Theory of Raman scattering in layered cuprate materials

C. M. Canali and S. M. Girvin
Department of Physics, Indiana University, Bloomington, Indiana 47405
(Received 20 September 1991; revised manuscript received 4 December 1991)

The line shape of Raman scattering in a two-dimensional Heisenberg antiferromagnet at zero temperature is studied within spin-wave theory, by using the Dyson-Maleev transformation. Besides the well-known dominant contribution coming from two-magnon scattering, a systematic analysis of the contribution coming from the production of four magnons is carried out. It is found that the four-magnon contribution is very small compared with the two-magnon intensity. However, it occurs at such large energies that the ratio of the first two frequency cumulants is enhanced by a factor of 2.5 for $S=\frac{1}{2}$, in fairly good agreement with recent series-expansion estimates. This is true despite the fact that the total line shape that we obtain is still in rather poor agreement with the experimental line shape obtained in experiments on undoped La_2CuO_4. As a by-product of the analysis of the effects of spin-wave interactions on the magnon propagator, the renormalization factor of the spin-wave velocity is computed to $O((1/S)^2)$. For $S=\frac{1}{2}$, the number that we find is $Z_c=1.177$, in very good agreement with the series-expansion result.

I. INTRODUCTION

Raman scattering from magnetic excitations was intensely studied more than two decades ago for different antiferromagnetic materials with effective spin S equal to or greater than 1. At that time it was shown that a possible source of photon-magnon interaction can involve a "two-magnon process,"[1] which can be described by a phenomenological photon–spin-pair coupling. Subsequently, within this model, a lineshape analysis based on a two-magnon scattering spin-wave theory was developed by Parkinson,[2] and this turned out to be extremely successful in reproducing the experimental curve. In particular, excellent agreement between theory and experiment[3] was found for K_2NiF_4, which is well described by a two-dimensional spin $S=1$ Heisenberg antiferromagnet (HAFM).

Soon after the high-temperature superconductors were discovered, the same kind of Raman-scattering experiments[4–6] were performed on the insulating phase of La_2CuO_4, which is believed to be a quasi-two-dimensional spin $S=\frac{1}{2}$ HAFM. As in the previously studied K_2NiF_4, the experimental spectrum shows a well-defined peak and satisfies the selection rules appropriate to magnetic spin-pair excitations. However, in contrast with the spin $S=1$ case, the peak linewidth is very broad and the spectrum has a very long tail far beyond the maximum energy that a magnon pair can have, extending into the energy range of four-magnon excitations. As a result, the old line shape analysis yields a theoretical spectrum in considerable disagreement with the experiment, even though the peak position gives a reasonable value of the exchange constant J. The anomalously broad spectrum is believed to be an intrinsic characteristic of spin $S=\frac{1}{2}$ systems, and the fact that Parkinson's spin-wave theory[2] does not provide good agreement with the experiment may simply mean that quantum fluctuations, which are presumably more important in this case, have not been included adequately. Strong support for this explanation was given by the calculation, within this model, of the first three frequency moments of the line shape by Singh *et al.*[7] Using series-expansion techniques, they obtained frequency moments in very good agreement with the experimental values. In particular, the first moment gives an estimate of the exchange constant $J\approx 1030\ \mathrm{cm}^{-1}$, consistent with the value obtained from other experiments. The ratio of the peak width to its position—which provides a parameter-free check of the theory—is also very close to the experimental value. This seems to imply that the effective photon–spin-pair coupling and the two-dimensional HAFM Hamiltonian are indeed the correct model describing the problem. However, the first three moments of a spectrum cannot define completely its line shape and a real theory of the line shape is still lacking.

More recently there have been some attempts[8–12] to tackle the problem using finite-size lattice calculations, with the argument that, since Raman scattering is primarily dominated by short-wavelength excitations, it should be possible to get useful information from small systems. Most of these calculations were performed on a 4×4 lattice.[13] The exact diagonalization of this system reveals very little structure: essentially three peaks. The highest one is clearly a two-magnon peak, while the other two are identifiable as four-magnon peaks. Despite the fact that these results do not resemble at all the broad peak found experimentally, it is interesting that the first three cumulants of the distribution are in good agreement with the experiments and with Singh's calculations. Of course, a 4×4 lattice is still very small, especially if one considers that, in the series-expansion calculations, there are contributions from spin-spin correlations with spins as far as ten sites apart along any axis.[14]

Another rather different approach, based on the "flux-phase" description of the $S=\frac{1}{2}$ HAMF, has been proposed by Hsu,[15] who simply describes the Raman spec-

trum as a convolution of two noninteracting flux-phase spin waves multiplied by the correct polarization- and momentum-dependent weighting factor. The spectrum that he gets is naturally broader than Parkinson's result and resembles better the experimental line shape. This is simply due to the anomalous [with respect to ordinary linear-spin-wave (LSW) theory] line shape of the one-spin-wave density of states that his dispersion yields. However, there seems to be some doubts that this dispersion correctly describes the short-wavelength excitations of the $S=\frac{1}{2}$ HAFM and, furthermore, this approach, although quite original and appealing, cannot be easily improved in a systematic way.

In a recent paper, Wang[16] employed a two-dimensional extension of the Wigner-Jordan transformation to map the spin variables of the $S=\frac{1}{2}$ HAFM into spinless fermion variables. The Raman spectrum is then studied within the "in-phase flux state of this model,"[17] which is a *disordered* spin state with gapless excitations, similar to the flux phase discussed by Affleck and Martson.[18] Apart from this mapping, the calculation is then carried out in a way very similar to Parkinson's theory of two-magnon scattering, the difference being that here the quasiparticles are fermionlike with a different dispersion. The resulting line shape is claimed to be in excellent agreement with experiment. We disagree on this: indeed the line shape, like the one obtained by Parkinson, has a natural cutoff at twice the maximum value of the quasiparticle excitation energy—which, for the in-phase flux state, is very close to the conventional spin-wave value—and totally misses the long tail at high frequencies which is, in fact, one of the main puzzles of the experimental line shape. Also, we think that Parkinson's line shape, reported in Wang's paper as a comparison, has not been drawn correctly: actually, Parkinson's line shape should be much narrower than the experimental line shape.[19] Finally, a more fundamental objection to this theory is that the in-phase flux state is a disordered phase while there is, by now, considerable numerical evidence that the $S=\frac{1}{2}$ HAFM ground state has a finite, nonzero magnetization. On the other hand, if the magnetization is forced to be nonzero (this gives rise to the "Néel flux phase"[16]), the elementary excitations in this model are no longer gapless, in contrast with what we aspect from the rotational invariance of the Heisenberg model.

In this paper we shall study the Raman-scattering line shape at $T=0$ within the framework of conventional spin-wave theory. Our purpose will be to try to go beyond the well-known "two-magnon" scattering and compute, in a systematic way, the contribution to the scattering due to the production of four magnons. We want to see how the line shape *and* the first few frequency moments are modified by the four-magnon contribution. Our terms of comparison will be the series-expansion results and the experiment. In particular, the question that we want to answer is: is it possible to derive a *line shape* whose *moments* agree with Singh's results and, in this case, how does this curve compare with the experiment?

We choose to work within the Dyson-Maleev (DM) formalism,[20,21] rather than the more common Holstein-Primakoff (HP) formalism, for many technical reasons. It has been recognized for a long time[20,22] that the DM formalism has many advantages if one needs really to go beyond LSW theory within a perturbation scheme, mainly because the interactions between spin waves are much better handled than in HP so that the unphysical singularities caused by the long-wavelength spin waves cancel out.[23] The price that we have to pay is to work explicitly within a non-Hermitian theory. In the past the DM formalism was used to study mostly static (i.e., thermodynamic) properties of the HAFM, or, when dynamical quantities were computed, the calculations were always carried out close to the "on-shell" condition (see Sec. III). In that case, the non-Hermiticity of the theory did not case any problem. Not much is known about the study of fully dynamical quantities where some important physics occurs far off the mass shell, as in our problem. We will see that, in this case, some difficulties connected with the non-Hermiticity of the formalism may indeed arise, but eventually everything works rather well if we are just interested in computing real physical observables. What we find is that all the numerous four-magnon contributions coming from the exchange Hamiltonian and the Raman-scattering operator hardly change the two-magnon line shape: for $S=\frac{1}{2}$, the integrated four-magnon intensity is only 2.9% of the integrated two-magnon intensity and for $S=1$ it is even smaller. However, the four-magnon intensity happens to be nonzero at such large energies that the ratio of the first two cumulants is modified by a factor of 2.5 for $S=\frac{1}{2}$, in good agreement with Singh's results, despite the rather poor *apparent* agreement between our line shape and the experimental line shape. For $S=1$, the four-magnon contribution seems to be even less relevant than for the $S=\frac{1}{2}$ case. However, again, it causes the ratio of the first two cumulants to be enhanced by almost 50%, in rough agreement with the series-expansion result.[14]

As a by-product of our study of the second-order magnon self-energy, which turns out to be the relevant quantity needed to evaluate the indirect four-magnon production caused by decay, we have also computed the correction, to second order in $(1/S)$, of the magnon dispersion and the renormalization constant of the spin-wave velocity, Z_c. The value of Z_c that we get for $S=\frac{1}{2}$ is $Z_c=1.177\pm0.001$, in very good agreement with the series-expansion result 1.18 ± 0.02 obtained by Singh and Singh and Huse.[24] The $(1/S)^2$ correction to the magnon dispersion is positive for all values of the wave vectors inside the antiferromagnetic Brillouin zone and it is less than 3% of the first order (in $1/S$) result, strengthening the belief that the spin-wave expansion is indeed a very good asymptotic expansion.

The paper is organized in the following way. In Sec. II we introduce the basic formalism: Sec. II A describes the Heisenberg Hamiltonian in the Dyson-Maleev representation; in Sec. II B the boson Green's function and perturbation theory at $T=0$ are introduced; in Sec. II C the Raman-scattering Hamiltonian and cross section are introduced. Section III is devoted to a detailed analysis of the Raman-scattering line shape: the two-magnon scattering is derived in Sec. III A; in Sec. III B we discuss the scattering involving the direct production of four

magnons; in Sec. III C interference precesses between two-magnon states and four-magnon states are considered; in Sec. III D we analyze the total Raman line shape due to all these different processes. Finally, Sec. IV contains the concluding remarks of this paper.

II. FORMALISM

A. Heisenberg Hamiltonian in the Dyson-Maleev boson representation

The Hamiltonian of the quantum HAFM is given by

$$H=J\sum_{\langle ij\rangle}\mathbf{S}_i\cdot\mathbf{S}_j=J\sum_{\langle ij\rangle}[S_i^zS_j^z+\tfrac{1}{2}(S_i^+S_j^-+S_i^+S_j^+)]\ . \tag{2.1}$$

The sum $\langle ij\rangle$ runs over bonds in a square lattice whose lattice spacing is a. Sites i belong to the sublattice A ("up") and sites j belong to the sublattice B ("down"). Sublattices A and B are both square lattices rotated by an angle of 45° with respect to the original lattice; their lattice spacing is $\sqrt{2}a$. Let us assume that each sublattice consists of N sites. The units are such that the positive quantity J has dimensions of an energy and the spin operators are dimensionless.

In order to apply standard many-body techniques for boson systems, let us transform the spin Hamiltonian given in Eq. (2.1) into a boson Hamiltonian by using the Dyson-Maleev transformation,[20,21] which, in the case of nonfrustrated antiferromagnetic coupling, is conveniently written as (see Appendix A)

$$\begin{aligned}S_i^z&=S-a_i^\dagger a_i\ ,\\ S_i^+&=(2S)^{1/2}\left[1-\frac{a_i^\dagger a_i}{2S}\right]a_i\ ,\\ S_i^-&=(2S)^{1/2}a_i^\dagger\ ,\end{aligned} \tag{2.2}$$

for sublattice A, and

$$\begin{aligned}S_j^z&=-S+b_j^\dagger b_j\ ,\\ S_j^+&=(2S)^{1/2}b_j^\dagger\left[1-\frac{b_j^\dagger b_j}{2S}\right]\ ,\\ S_j^-&=(2S)^{1/2}b_j\ ,\end{aligned} \tag{2.3}$$

for sublattice B. This representation of the spin operators obeys the correct spin commutation relations but constitutes a nonunitary transformation.

By using Eqs. (2.2) and (2.3) in Eq. (2.1), the spin Hamiltonian is turned into the following non-Hermitian boson Hamiltonian:

$$H_{\rm DM}=E_0'+H_0'+V_{\rm DM}'\ , \tag{2.4}$$

where

$$E_0'=-NJzS^2\ , \tag{2.5}$$

$$H_0'=JSz\left[\sum_i a_i^\dagger a_i+\sum_j b_j^\dagger b_j\right]+SJ\sum_{\langle ij\rangle}(a_i^\dagger b_j^\dagger+a_ib_j)\ , \tag{2.6}$$

$$V_{\rm DM}'=-J\sum_{\langle ij\rangle}(a_i^\dagger a_ib_j^\dagger b_j+\tfrac{1}{2}a_i^\dagger a_ia_ib_j+\tfrac{1}{2}a_i^\dagger b_j^\dagger b_j^\dagger b_j)\ . \tag{2.7}$$

Here z is the coordination number of the lattice, which is equal to four for a two-dimensional square lattice.

We introduce the Fourier transform of the boson operators

$$a_{\mathbf{k}}=N^{-1/2}\sum_i e^{i\mathbf{k}\cdot\mathbf{r}_i}a_i\ , \tag{2.8}$$

$$b_{\mathbf{k}}=N^{-1/2}\sum_i e^{-i\mathbf{k}\cdot\mathbf{r}_j}b_j\ , \tag{2.9}$$

where each summation is restricted to the relevant sublattice and $\mathbf{k}$ runs over the antiferromagnetic Brillouin zone. The quadratic part H_0' is then given by

$$H_0'=JSz\sum_{\mathbf{k}}[a_{\mathbf{k}}^\dagger a_{\mathbf{k}}+b_{\mathbf{k}}^\dagger b_k+\gamma_{\mathbf{k}}(a_{\mathbf{k}}^\dagger b_{\mathbf{k}}^\dagger+a_{\mathbf{k}}b_{\mathbf{k}})]\ , \tag{2.10}$$

where we have defined

$$\gamma_{\mathbf{k}}=\frac{1}{z}\sum_{\boldsymbol{\delta}}e^{ia\mathbf{k}\cdot\boldsymbol{\delta}}\ , \tag{2.11}$$

and the sum over $\boldsymbol{\delta}$ is over the $z=4$ unit vectors connecting site $\mathbf{i}$ with its nearest neighbors, namely, $\boldsymbol{\delta}=\pm\hat{\mathbf{x}},\pm\hat{\mathbf{y}}$, where $\hat{\mathbf{x}}$ and $\hat{\mathbf{y}}$ are the x and y directions along the bonds of the square lattice. Therefore,

$$\gamma_{\mathbf{k}}=\frac{\cos(k_xa)+\cos(k_ya)}{2}\ . \tag{2.12}$$

We now proceed to diagonalize H_0' with a Bogoliubov transformation

$$a_{\mathbf{k}}=u_{\mathbf{k}}\alpha_{\mathbf{k}}+v_{\mathbf{k}}\beta_{\mathbf{k}}^\dagger=u_{\mathbf{k}}(\alpha_{\mathbf{k}}-x_{\mathbf{k}}\beta_{\mathbf{k}}^\dagger)\ , \tag{2.13}$$

$$b_{\mathbf{k}}=u_{\mathbf{k}}\beta_{\mathbf{k}}+v_{\mathbf{k}}\alpha_{\mathbf{k}}^\dagger=u_{\mathbf{k}}(\beta_{\mathbf{k}}-x_{\mathbf{k}}\alpha_{\mathbf{k}}^\dagger)\ , \tag{2.14}$$

where the α's and β's satisfy the usual Bose commutation rules and

$$u_{\mathbf{k}}^2-v_{\mathbf{k}}^2=u_{\mathbf{k}}^2(1+x_{\mathbf{k}}^2)=1\ . \tag{2.15}$$

H_0' is then found to be diagonalized for

$$u_{\mathbf{k}}=[(1+\varepsilon_{\mathbf{k}})/2\varepsilon_k]^{1/2}\ , \tag{2.16}$$

$$v_{\mathbf{k}}=-[(1-\varepsilon_{\mathbf{k}})/2\varepsilon_{\mathbf{k}}]^{1/2}\ , \tag{2.17}$$

$$x_{\mathbf{k}}=-v_{\mathbf{k}}/u_{\mathbf{k}}[(1-\varepsilon_k)/(1+\varepsilon_{\mathbf{k}})]^{1/2}\ , \tag{2.18}$$

with

$$\varepsilon_{\mathbf{k}}=(1-\gamma_{\mathbf{k}})^{1/2}\ . \tag{2.19}$$

Other useful relations are

$$u_{\mathbf{k}}^2+v_{\mathbf{k}}^2=1/\varepsilon_{\mathbf{k}}\ , \tag{2.20}$$

$$u_{\mathbf{k}}v_{\mathbf{k}}=-\gamma_{\mathbf{k}}/2\varepsilon_{\mathbf{k}}\ . \tag{2.21}$$

We obtain

$$H_0' = JSz\sum_{\mathbf{k}}\varepsilon_{\mathbf{k}}(\alpha_{\mathbf{k}}^\dagger\alpha_{\mathbf{k}}+\beta_{\mathbf{k}}^\dagger\beta_{\mathbf{k}}+1)-NJSz\ . \tag{2.22}$$

When $V_{\rm DM}'$ is written in terms of α's and β's, we get a sum of complicated quartic terms. We then proceed to normal order these terms and we obtain

$$V_{\rm DM}' = -NJzS^2\left[\frac{r}{2S}\right]^2 + JzS\frac{r}{2S}\sum_{\mathbf{k}}\varepsilon_{\mathbf{k}}(\alpha_{\mathbf{k}}^\dagger\alpha_{\mathbf{k}}+\beta_{\mathbf{k}}^\dagger\beta_{\mathbf{k}})+V_{\rm DM}\ , \tag{2.23}$$

where

$$\begin{aligned}V_{\rm DM}\equiv :V_{\rm DM}':\equiv -\left[\frac{z}{4}\right]\frac{J}{N}\sum_{(1234)}\delta_G(1+2-3-4)(&V_{(1234)}^{(1)}\alpha_1^\dagger\alpha_2^\dagger\alpha_3\alpha_4+V_{(1234)}^{(2)}\alpha_1^\dagger\beta_2\alpha_3\alpha_4+V_{(1234)}^{(3)}\alpha_1^\dagger\alpha_2^\dagger\beta_3^\dagger\alpha_4\\&+V_{(1234)}^{(4)}\alpha_1^\dagger\alpha_3\beta_4^\dagger\beta_2+V_{(1234)}^{(5)}\beta_4^\dagger\alpha_3\beta_2\beta_1+V_{(1234)}^{(6)}\beta_4^\dagger\beta_3^\dagger\alpha_2^\dagger\beta_1\\&+V_{(1234)}^{(7)}\alpha_1^\dagger\alpha_2^\dagger\beta_3^\dagger\beta_4^\dagger+V_{(1234)}^{(8)}\beta_1\beta_2\alpha_3\alpha_4+V_{(1234)}^{(9)}\beta_4^\dagger\beta_3^\dagger\beta_2\beta_1)\ .\end{aligned} \tag{2.24}$$

The numerical constant r is defined by

$$r=1-\frac{1}{N}\sum_{\mathbf{k}}\varepsilon_{\mathbf{k}}\ , \tag{2.25}$$

and it is approximately equal to 0.158 in two dimensions. The constant and the quadratic terms in Eq. (2.23), coming from the normal ordering, are known as Oguchi corrections to the ground-state energy and the spin-wave dispersion, respectively.[25] The quartic interaction $V_{\rm DM}$ is the sum of nine terms. The vertex functions $V_{(1234)}^{(i)}$, $i=1,2,\ldots,9$ are given explicitly in Appendix B. Throughout the paper we shall use the abbreviations 1 for $\mathbf{k}_1$, 2 for $\mathbf{k}_2$, and so on. Also, in Eq. (2.24), the Kronecker δ, $\delta_G(1+2-3-4)$, expresses the conservation of momentum to within a reciprocal-lattice vector $\mathbf{G}$. Putting Eqs. (2.5), (2.22), and (2.23) together, we can finally rewrite H in the following form:

$$H_{\rm DM}=E_0+H_0+V_{\rm DM}\ , \tag{2.26}$$

where E_0 is the ground-state energy and is given by

$$E_0=-NJzS^2[\alpha(S)]^2\ , \tag{2.27}$$

where

$$\alpha(S)=1+\frac{r}{2S}\ . \tag{2.28}$$

The quadratic part H_0 describes a gas of noninteracting spin waves of two different species having the same dispersion, and is given by

$$H_0=\sum_{\mathbf{k}}\hbar\Omega_{\mathbf{k}}(\alpha_{\mathbf{k}}^\dagger\alpha_{\mathbf{k}}+\beta_{\mathbf{k}}^\dagger\beta_{\mathbf{k}})\ , \tag{2.29}$$

where the spin-wave dispersion is defined as

$$\Omega_{\mathbf{k}}=\frac{JzS\alpha(S)}{\hbar}\varepsilon_{\mathbf{k}}\ . \tag{2.30}$$

The maximum magnon energy is

$$\mathcal{E}_{\max}=\hbar\Omega_{\max}=JzS\alpha(S)\ . \tag{2.31}$$

The momentum-conserving potential $V_{\rm DM}$ represents the interactions between spin waves. It presents some differences with respect to potentials of standard form. First it is not simply a two-body interaction because there are terms, like $V_{(1234)}^{(7)}\alpha_1^\dagger\alpha_2^\dagger\beta_3^\dagger\beta_4^\dagger$, representing the simultaneous creation of four particles. Second, it is nonlocal, so that the vertex functions depend not only on the momentum transfer between two incoming magnons, but also on their momenta separately. Third, it is non-Hermitian. None of these facts causes any calculational problem since we can still use all the techniques of many-body theory for bosons, being careful to avoid implicitly assuming $V_{\rm DM}=V_{\rm DM}^\dagger$. Finally, we would like to emphasize that $V_{\rm DM}$ is what distinguishes the Dyson-Maleev theory from the analogous theory carried out by using the Holstein-Primakoff transformation: in the latter case one obtains the same expressions for E_0 and H_0 but the quartic terms are different. We will see that this difference plays an important role in the perturbation theory that we are about to describe.

B. Boson Green's function and perturbation theory at $T=0$

In this paper we are interested in studying correlation functions of the form

$$\langle\psi_0|\mathcal{T}\Lambda(t_1)\Lambda(t_2)|\psi_0\rangle\ , \tag{2.32}$$

where $\Lambda(t_1)=e^{iHt/\hbar}\Lambda e^{-iHt/\hbar}$ is a time-dependent spin operator in the Heisenberg picture and $|\psi_0\rangle$ is the ground state. Dyson[20] was able to prove that the expectation value of spin operators was equal to the expectation value of the corresponding boson operators (obtained via the DM transformation), provided that the "unphysical" boson states are ruled out. A boson state is said to be unphysical when there exists a site in the lattice occupied by more than $2S$ bosons. The constraint arising from ruling out the unphysical boson states is the origin of what is called the *kinematic interaction*, in contrast to the *dynamical interaction* represented, as we have just seen, by the quartic term $V_{\rm DM}$ in the boson Hamiltonian. If the constraint is satisfied, the correspondence is exact. In

fact, it is not known how to enforce the constraint exactly. What is known[20] is that, in the case of a *ferromagnet* in $D=3$ dimensions, the kinematic interaction is exponentially small at low temperatures (i.e., for $T \ll T_c$) and therefore can be safely neglected. For an antiferromagnet, the situation is much less clear then for a ferromagnet, even though it was argued[22] that, at least in $D=3$, the neglect of the kinematic interaction cannot introduce serious errors at low temperatures, namely, far below the Néel temperature. Of course, in our case, $D=2$, and this approximation is certainly not on firm ground. However, here we want to study the problem strictly at $T=0$, where it is by now generally believed that the system possesses long-range order, so that perhaps the arguments used in the $D=3$ case below the Néel temperature, are still valid. Therefore, we shall make the same approximation: we shall regard the HAFM excitations as an interacting boson gas and evaluate the boson correlation functions without explicitly projecting out the unphysical states. The second approximation that we will make is to treat the quartic terms in a perturbation expansion at $T=0$ around the LSW ground state, namely, we will assume that the spin waves interact weakly and we will use H_0 as the unperturbed Hamiltonian.

Let us define all the basic propagators[22]

$$iG_{\alpha\alpha}(\mathbf{k};t-t')=\langle\psi_0|\mathcal{T}\alpha_{\mathbf{k}}(t)\alpha_{\mathbf{k}}^{\dagger}(t')|\psi_0\rangle\ , \tag{2.33}$$

$$iG_{\beta\beta}(\mathbf{k};t-t')=\langle\psi_0|\mathcal{T}\beta_{\mathbf{k}}^{\dagger}(t)\beta_{\mathbf{k}}(t')|\psi_0\rangle\ , \tag{2.34}$$

$$iG_{\alpha\beta}(\mathbf{k};t-t')=\langle\psi_0|\mathcal{T}\alpha_{\mathbf{k}}(t)\beta_{\mathbf{k}}(t')|\psi_0\rangle\ , \tag{2.35}$$

$$iG_{\beta\alpha}(\mathbf{k};t-t')=\langle\psi_0|\mathcal{T}\beta_{\mathbf{k}}^{\dagger}(t)\alpha_{\mathbf{k}}^{\dagger}(t')|\psi_0\rangle\ . \tag{2.36}$$

We introduce the Fourier representations according to

$$G_{\mu\nu}(\mathbf{k};t-t')=\frac{1}{2\pi}\int_{-\infty}^{+\infty}d\omega\, e^{-i\omega(t-t')}G_{\mu\nu}(\mathbf{k},\omega)\ , \tag{2.37}$$

or equivalently

$$G_{\mu\nu}(\mathbf{k},\omega)=\int_{-\infty}^{+\infty}d(t-t')e^{i\omega(t-t')}G_{\mu\nu}(\mathbf{k};t-t')\ . \tag{2.38}$$

Here the Greek letters μ,ν run over α and β. The unperturbed Green's functions $G_{\mu\nu}^{(0)}(\mathbf{k},\omega)$ are easy to compute:

$$G_{\alpha\alpha}^{(0)}(\mathbf{k};t-t')=-i\Theta(t-t')e^{-i\Omega_{\mathbf{k}}(t-t')}\ , \tag{2.39}$$

$$G_{\beta\beta}^{(0)}(\mathbf{k};t-t')=-i\Theta(t'-t)e^{i\Omega_{\mathbf{k}}(t-t')}\ , \tag{2.40}$$

$$G_{\alpha\beta}^{(0)}(\mathbf{k};t-t')=G_{\beta\alpha}^{(0)}(\mathbf{k};t-t')=0\ , \tag{2.41}$$

and their Fourier transforms are

$$G_{\alpha\alpha}^{(0)}(\mathbf{k},\omega)=\frac{1}{\omega-\Omega_{\mathbf{k}}+i\eta}\ , \tag{2.42}$$

$$G_{\beta\beta}^{(0)}(\mathbf{k},\omega)=-\frac{1}{\omega+\Omega_{\mathbf{k}}-i\eta}\ . \tag{2.43}$$

We will associate with $G_{\alpha\alpha}$, $G_{\beta\beta}$, $G_{\alpha\alpha}^{(0)}$, and $G_{\beta\beta}^{(0)}$ the symbols shown in Fig. 1.

The Green's functions $G_{\mu\nu}$ satisfy a matrix Dyson's equation

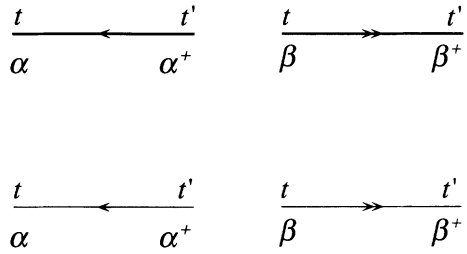

FIG. 1. Diagrammatic representation of the α and β propagators. A boldface line with a single arrow oriented from t' to t represents $G_{\alpha\alpha}(\mathbf{k};t-t')$. A boldface line with a double arrow oriented from t to t' represents $G_{\beta\beta}(\mathbf{k};t-t')$. A light line with a single arrow oriented from t' to t represents $G_{\alpha\alpha}^{(0)}(\mathbf{k};t-t')$. A light line with a double arrow oriented from t to t' represents $G_{\beta\beta}^{(0)}(\mathbf{k};t-t')$.

$$G_{\mu\nu}(\mathbf{k},\omega)=G_{\mu\nu}^{(0)}(\mathbf{k},\omega)+\sum_{\gamma,\delta}G_{\mu\gamma}^{(0)}(\mathbf{k},\omega)\Sigma_{\gamma\delta}(\mathbf{k},\omega)G_{\delta\nu}(\mathbf{k},\omega)\ , \tag{2.44}$$

where the self-energy $\Sigma_{\gamma\delta}(\mathbf{k},\omega)$ can be expressed in the usual kind of diagrammatic expressions. From the symmetry of the Hamiltonian with respect to the interchange $\alpha_{\mathbf{k}}\Longleftrightarrow\beta_{\mathbf{k}}^{\dagger}$, we obtain the following relations:

$$\Sigma_{\alpha\alpha}(\mathbf{k},\omega)=\Sigma_{\beta\beta}(\mathbf{k},-\omega)\ , \tag{2.45}$$

$$\Sigma_{\alpha\beta}(\mathbf{k},\omega)=\Sigma_{\beta\alpha}(\mathbf{k},-\omega)\ . \tag{2.46}$$

Furthermore, $\Sigma_{\gamma\delta}(\mathbf{k},\omega)$ has the symmetry of the square lattice and, in particular,

$$\Sigma_{\gamma\delta}(\mathbf{k},\omega)=\Sigma_{\gamma\delta}(-\mathbf{k},\omega)\ . \tag{2.47}$$

We will see that $\Sigma_{\gamma\delta}(\mathbf{k},\omega)$ is small compared to the unperturbed energy $\Omega_{\mathbf{k}}$, so that, at leading order in $\|\underline{\Sigma}(\mathbf{k},\omega)\|/\Omega_{\mathbf{k}}$, the solution of Eq. (2.44) may be approximated as[22]

$$G_{\alpha\alpha}(\mathbf{k},\omega)=\frac{1}{\omega-\Omega_{\mathbf{k}}-\Sigma_{\alpha\alpha}(\mathbf{k},\omega)+i\eta}\ , \tag{2.48}$$

$$G_{\beta\beta}(\mathbf{k},\omega)=-\frac{1}{\omega+\Omega_{\mathbf{k}}+\Sigma_{\beta\beta}(\mathbf{k},\omega)-i\eta}\ , \tag{2.49}$$

$$G_{\alpha\beta}(\mathbf{k},\omega)=\Sigma_{\alpha\beta}(\mathbf{k},\omega)G_{\alpha\alpha}(\mathbf{k},\omega)G_{\beta\beta}(\mathbf{k},\omega)\ , \tag{2.50}$$

$$G_{\beta\alpha}(\mathbf{k},\omega)=\Sigma_{\beta\alpha}(\mathbf{k},\omega)G_{\alpha\alpha}(\mathbf{k},\omega)G_{\beta\beta}(\mathbf{k},\omega)\ . \tag{2.51}$$

C. Raman-scattering Hamiltonian and cross section at $T=0$

If we assume that there exists an effective spin-pair Hamiltonian[1] with only nearest-neighbor coupling, describing the Raman scattering in a HAFM—the nearest-neighbor condition is consistent with having nearest-neighbor Heisenberg Hamiltonian for the unperturbed system—then group theory[26] shows that, for a lattice with square symmetry, only the B_{1g} mode is Raman active and the scattering Hamiltonian has the form

$$\Lambda = B\sum_{i,\delta} P(\mathbf{E}_{\rm inc},\mathbf{E}_{\rm sc};\delta)\mathbf{S}_i\cdot\mathbf{S}_{i+\delta}\ , \tag{2.52}$$

where $\mathbf{E}_{\rm inc}$ and $\mathbf{E}_{\rm sc}$ are, respectively, the initial (incident) and the final (scattered) polarization vectors of the scattered light and the site-independent function $P(\mathbf{E}_{\rm inc},\mathbf{E}_{\rm sc};\delta)$ is defined by

$$P(\mathbf{E}_{\rm inc},\mathbf{E}_{\rm sc};\delta) = [\tfrac{1}{2}\mathbf{E}_{\rm inc}\cdot\mathbf{E}_{\rm sc} - (\delta\cdot\mathbf{E}_{\rm inc})(\delta\cdot\mathbf{E}_{\rm sc})]\ . \tag{2.53}$$

B is an undetermined constant.

We can also rewrite the scattering Hamiltonian in the form

$$\Lambda = \frac{B}{2}\mathcal{P}(\mathbf{E}_{\rm inc},\mathbf{E}_{\rm sc})\sum_j \mathbf{S}_j\cdot(\mathbf{S}_{j+\hat{y}} - \mathbf{S}_{j+\hat{x}})\ , \tag{2.54}$$

where the polarization function, $\mathcal{P}(\mathbf{E}_{\rm inc},\mathbf{E}_{\rm sc})$, is

$$\mathcal{P}(\mathbf{E}_{\rm inc},\mathbf{E}_{\rm sc}) = (E^x_{\rm inc}E^x_{\rm sc} - E^y_{\rm inc}E^y_{\rm sc})\ , \tag{2.55}$$

and the sum over j in Eq. (2.54) runs now over the whole lattice. Notice incidentally that the Heisenberg Hamiltonian can be written in a similar way:

$$H = J\sum_j \mathbf{S}_j\cdot(\mathbf{S}_{j+\hat{y}} + \mathbf{S}_{j+\hat{x}})\ . \tag{2.56}$$

Equations (2.54) and (2.56) emphasize the transformation properties of H and Λ under the symmetry group of the square lattice.

The scattering intensity at $T=0$ is given by Fermi's Golden Rule

$$I(\mathcal{E}) = \frac{2\pi}{\hbar}\sum_n \delta(\mathcal{E} - (\mathcal{E}_n - \mathcal{E}_0))|\langle\psi_0|\Lambda|\psi_n\rangle|^2\ , \tag{2.57}$$

where $|\psi_0\rangle$ is the ground state and $|\psi_n\rangle$ are the excited states of the full Heisenberg Hamiltonian.

Let us define the following time-ordered Green's function at $T=0$:

$$iG_\Lambda(t-t') = \langle\psi_0|\mathcal{T}\Lambda(t)\Lambda(t')|\psi_0\rangle\ , \tag{2.58}$$

and its Fourier transform

$$\tilde{G}_\Lambda(\omega) = \int_{-\infty}^{+\infty} d(t-t')e^{i\omega(t-t')}G_\Lambda(t-t')\ . \tag{2.59}$$

We have the relation

$$I(\mathcal{E}) = -\frac{2}{\hbar}\mathrm{Im}\tilde{G}_\Lambda(\omega = \mathcal{E}/\hbar)\ . \tag{2.60}$$

We want to evaluate $\tilde{G}_\Lambda(\omega)$ by using a perturbation expansion at $T=0$. In order to do this, let us rewrite the Raman operator Λ in terms of boson operators, following exactly the same procedure used for the bosonization of the Heisenberg Hamiltonian. We obtain

$$\Lambda = B\sum_{i,\delta} P(\mathbf{E}_{\rm inc},\mathbf{E}_{\rm sc};\delta)[-S^2 + S(a_i^\dagger a_i + b_{i+\delta}^\dagger b_{i+\delta}) + S(a_i b_{i+\delta} + a_i^\dagger b_{i+\delta}^\dagger) - a_i^\dagger a_i b_{i+\delta}^\dagger b_{i+\delta} - \tfrac{1}{2}(a_i^\dagger a_i a_i b_{i+\delta} + a_i^\dagger b_{i+\delta}^\dagger b_{i+\delta}^\dagger b_{i+\delta})]\ . \tag{2.61}$$

Since

$$\sum_\delta P(\mathbf{E}_{\rm inc},\mathbf{E}_{\rm sc};\delta) = 0\ , \tag{2.62}$$

the first two terms inside the square bracket vanish. Therefore, we are left with the following expression:

$$\Lambda = \Lambda_0' + \Lambda_1'\ , \tag{2.63}$$

where

$$\Lambda_0' = BS\sum_{i,\delta} P(\mathbf{E}_{\rm inc},\mathbf{E}_{\rm sc};\delta)(a_i b_{i+\delta} + a_i^\dagger b_{i+\delta}^\dagger)\ , \tag{2.64}$$

$$\Lambda_1' = -B\sum_{i,\delta} P(\mathbf{E}_{\rm inc},\mathbf{E}_{\rm sc};\delta)[a_i^\dagger a_i b_{i+\delta}^\dagger b_{i+\delta} + \tfrac{1}{2}(a_i^\dagger a_i a_i b_{i+\delta} + a_i^\dagger a_i b_{i+\delta}^\dagger b_{i+\delta}^\dagger b_{i+\delta})]\ . \tag{2.65}$$

Next, we go to Fourier space and replace a's and b's with α's and β's, obtaining, after normal ordering, the quartic terms

$$\Lambda_0' = \frac{B}{2}\mathcal{P}(\mathbf{E}_{\rm inc},\mathbf{E}_{\rm sc})zS\sum_{\mathbf{k}}\frac{\tilde{\gamma}_{\mathbf{k}}}{\varepsilon_{\mathbf{k}}}[(\alpha_{\mathbf{k}}\beta_{\mathbf{k}} + \alpha_{\mathbf{k}}^\dagger\beta_{\mathbf{k}}^\dagger) - \gamma_{\mathbf{k}}(\alpha_{\mathbf{k}}^\dagger\alpha_{\mathbf{k}} + \beta_{\mathbf{k}}^\dagger\beta_{\mathbf{k}})]\ , \tag{2.66}$$

$$\Lambda_1' = \frac{r}{2S}\Lambda_0' + \Lambda_1\ , \tag{2.67}$$

$$\Lambda_1 = -\frac{B}{2}\mathcal{P}(\mathbf{E}_{\rm inc},\mathbf{E}_{\rm sc})\frac{z}{4N}\sum_{(1234)}\delta_{\mathbf{G}}(1+2-3-4)[\tilde{V}^{(1)}_{(1234)}\alpha_1^\dagger\alpha_2^\dagger\alpha_3\alpha_4 + \tilde{V}^{(2)}_{(1234)}\alpha_1^\dagger\beta_2\alpha_3\alpha_4 + \tilde{V}^{(3)}_{(1234)}\alpha_1^\dagger\alpha_2^\dagger\beta_3^\dagger\alpha_4 + \tilde{V}^{(4)}_{(1234)}\alpha_1^\dagger\alpha_3\beta_4^\dagger\beta_2 + \tilde{V}^{(5)}_{(1234)}\beta_4^\dagger\alpha_3\beta_2\beta_1 + \tilde{V}^{(6)}_{(1234)}\beta_4^\dagger\beta_3^\dagger\alpha_2^\dagger\beta_1 + \tilde{V}^{(7)}_{(1234)}\alpha_1^\dagger\alpha_2^\dagger\beta_3^\dagger\beta_4^\dagger + \tilde{V}^{(8)}_{(1234)}\beta_1\beta_2\alpha_3\alpha_4 + \tilde{V}^{(9)}_{(1234)}\beta_4^\dagger\beta_3^\dagger\beta_2\beta_1]\ , \tag{2.68}$$

where the symmetry factor of the B_{1g} mode, $\tilde{\gamma}_{\mathbf{k}}$, is defined as

$$\tilde{\gamma}_{\mathbf{k}}=\frac{\cos(k_x a)-\cos(k_y a)}{2} . \tag{2.69}$$

The explicit expressions for the vertices $\tilde{V}^{(i)}_{(1234)}$, $i=1,2,\ldots,9$, are given in Appendix B. Notice that the symmetry factor $\tilde{\gamma}_{\mathbf{k}}$ and the polarization factor $\mathcal{P}(\mathbf{E}_{\rm inc},\mathbf{E}_{\rm sc})$ are completely decoupled in Eqs. (2.66) and (2.68).

We can finally rewrite Λ in the form

$$\Lambda=\Lambda_0+\Lambda_1 , \tag{2.70}$$

where

$$\Lambda_0=\frac{B}{2}\mathcal{P}(\mathbf{E}_{\rm inc},\mathbf{E}_{\rm sc})zS\alpha(S) \times\sum_{\mathbf{k}}\frac{\tilde{\gamma}_{\mathbf{k}}}{\varepsilon_{\mathbf{k}}}[(\alpha_{\mathbf{k}}\beta_{\mathbf{k}}+\alpha^{\dagger}_{\mathbf{k}}\beta^{\dagger}_{\mathbf{k}})-\gamma_{\mathbf{k}}(\alpha^{\dagger}_{\mathbf{k}}\alpha_{\mathbf{k}}+\beta^{\dagger}_{\mathbf{k}}\beta_{\mathbf{k}})] . \tag{2.71}$$

Therefore, the computation of $G_{\Lambda}(t-t')$ will involve the computation of the following four correlation functions:

(1) A two-magnon correlation function

$$G_{\Lambda_0}(t-t')=-i\langle\psi_0|\mathcal{T}\Lambda_0(t)\Lambda_0(t')|\psi_0\rangle . \tag{2.72}$$

(2) A four-magnon correlation function

$$G_{\Lambda_1}(t-t')=-i\langle\psi_0|\mathcal{T}\Lambda_1(t)\Lambda_1(t')|\psi_0\rangle . \tag{2.73}$$

(3) Two "interference" correlation functions

$$G_{\Lambda_{01}}(t-t')=-i\langle\psi_0|\mathcal{T}\Lambda_0(t)\Lambda_1(t')|\psi_0\rangle , \tag{2.74}$$

$$G_{\Lambda_{10}}(t-t')=-i\langle\psi_0|\mathcal{T}\Lambda_1(t)\Lambda_0(t')|\psi_0\rangle . \tag{2.75}$$

Since

$$G_{\Lambda_{01}}(t-t')=G_{\Lambda_{10}}(t'-t) , \tag{2.76}$$

or equivalently

$$\tilde{G}_{\Lambda_{01}}(\omega)=\tilde{G}_{\Lambda_{10}}(-\omega) , \tag{2.77}$$

it will be enough to compute either one of them. Therefore, the total Raman-scattering intensity can be written as the sum of four contributions:

$$I(\mathcal{E})=I_{\Lambda_0}(\mathcal{E})+I_{\Lambda_1}(\mathcal{E})+I_{\Lambda_{01}}(\mathcal{E})+I_{\Lambda_{10}}(\mathcal{E}) , \tag{2.78}$$

where

$$I_{\Lambda_0}(\mathcal{E})=-\frac{2}{\hbar}\mathrm{Im}[\tilde{G}_{\Lambda_0}(\omega=\mathcal{E}/\hbar)] , \tag{2.79}$$

and so on.

III. STUDY OF THE RAMAN-SCATTERING LINE SHAPE

A. Two-magnon Raman scattering

In this section we want to study the correlation function $G_{\Lambda_0}(\omega)$ describing the multiple scattering of a pair of magnons. The results that we are going to derive here were first obtained by Parkinson[2] using an equation-of-motion formalism and subsequently by Davis *et al.*[27] using essentially the same approach that we have adopted here but at finite temperatures. Nevertheless, we think it useful to repeat their derivation in order to set up a coherent notation for our $T=0$ analysis and to discuss all the other contributions that were disregarded in those previous works, which can be important for the spin $S=\frac{1}{2}$ case. The Fourier transform of $G_{\Lambda_0}(t-t')$ is written in the form

$$G_{\Lambda_0}(\omega)=N(B/2)^2 g(\mathbf{E}_{\rm inc},\mathbf{E}_{\rm sc})[zS\alpha(S)]^2\frac{1}{N}\sum_{\mathbf{k},\mathbf{k}'}\tilde{\gamma}_{\mathbf{k}}\tilde{\gamma}_{\mathbf{k}'}\left[\frac{1}{\varepsilon_{\mathbf{k}}}\frac{1}{\varepsilon_{\mathbf{k}'}}\chi^{(1)}_{\mathbf{k}\mathbf{k}'}(\omega)-\frac{\gamma_{\mathbf{k}'}}{\varepsilon_{\mathbf{k}}\varepsilon_{\mathbf{k}'}}[\chi^{(2)}_{\mathbf{k}\mathbf{k}'}(\omega)+\chi^{(2)}_{\mathbf{k}\mathbf{k}'}(-\omega)]+\frac{\gamma_{\mathbf{k}}}{\varepsilon_{\mathbf{k}}}\frac{\gamma_{\mathbf{k}'}}{\varepsilon_{\mathbf{k}'}}\chi^{(3)}_{\mathbf{k}\mathbf{k}'}(\omega)\right] , \tag{3.1}$$

where

$$g(\mathbf{E}_{\rm inc},\mathbf{E}_{\rm sc})=(E^x_{\rm inc}E^x_{\rm sc}-E^y_{\rm inc}E^y_{\rm sc})^2 , \tag{3.2}$$

$$\chi^{(1)}_{\mathbf{k}\mathbf{k}'}(\omega)=[\Pi^{(1)}_{\mathbf{k}\mathbf{k}'}(\omega)+\Pi^{(2)}_{\mathbf{k}\mathbf{k}'}(\omega)+\Pi^{(3)}_{\mathbf{k}\mathbf{k}'}(\omega)+\Pi^{(3)}_{\mathbf{k}'\mathbf{k}}(-\omega)] , \tag{3.3}$$

$$\chi^{(2)}_{\mathbf{k}\mathbf{k}'}(\omega)=[\Pi^{(4)}_{\mathbf{k}\mathbf{k}'}(\omega)+\Pi^{(5)}_{\mathbf{k}\mathbf{k}'}(\omega)+\Pi^{(6)}_{\mathbf{k}'\mathbf{k}}(-\omega)+\Pi^{(7)}_{\mathbf{k}'\mathbf{k}}(-\omega)] , \tag{3.4}$$

$$\chi^{(3)}_{\mathbf{k}\mathbf{k}'}(\omega)=[\Pi^{(8)}_{\mathbf{k}\mathbf{k}'}+\Pi^{(9)}_{\mathbf{k}\mathbf{k}'}(\omega)+\Pi^{(10)}_{\mathbf{k}\mathbf{k}'}(\omega)+\Pi^{(8)}_{\mathbf{k}'\mathbf{k}}(-\omega)] , \tag{3.5}$$

and $\Pi^{(i)}_{\mathbf{k}\mathbf{k}'}(\omega)$, $i=1,2,\ldots,10$, are the Fourier transforms of the following ten two-particle Green's functions:

$$\Pi^{(1)}_{\mathbf{k}\mathbf{k}'}(t-t')=-i\langle\psi_0|\mathcal{T}\alpha_{\mathbf{k}}(t)\beta_{\mathbf{k}}(t)\alpha_{\mathbf{k}'}(t')\beta_{\mathbf{k}'}(t')|\psi_0\rangle , \tag{3.6a}$$

$$\Pi^{(2)}_{\mathbf{k}\mathbf{k}'}(t-t')=-i\langle\psi_0|\mathcal{T}\alpha^{\dagger}_{\mathbf{k}}(t)\beta^{\dagger}_{\mathbf{k}}(t)\alpha^{\dagger}_{\mathbf{k}'}(t')\beta^{\dagger}_{\mathbf{k}'}(t')|\psi_0\rangle , \tag{3.6b}$$

$$\Pi^{(3)}_{\mathbf{k}\mathbf{k}'}(t-t')=-i\langle\psi_0|\mathcal{T}\alpha_{\mathbf{k}}(t)\beta_{\mathbf{k}}(t)\alpha^{\dagger}_{\mathbf{k}'}(t')\beta^{\dagger}_{\mathbf{k}'}(t')|\psi_0\rangle , \tag{3.6c}$$

$$\Pi^{(4)}_{\mathbf{k}\mathbf{k}'}(t-t')=-i\langle\psi_0|\mathcal{T}\alpha_{\mathbf{k}}(t)\beta_{\mathbf{k}}(t)\alpha^{\dagger}_{\mathbf{k}'}(t')\alpha_{\mathbf{k}'}(t')|\psi_0\rangle , \tag{3.6d}$$

$$\Pi^{(5)}_{\mathbf{k}\mathbf{k}'}(t-t') = -i\langle\psi_0|\mathcal{T}\alpha_{\mathbf{k}}(t)\beta_{\mathbf{k}}(t)\beta^{\dagger}_{\mathbf{k}'}(t')\beta_{\mathbf{k}'}(t')|\psi_0\rangle \ , \quad (3.6e)$$

$$\Pi^{(6)}_{\mathbf{k}\mathbf{k}'}(t-t') = -i\langle\psi_0|\mathcal{T}\alpha^{\dagger}_{\mathbf{k}}(t)\alpha_{\mathbf{k}}(t)\alpha^{\dagger}_{\mathbf{k}'}(t')\beta^{\dagger}_{\mathbf{k}'}(t')|\psi_0\rangle \ , \quad (3.6f)$$

$$\Pi^{(7)}_{\mathbf{k}\mathbf{k}'}(t-t') = -i\langle\psi_0|\mathcal{T}\beta^{\dagger}_{\mathbf{k}}(t)\beta_{\mathbf{k}}(t)\alpha^{\dagger}_{\mathbf{k}'}(t')\beta^{\dagger}_{\mathbf{k}'}(t')|\psi_0\rangle \ , \quad (3.6g)$$

$$\Pi^{(8)}_{\mathbf{k}\mathbf{k}'}(t-t') = -i\langle\psi_0|\mathcal{T}\alpha^{\dagger}_{\mathbf{k}}(t)\alpha_{\mathbf{k}}(t)\beta^{\dagger}_{\mathbf{k}'}(t')\beta_{\mathbf{k}'}(t')|\psi_0\rangle \ , \quad (3.6h)$$

$$\Pi^{(9)}_{\mathbf{k}\mathbf{k}'}(t-t') = -i\langle\psi_0|\mathcal{T}\alpha^{\dagger}_{\mathbf{k}}(t)\alpha_{\mathbf{k}}(t)\alpha^{\dagger}_{\mathbf{k}'}(t')\alpha_{\mathbf{k}'}(t')|\psi_0\rangle \ , \quad (3.6i)$$

$$\Pi^{(10)}_{\mathbf{k}\mathbf{k}'}(t-t') = -i\langle\psi_0|\mathcal{T}\beta^{\dagger}_{\mathbf{k}}(t)\beta_{\mathbf{k}}(t)\beta^{\dagger}_{\mathbf{k}'}(t')\beta_{\mathbf{k}'}(t')|\psi_0\rangle \ . \quad (3.6j)$$

In principle, we should now compute all of these ten correlation functions. However, Davis *et al.* argued that, in order to compute $G_{\Lambda_0}(\omega)$, we just need to compute $\chi^{(1)}_{\mathbf{k}\mathbf{k}'}(\omega)$ and we can ignore $\chi^{(2)}_{\mathbf{k}\mathbf{k}'}(\omega)$ and $\chi^{(3)}_{\mathbf{k}\mathbf{k}'}(\omega)$. Furthermore, only $\Pi^{(3)}_{\mathbf{k}\mathbf{k}'}(\omega)$ is relevant in the computation of $\chi^{(1)}_{\mathbf{k}\mathbf{k}'}(\omega)$. Two arguments support these approximations. First, we know, from simple phase-space considerations, that the two-magnon scattering is dominated by zone boundary magnons, where $|\gamma_{\mathbf{k}}/\varepsilon_{\mathbf{k}}|\approx 0$. This allows us to say that $\chi^{(2)}_{\mathbf{k}\mathbf{k}'}(\omega)$ and $\chi^{(3)}_{\mathbf{k}\mathbf{k}'}(\omega)$ should be negligible with respect to $\chi^{(1)}_{\mathbf{k}\mathbf{k}'}(\omega)$. Second, $\Pi^{(3)}_{\mathbf{k}\mathbf{k}'}(\omega)$ is the only correlation function, among the ten, which has a nonzero contribution in the noninteracting case. All the others vanish when the spin-wave interactions coming from the Hamiltonian are turned off. Davis *et al.* claimed that higher-order corrections of these Green's functions can be also ignored for the same reasons. However, in their analysis, they were considering only three vertices of the Hamiltonian, namely, $V^{(1)}$, $V^{(4)}$, $V^{(9)}$, neglecting all the others. Here we want to keep all of them. Therefore, we will first restrict ourselves to $\Pi^{(3)}_{\mathbf{k}\mathbf{k}'}(\omega)$, which is the only one that can be easily interpreted as a two-magnon Green's function and which, indeed, gives rise to the dominant two-magnon peak. But we shall go back to $\Pi^{(1)}$, $\Pi^{(2)}$, etc., in Sec. III A 3 and discuss the importance of their first nonvanishing terms.

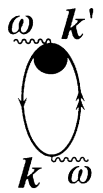

FIG. 2. Diagrammatic representation of $\Pi^{(3)}_{\mathbf{k}\mathbf{k}'}(\omega)$. The solid lines are the α and β propagators, while the solid circle represent the vertex function, $\Gamma_{\mathbf{k}\mathbf{k}'}(\omega,\omega')$.

1. *Bethe-Salpeter equation for* $\Pi^{(3)}_{\mathbf{k}\mathbf{k}'}(\omega)$

Let us focus our attention on $\Pi^{(3)}_{\mathbf{k}\mathbf{k}'}(\omega)$. We can easily write down[27] a general expression for it in terms of the full α and β propagators $G_{\alpha\alpha}(\mathbf{k},\omega)$, $G_{\beta\beta}(\mathbf{k},\omega)$, and a vertex function $\Gamma_{\mathbf{k}\mathbf{k}'}(\omega,\omega')$. The diagrammatic representation is given in Fig. 2 and explicitly is

$$\Pi^{(3)}_{\mathbf{k}\mathbf{k}'}(\omega) = i\int \frac{d\omega'}{2\pi} G_{\alpha\alpha}(\mathbf{k},\omega+\omega')G_{\beta\beta}(\mathbf{k},\omega')\Gamma_{\mathbf{k}\mathbf{k}'}(\omega,\omega') \ . \quad (3.7)$$

The vertex function satisfies the following Bethe-Salpeter equation:

$$\Gamma_{\mathbf{k}\mathbf{k}'}(\omega,\omega') = \delta_{\mathbf{k}\mathbf{k}'} + \frac{Jz}{4N}\left(-\frac{i}{\hbar}\right)\sum_{k_1}\int\frac{d\omega_1}{2\pi}\mathcal{V}^{\alpha\beta}_{\mathbf{k}\mathbf{k}_1\mathbf{k}_1\mathbf{k}}(\omega',\omega_1)G_{\alpha\alpha}(\mathbf{k}_1,\omega+\omega_1)G_{\beta\beta}(\mathbf{k}_1,\omega_1)\Gamma_{\mathbf{k}\mathbf{k}'}(\omega,\omega_1) \ . \quad (3.8)$$

Here $\mathcal{V}^{\alpha\beta}_{\mathbf{k}\mathbf{k}_1\mathbf{k}_1\mathbf{k}}(\omega',\omega_1)$ is the sum of all the irreducible interaction parts. Equation (3.8) is represented in Fig. 3, while in Fig. 4 we show the only first-order contribution to $\mathcal{V}^{\alpha\beta}_{\mathbf{k}\mathbf{k}_1\mathbf{k}_1\mathbf{k}}$ and the several second-order terms.

In order to solve these coupled equations, it is much more convenient to directly compute $G_{\Lambda_0}(\omega)$ rather than $\Pi^{(3)}_{\mathbf{k}\mathbf{k}'}(\omega)$. We have

$$G_{\Lambda_0}(\omega)\approx G^{+}_{\Lambda_0}(\omega)+G^{+}_{\Lambda_0}(-\omega) \ , \quad (3.9)$$

where

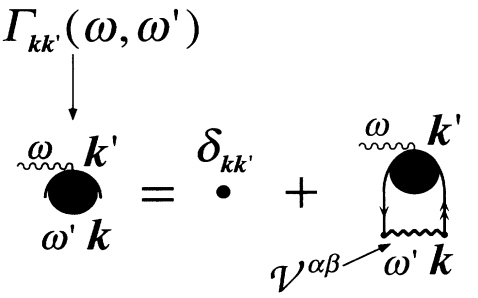

FIG. 3. Bethe-Salpeter equation for $\Gamma_{\mathbf{k}\mathbf{k}'}(\omega,\omega')$.

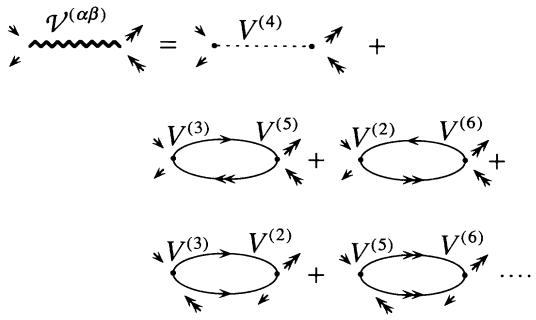

FIG. 4. First contributions to $\mathcal{V}^{\alpha\beta}_{\mathbf{k}\mathbf{k}_1\mathbf{k}_1\mathbf{k}}$.

$$G^{+}_{\Lambda_0}(\omega)=N(B/2)^2 g(\mathbf{E}_{\rm inc},\mathbf{E}_{\rm sc})[zS\alpha(S)]^2 \times\frac{1}{N}\sum_{\mathbf{k},\mathbf{k}'}\frac{\tilde{\gamma}_{\mathbf{k}}}{\varepsilon_{\mathbf{k}}}\frac{\tilde{\gamma}_{\mathbf{k}'}}{\varepsilon_{\mathbf{k}'}}\Pi^{(3)}_{\mathbf{k}\mathbf{k}'}(\omega)\ . \tag{3.10}$$

Using Eq. (3.7) we can write

$$G^{+}_{\Lambda_0}(\omega)=N(B/2)^2 g(\mathbf{E}_{\rm inc},\mathbf{E}_{\rm sc})z[S\alpha(S)]^2\frac{i}{N} \times\int\frac{d\omega'}{2\pi}\sum_{\mathbf{k}}\frac{f_{\mathbf{k}}}{\varepsilon_{\mathbf{k}}}G_{\alpha\alpha}(\mathbf{k},\omega+\omega') \times G_{\beta\beta}(\mathbf{k},\omega')\Gamma_{\mathbf{k}}(\omega,\omega')\ , \tag{3.11}$$

where $f_{\mathbf{k}}\equiv(z/2)\tilde{\gamma}_{\mathbf{k}}=2\tilde{\gamma}_{\mathbf{k}}$, and we have introduced a vertex function $\Gamma_{\mathbf{k}}(\omega,\omega')$:

$$\Gamma_{\mathbf{k}}(\omega,\omega')=\sum_{\mathbf{k}'}\frac{f_{\mathbf{k}'}}{\varepsilon_{\mathbf{k}'}}\Gamma_{\mathbf{k}\mathbf{k}'}(\omega,\omega')\ . \tag{3.12}$$

$\Gamma_{\mathbf{k}}(\omega,\omega')$ satisfies the equation

$$\Gamma_{\mathbf{k}}(\omega,\omega')=\frac{f_{\mathbf{k}}}{\varepsilon_{\mathbf{k}}}+\frac{Jz}{4N}\left[\frac{-i}{\hbar}\right] \times\sum_{\mathbf{k}_1}\int\frac{d\omega_1}{2\pi}\mathcal{V}^{\alpha\beta}_{\mathbf{k}\mathbf{k}_1\mathbf{k}_1\mathbf{k}}(\omega',\omega_1) \times G_{\alpha\alpha}(\mathbf{k}_1,\omega+\omega_1) \times G_{\beta\beta}(\mathbf{k},\omega_1)\Gamma_{\mathbf{k}_1}(\omega,\omega_1)\ . \tag{3.13}$$

2. *Ladder approximation*

In order to get a solution of the two coupled equations, Eqs. (3.11) and (3.13), we need to make a consistent (conserving) approximation to the magnon propagators and to the irreducible interaction function $\mathcal{V}^{\alpha\beta}_{\mathbf{k}\mathbf{k}_1\mathbf{k}_1\mathbf{k}}$. The lowest approximation is, of course, to neglect the interactions all together: in this case we just have two noninteracting magnons effectively excited by light. Replacing $G_{\alpha\alpha}$ and $G_{\beta\beta}$ by $G^{(0)}_{\alpha\alpha}$ and $G^{(0)}_{\beta\beta}$ and $\Gamma_{\mathbf{k}}$ by $f_{\mathbf{k}}/\varepsilon_{\mathbf{k}}$, we easily get

$$G^{+}_{\Lambda_0}(\omega)=N(B/2)^2 g(\mathbf{E}_{\rm inc},\mathbf{E}_{\rm sc})z[S\alpha(S)]^2 L^{(2)}(\omega)\ , \tag{3.14}$$

where

$$L^{(m)}(\omega)=\frac{i}{N}\int\frac{d\omega'}{2\pi}\sum_{\mathbf{k}}\frac{f^2_{\mathbf{k}}}{(\varepsilon_{\mathbf{k}})^m}G^{(0)}_{\alpha\alpha}(\mathbf{k},\omega+\omega')G^{(0)}_{\beta\beta}(\mathbf{k},\omega') =\frac{1}{N\Omega_{\max}}\sum_{\mathbf{k}}\frac{f^2_{\mathbf{k}}}{(\varepsilon_k)^m}\frac{1}{\tilde{\omega}-2\varepsilon_{\mathbf{k}}+i\eta}\ , \tag{3.15}$$

and we have introduced the dimensionless frequency

$$\tilde{\omega}=\omega/\Omega_{\max}\ . \tag{3.16}$$

It will be also convenient to introduce

$$l^{(m)}(\tilde{\omega})=\Omega_{\max}L^{(m)}(\omega)=\sum_{\mathbf{k}}\frac{f^2_{\mathbf{k}}}{(\varepsilon_{\mathbf{k}})^m}\frac{1}{\tilde{\omega}-2\varepsilon_{\mathbf{k}}+i\eta}\ . \tag{3.17}$$

The scattering intensity for the Stoke's case ($\mathcal{E}>0$) is therefore

$$I_{\Lambda_0}(\mathcal{E})=-\frac{2}{\hbar}\mathrm{Im}[\tilde{G}_{\Lambda_0}(\omega=\mathcal{E}/\hbar)] =\frac{2\pi}{\hbar}N(B/2)^2 g(\mathbf{E}_{\rm inc},\mathbf{E}_{\rm sc})(1/\Omega_{\max})[zS\alpha(S)]^2 \times\sum_{\mathbf{k}}\frac{\tilde{\gamma}^2_{\mathbf{k}}}{\varepsilon^2_{\mathbf{k}}}\delta(\tilde{\omega}-2\varepsilon_{\mathbf{k}})\ . \tag{3.18}$$

Apart from the symmetrization of the B_{1g} mode, $\tilde{\gamma}^2_{\mathbf{k}}/\varepsilon^2_{\mathbf{k}}$, Eq. (3.18) is nothing but the joint density of states of two noninteracting magnons with momentum $\mathbf{k}$ and $-\mathbf{k}$ and energy ε_k in units of $JzS\alpha(S)$. The curve has a cutoff at the maximum energy that a two-magnon state can have, namely, $2JzS\alpha(S)$, where, in fact, there is a Van Hove singularity, (see Fig. 6, dotted lines). This singularity in the Raman spectrum is, of course, unphysical and it is due to the neglect of all possible magnon interactions. In fact, the interaction cannot be neglected since the two magnons are created close to each other in real space.[26]

Therefore, the next step is to introduce magnon interactions at the lowest order, by approximating $\mathcal{V}^{\alpha\beta}$ by its first-order irreducible interaction part and, consistently, to correct the magnon propagators by the first-order self-energy. For the vertex part, we simply have

$$\mathcal{V}^{\alpha\beta}_{\mathbf{k}\mathbf{k}_1\mathbf{k}_1\mathbf{k}}(\omega',\omega_1)=V^{(4)}_{\mathbf{k}\mathbf{k}_1\mathbf{k}_1\mathbf{k}}\ . \tag{3.19}$$

As far as the correction to the propagators is concerned, we show in Appendix D that the first-order magnon self-energy vanishes at $T=0$. Therefore, again we can use the bare expressions $G^{(0)}_{\alpha\alpha}$ and $G^{(0)}_{\beta\beta}$ in Eq. (3.11). Equations (3.11) and (3.13) are now rewritten in the form

$$G^{+}_{\Lambda_0}(\omega)=N(B/2)^2 g(\mathbf{E}_{\rm inc},\mathbf{E}_{\rm sc})z[S\alpha(S)]^2\frac{i}{N}\int\frac{d\omega'}{2\pi}\sum_{\mathbf{k}}\frac{f_{\mathbf{k}}}{\varepsilon_{\mathbf{k}}} \times G^{(0)}_{\alpha\alpha}(\mathbf{k},\omega+\omega')G^{(0)}_{\beta\beta}(\mathbf{k},\omega')\Gamma_{\mathbf{k}}(\omega,\omega')\ , \tag{3.20}$$

$$\Gamma_{\mathbf{k}}(\omega,\omega')=\frac{f_{\mathbf{k}}}{\varepsilon_{\mathbf{k}}}+\frac{Jz}{4N}\left[\frac{-i}{\hbar}\right]\times\sum_{\mathbf{k}_1}\int\frac{d\omega_1}{2\pi}V^{(4)}_{\mathbf{k}\mathbf{k}_1\mathbf{k}_1\mathbf{k}}\times G^{(0)}_{\alpha\alpha}(\mathbf{k}_1,\omega+\omega_1)\times G^{(0)}_{\beta\beta}(\mathbf{k},\omega_1)\Gamma_{\mathbf{k}_1}(\omega,\omega_1)\ . \quad (3.21)$$

$\Gamma_{\mathbf{k}_1}(\omega,\omega')$ now satisfies a ladder-approximation Bethe-Salpeter equation. It is easy to see that, in this approximation, $\Pi^{(3)}_{\mathbf{k}\mathbf{k}'}$ is given by an infinite sum of bubbles with ladder interactions (see Fig. 5), representing the fact that the magnon pair undergoes repeated scattering. This is very similar to the situation that we encounter in the RPA of more familiar problems, the main difference being that, due to the nonlocality of $V^{(4)}_{\mathbf{k}\mathbf{k}_1\mathbf{k}_1,\mathbf{k}}$, the sum of the bubbles is not a straightforward geometric series. Nevertheless, an exact solution for $G^{+}_{\Lambda_0}(\omega)$ can still be obtained, and the result is[27]

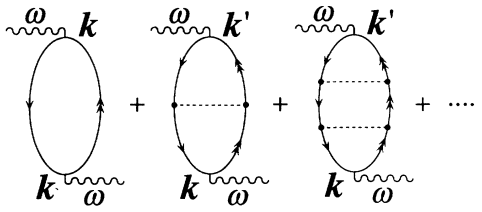

FIG. 5. Two-magnon scattering (ladder) diagrams contributing to $\Pi^{(3)}$.

$$G^{+}_{\Lambda_0}(\omega)=N(B/2)^2 g(\mathbf{E}_{\rm inc},\mathbf{E}_{\rm sc})z[S\alpha(S)]^2\left[\frac{L^{(2)}-\frac{1}{2}(J/\hbar)(L^{(1)}L^{(1)}-L^{(0)}L^{(2)})}{1+\frac{1}{2}(J/\hbar)(L^{(0)}+L^{(2)})-\frac{1}{4}(J/\hbar)^2(L^{(1)}L^{(1)}-L^{(0)}L^{(2)})}\right], \quad (3.22)$$

or, in terms of the dimensionless $l^{(m)}$

$$G^{+}_{\Lambda_0}(\omega)=N(B/2)^2 g(\mathbf{E}_{\rm inc},\mathbf{E}_{\rm sc})z[S\alpha(S)]^2(1/\Omega_{\max})\left[\frac{l^{(2)}-[1/2zS\alpha(S)](l^{(1)}l^{(1)}-l^{(0)}l^{(2)})}{1+[1/2zS\alpha(S)](l^{(0)}+l^{(2)})-[1/2zS\alpha(S)]^2(l^{(1)}l^{(1)}-l^{(0)}l^{(2)})}\right]. \quad (3.23)$$

The derivation of Eq. (3.22) is given in Appendix C.

The line shape obtained from the imaginary part of $G^{+}_{\Lambda_0}(\omega)$ given in Eq. (3.23) is shown in Fig. 6(a) for $S=\frac{1}{2}$, and in Fig. 6(b) for $S=1$, respectively. We will refer to it as the two-magnon spin-wave (SW) line shape. We can see that this line shape still has a cutoff at $\mathcal{E}=2\mathcal{E}_{\max}=2[JzS\alpha(S)]$ because this is the maximum possible energy that a pair of on-shell (undamped) magnons can have. The unphysical singularity has disappeared and the curve peaks at

$$\mathcal{E}_{\rm peak}=1.46\mathcal{E}_{\max}=3.38J \quad \text{for } S=\tfrac{1}{2}\ , \quad (3.24)$$

$$\mathcal{E}_{\rm peak}=1.71\mathcal{E}_{\max}=7.38J \quad \text{for } S=1\ . \quad (3.25)$$

Notice that, if Oguchi's corrections are disregarded—this means that the dispersion is $JzS\epsilon_{\mathbf{k}}$—, the curve peaks at

$$\mathcal{E}_{\rm peak}=1.38(zSJ)=2.76J \quad \text{for } S=\tfrac{1}{2}\ , \quad (3.26)$$

$$\mathcal{E}_{\rm peak}=1.69(zSJ)=6.76J \quad \text{for } S=1\ . \quad (3.27)$$

We would like to emphasize that the Oguchi corrections change, though slightly, the line shape and not simply the overall energy scale. This comes about because apart from renormalizing the energy scale, the factor $\alpha(S)$ appears in a nontrivial way in Eq. (3.23). The importance of this correction turns out to be more relevant for $S=\frac{1}{2}$ than for $S=1$. This point is often overlooked in the literature.

It is interesting, at this point, to compare the two-magnon SW scattering line shape derived here, with the analogous expression originally derived by Parkinson,[2] which we will call two-magnon Néel line shape (see below). Equation (3.23) is formally different from Parkinson's expression. In Parkinson's derivation, the ground state of the unperturbed system is taken to be the naive Néel state and the magnon dispersion is the linear-spin-wave expression without the Oguchi correction. In the formalism presented here, the unperturbed ground state is the spin-wave ground state which contains quantum fluctuations. A comparison of the line shape obtained from the Parkinson formalism with the line shape of Fig. 6 shows that, in the latter case, the two-magnon peak is shifted towards higher frequencies, mainly because of the Oguchi correction. If we insert the Oguchi correction *by hand* in Parkinson's expression and we rescale the energy scale by the same factor as well, then the line shape becomes almost undistinguishable from the one shown in Fig. 6: they differ only a little for small frequencies.[27] However, in contrast with the formalism presented in this paper, the method used by Parkinson cannot be easily improved in order to take into account corrections to the two-magnon scattering coming from higher-order terms of the Heisenberg Hamiltonian and the Raman-scattering operator.

Since the two-magnon density of states is so sharply peaked near the zone edge, one can easily see that

$L^{(0)} \approx L^{(1)} \approx L^{(2)}$ because the factor $1/(\varepsilon_k^m)$ in the definition of $L^{(m)}$ is approximately equal to one. With this approximation, Eq. (3.22) simplifies considerably and assumes the following, more standard, RPA form:

$$G^{+}_{\Lambda_0}(\omega) = N(B/2)^2 g(\mathbf{E}_{\rm inc}, \mathbf{E}_{\rm sc}) z [S\alpha(S)]^2 \times \left[\frac{L^{(0)}}{1 + (J/h)(L^{(0)})} \right] . \tag{3.28}$$

We have checked that the line shape does not change very much if we make this approximation. Notice also that Eq. (3.28) can be obtained directly from the sum of the ladder bubbles for $\Pi^{(3)}_{\mathbf{k},\mathbf{k}'}$ since, if we make the approximation $1/(\varepsilon_k^m) \approx 1$, then this sum reduces to a simple geometric series (see Appendix E).

If we expand Eq. (3.23) in powers of S, we can see that, apart from the overall energy-scale factor $1/\Omega_{\rm max}$, the dominant term is of $O(S^2)$ and comes from the "bare bubble," representing the two-noninteracting-magnon case. As we will see, this is going to be important when we compare the relative intensity of the two-magnon contribution with the four-magnon contributions and it will bring about the main difference between the $S=\frac{1}{2}$ case and the $S=1$ case.

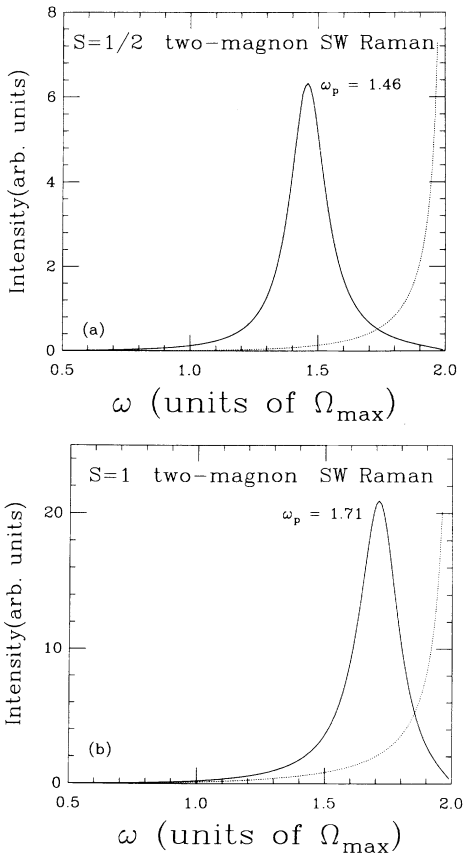

FIG. 6. Line shape of the two-magnon SW Raman scattering. The two magnons are on-shell and their lifetime is infinite (no damping), although they can repeatedly interact with each other. Solid lines represent the interacting case, Eq. (3.23); dotted lines, the noninteracting case, Eq. (3.18). (a) $S=\frac{1}{2}$. (b) $S=1$.

At the end of this section we want to compute the first three frequency moments and cumulants of the Raman intensity. We introduce some notation that will also be useful later on.

The nth moment of the spectrum is defined as

$$\rho_n = \frac{1}{I_T} \int d\omega\, \omega^n I(\omega) , \tag{3.29}$$

where

$$I_T = \int d\omega\, I(\omega) . \tag{3.30}$$

It is convenient to also define the cumulants[7]

$$M_1 = \rho_1 , \tag{3.31}$$

$$(M_n)^n = \frac{1}{I_T} \int d\omega (\omega - \rho_1)^n I(\omega) , \quad n > 1 . \tag{3.32}$$

The first cumulant, M_1, gives the mean position of the scattered intensity, while the second and third cumulants M_2 and M_3 measure the width and the asymmetry of the line shape. These cumulants provide a parameter-free test of the theory: the predicted ratio M_2/M_1 relates the spin-pair linewidth to the central frequency, and it is independent of J. Similarly, the ratio M_3/M_1 is an estimate of the skewness of the line shape and gives a bound on the high-energy tail of the spectrum.

In the first column of Table I we show the first three cumulants of the two-magnon SW line shape for $S=\frac{1}{2}$. (These values can be compared with the results obtained from Parkinson's two-magnon Néel theory[28]). If we compare these results with the series-expansion results[7] and the results obtained from experiments on the undoped (insulting) phase of La_2CuO_4 (Refs. 4 and 7) (see columns 3 and 5 of Table I), we can see that, while the first two-magnon SW cumulant is not far from the series-expansion estimate and yields a reasonable value of the exchange constant J, the second and third two-magnon SW cumulants are in disagreement both with the experiments and the series expansion. In particular, the ratio of the second to the first cumulant, as derived in the two-magnon SW calculation, is smaller by a factor of 2. Indeed, a direct comparison of the two-magnon SW spectrum [see Fig. 6(a)] with the experimental line shape[19] reveals that the latter is much broader than the former and has a very long tail at high frequencies, far beyond the maximum energy that a magnon pair can have. It has been claimed[7] that this anomalously broad spectrum is an intrinsic characteristic of the $S=\frac{1}{2}$ systems.

For $S=1$, the two-magnon SW line shape shown in Fig. 6(b) is in excellent agreement with the line shape obtained in experiments on K_2NiF_4.[3] In Table II we show the moments for the $S=1$ case as computed from the two-magnon SW theory and from series-expansion techniques.[14] We see that, in this case, the agreement between the two is much better, even though the two-magnon SW value for M_2/M_1 is 30% smaller than the series-expansion result.[14] We will try to explain this different behavior of $S=\frac{1}{2}$ and $S=1$ in the next sections, within the same spin-wave formalism.

TABLE I. First three frequency cumulants from different formalisms: $S=\frac{1}{2}$ case.

	Two-magnon SW	Two-magnon–four-magnon	Series expansion Ref. 7	Exact diagonalization Refs. 9 and 10	Experiment[a] Refs. 4 and 7
M_1/J	3.37	3.51	3.58±0.06	3.24	3700
M_2/J	0.363	0.922	0.81±0.05	0.797	1050
M_3/J	−0.337	1.498	1.00±0.14	1.14	1000
M_2/M_1	0.108	0.263	0.23±0.02	0.245	0.27±0.03
M_3/M_1	−0.100	0.427	0.27	0.352	0.27

[a]The experimental values for M_1, M_2, M_3 are in units of cm^{-1}.

2. *Second-order self-energy and/or vertex insertions Indirect four-magnon production*

The two-magnon scattering intensity obtained in Sec. III A 2 is rigorously zero above $\tilde{\omega}=2$ because the Green's functions contain no imaginary part above this energy. As previously stated, experimental observations show—particularly for the two-dimensional $S=\frac{1}{2}$ HAFM, such as the undoped insulating La_2CuO_4—a nonzero intensity above this energy. It is possible to imagine that this broadening of the line shape towards higher frequencies is, at least partly, the effect of some sort of damping mechanism of the one-magnon states, due to two-magnon scattering. We want to concentrate on this here and we shall discuss the other possible source of intensity above the $\tilde{\omega}=2$ cutoff, namely, the direct production by light of more than two particles, in the next section. The possibility of any sort of damping has been already excluded at the level of first-order perturbation theory, where we saw that the magnon self-energy $\Sigma^{(1)}_{\alpha\alpha}(\mathbf{k},\omega)$ is identically zero at $T=0$ (see Appendix D). Furthermore, as discussed in the same appendix, we know that, at $T=0$, the magnon spectrum has a negative curvature for all $\mathbf{k}$ and therefore magnons cannot decay spontaneously: the imaginary part of the self-energy vanishes at any order in perturbation theory when ω is on shell; that is, the on-shell magnon lifetime is infinite at $T=0$.[22,29,23] It is therefore unjustified to use a phenomenological damping parameter in the Green's function of the single magnon to explain the anomalously broad Raman width for $S=\frac{1}{2}$. What we should consider, instead, is a possible *off-shell* decay which could provide a nonzero intensity to the single magnon spectral density away from the spin-wave peak and, consequently, a long tail to the two-magnon Raman scattering in the high-energy ($\tilde{\omega}>2$) region. Therefore, we must go back to the two general equations of the theory, Eqs. (3.11) and (3.13), and insert in there the expressions for the magnon propagators and for the irreducible vertex function $\mathcal{V}^{\alpha\beta}$ corrected by second-order (in V_{DM}) processes.

First of all, the magnon propagators should be dressed with the second-order self-energy diagrams. A detailed analysis of the second-order magnon self-energy is carried out in Appendix D. There we show that the second-order *on-shell* self-energy vanishes linearly as $\mathbf{k}\to 0$, as it must be because of the rotational invariance of the Heisenberg model. We also compute numerically both the real and the imaginary part of $\Sigma^{(2)}_{\alpha\alpha}(\mathbf{k},\omega)$, as a function of ω, for several values of $\mathbf{k}$. We show that, for $S=\frac{1}{2}$, the second-order self-energy increases for first-order magnon dispersion $\Omega_{\mathbf{k}}$ only by 1.5–3%. As a result, the renormalization constant of spin-wave velocity, Z_c, to second order in $(1/S)$, turns out to be 1.177 for $S=\frac{1}{2}$, very close to the series expansion result 1.18±0.02, obtained by Singh.[24] Recently the $1/S^2$ correction to the self-energy has been calculated within the Holstein-Primakoff formalism.[30] In contrast with our results, the HP second-order self-energy is negative, lowering the spin-wave energy. For $\mathbf{k}$ vectors close to the zone center, the second-order correction to the first-order result is rather small, approximately 2%. On the other hand, the second-order result deviates appreciably from the first-order result near the zone boundary, where the magnon dispersion is decreased by approximately 15%.

Since the self-energy $\Sigma(\mathbf{k},\omega)$, as a function of $\mathbf{k}$, still has the point-group symmetry of the square (sub) lattice, the derivation of Eq. (3.22) still goes through unchanged when we dress the propagator if we use $\mathcal{V}^{\alpha\beta}=V^{(4)}$ (i.e.,

TABLE II. First three frequency cumulants from different formalisms: $S=1$ case.

	Two-magnon Néel[a] Ref. 2	Two-magnon SW	Two-magnon–four-magnon	Series expansion Ref. 14
M_1/J	6.64	7.18	7.25	7.22±0.02
M_2/J	0.59	0.72	1.06	
M_3/J	−0.69	−0.90	1.62	
M_2/M_1	0.09	0.10	0.146	0.12±0.03
M_3/M_1	−0.10	−0.13	0.22	

[a]In the derivation given by Parkinson, the ground state is the Néel state.

the ladder approximation); the only difference is that now, in the definition of $L^{(m)}(\omega)$ given in Eq. (3.15), $G^{(0)}_{\alpha\alpha}$ is replaced by $G^{(2)}_{\alpha\alpha}$. Apart from some technical difficulties, this can be done with enough hard work. However, in order to be truly consistent, we should modify the vertex interaction $\mathcal{V}^{\alpha\beta}$ as well.

Typical second-order vertex corrections to $\Pi^{(3)}_{\mathbf{k}\mathbf{k}'}$, from which we can extract a second-order correction to $\nu^{\alpha\beta}$, are shown in Fig. 23 of Appendix E, diagrams $\mathcal{E}_5$–$\mathcal{E}_8$. These diagrams can be roughly thought of as polarization processes which modify the interaction between the two "main" Raman magnons α and β. Of course, with these corrections taken into account, it is not possible any more to obtain an exact solution for $G^{+}_{\Lambda_0}(\omega)$. Therefore, we first carried out the following, less ambitious task: instead of dressing the bare magnon propagator and correct the vertex function $\mathcal{V}^{\alpha\beta}$, we simply summed up all the second-order diagrams contributing to $\Pi^{(3)}_{\mathbf{k}\mathbf{k}'}$. These diagrams with their analytical expressions can be found in Appendix E, Fig. 23. In order to be consistent, we also considered similar diagrams contributing to the other nine correlation functions, $\Pi^{(1)}_{\mathbf{k}\mathbf{k}'}$, $\Pi^{(2)}_{\mathbf{k}\mathbf{k}'}$, $\Pi^{(4)}_{\mathbf{k}\mathbf{k}'}$, etc. This procedure can be justified remembering that these diagrams, which are of order $O(1/S^0)$, are going to be the leading-order terms in a $1/S$ expansion of the results obtained when self-energy and vertex corrections are properly inserted in Eqs. (3.11) and (3.13). In particular, these diagrams should give the main contribution to the spectrum in the four-magnon region from off-shell decay. We will come back to this point later and we will see that, in fact, this is what happens. The computation of the imaginary part of these diagrams is still quite problematic in the energy region $\tilde{\omega}<2$, when the diagram is "cut" at the level of a two-magnon state. The problem here is not so much the Van Hove singularity at $\tilde{\omega}=2$ that we have already encountered—this can be fixed by adding ladders to the diagrams—but it is rather the fact that the mathematical expressions are not well defined due to the existence of on-shell intermediate states. This is the case, in particular, for the self-energy diagrams $\mathcal{E}_1$–$\mathcal{E}_4$, where the square of the same energy denominator occurs. Let us consider, for now, the case in which the imaginary part is taken only at the level of the four-magnon states, so that the two-magnon energy denominators are real numbers, positive for $\tilde{\omega}>2$. Notice that, in this case, the fact that the four magnons do not interact does not cause any singularity because of the large phase space available [see Fig. 12(a), showing the four-magnon density of states]. When we take the imaginary part of these diagrams at the level of the four-magnon states, we end up with the following kind of *eight-dimensional* integral:

$$\sum_{(1234)} \left[\delta_{\mathbf{G}}(1+2-3-4)\delta(\tilde{\omega}-\varepsilon_1-\varepsilon_2-\varepsilon_3-\varepsilon_4) \left[\frac{1}{\tilde{\omega}-2\varepsilon_1} \right]^2 V^{(2)}_{(1234)} V^{(3)}_{(3421)} \right] . \tag{3.33}$$

Since this is the first one of numerous multidimensional integrals that we shall encounter in this paper, we want to comment here on some of its characteristics and the numerical techniques that we have used to compute it. First of all, the momentum conservation δ function is used to reduce the eight-dimensional integral to a six-dimensional integral, with the umklapp procedure that we discuss in Appendix B. As was shown by Kopietz,[23] the product of the two Dyson-Maleev vertices, that enter in all these integrals, is a well-behaved function of the momenta. Therefore, the integrand is a regular function of the momentum variables. Secondly, the frequency δ function is implemented when we integrate over one the remaining three two-dimensional variables, say $\mathbf{k}_3$, while we keep the other two, $\mathbf{k}_1$ and $\mathbf{k}_2$, fixed. This is done by dividing the HAFM Brilloiun zone in triangles and linearizing the integrand inside each triangle. The contribution to the spectral density from each triangle is then trivially computed with a spline technique. The remaining four-dimensional integral is done very simply by summing a discrete number of points inside the Brillouin zone. Typically we have chosen lattices of size 20×20 for all of the three $\mathbf{k}$ vectors. To check the convergence we have increased the size of the lattice up to 40×40 (in this case we have taken advantage of the symmetry properties of the Brillouin zone by integrating the last $\mathbf{k}$ vector over $\frac{1}{8}$ of the zone). Our results converge quite well already with a 20×20 lattice size. The line shapes that we get are generally rather smooth, except for the interference diagrams (See Sec. III C), where even with the largest possible lattice the curves display some noise.

The results that we obtain from the relevant second-order contributions to $\Pi^{(3)}$ (diagrams $\mathcal{E}_1$, $\mathcal{E}_2$, $\mathcal{E}_5$, $\mathcal{E}_6$, $\mathcal{E}_7$, and $\mathcal{E}_8$) are represented by the dashes lines of Fig. 7. We can see that the intensity coming from these processes is 2 orders of magnitude smaller than that of the two-magnon peak for $S=\frac{1}{2}$. Furthermore, the intensity coming from the diagrams with self-energy insertions happens to be negative in the energy range $2<\tilde{\omega}<3.4$, where, as we show in Appendix D, the imaginary part of the second-order magnon self-energy, $\Sigma^{(2)}(\mathbf{k},\omega)$, as a function of ω is indeed negative. Although the contributions coming from the vertex insertions is positive in the same region, the total sum of all the relevant diagrams contributing to $\Pi^{(3)}$ is still partly negative. The fact that the spectral density of $\Pi^{(3)}$ can be negative should not be a surprise, since the boson Hamiltonian itself is not Hermitian and therefore it is very possible that *boson correlation functions* have this anomalous characteristic. Of

course if this formalism is a correct approach to the original spin problem, then *spin correlation functions,* when written in terms of the corresponding boson correlation functions, must have positive definite spectral densities,

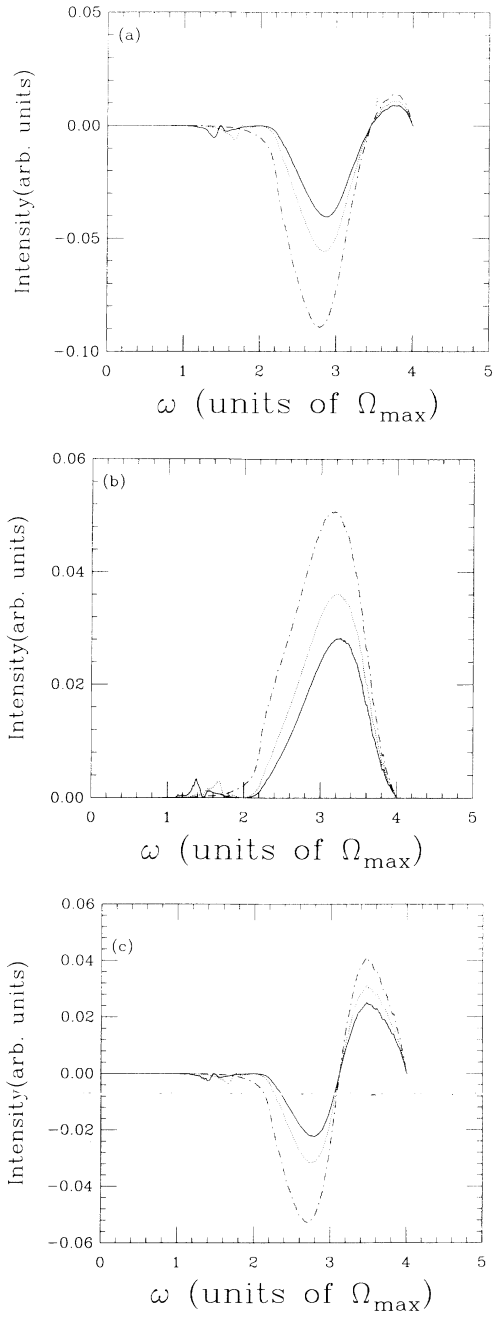

FIG. 7. Raman intensity coming from second-order diagrams contributing to $\Pi^{(3)}$, see Appendix E. The imaginary part is taken by cutting the diagrams at the level of the four-magnon state. The solid curve are for the $S=\frac{1}{2}$ case, and the two main magnons interact via "ladders." The dotted curves are for the $S=1$ case and the two main magnons interact via "ladders." The dashed curves are for the case in which the two main magnons are noninteracting, which is equivalent to $S=\infty$. (a) From self-energy insertions, diagrams $\mathcal{E}_1$ and $\mathcal{E}_2$. (b) From vertex corrections, diagrams $\mathcal{E}_5$–$\mathcal{E}_8$. (c) Total sum of all.

provided that all the contributions from the different boson terms are correctly summed. In our case the relevant spin correlation function is the Raman-scattering correlation function given in Eq. (2.58). Therefore, it is this correlation function that must have (and indeed has) a positive definite spectral density and not the single boson terms in which it can be decomposed.

So far we have restricted ourselves to the diagrams coming from $\Pi^{(3)}$ only, using the argument that all the others should be much smaller than these. We want now to see how smaller they really are, particularly in view of possible cancellations of the negative contribution that we have just mentioned. We have therefore evaluated all the second-order diagrams contributing to $\Pi^{(i)}$, $i=1,2,4,\ldots,10$ (see Appendix E), obtaining the following results.

(1) $\Pi^{(1)}$ and $\Pi^{(2)}$—which together with $\Pi^{(3)}$ define $\chi^{(1)}$—do not give any contribution to the $\tilde{\omega}>2$ region.

(2) $\Pi^{(4)}$, $\Pi^{(5)}$, $\Pi^{(6)}$, and $\Pi^{(7)}$— which define $\chi^{(2)}$—do have a nonzero contribution for $\tilde{\omega}>2$, but this is at least 1 order of magnitude smaller than the one coming from $\Pi^{(3)}$. As we said at the beginning of Sec. III, this is due to the fact that $\chi^{(2)}$ is multiplied by the factor $\gamma_{\mathbf{k}}$, which vanishes for zone-edge wave vectors.

(3) Even smaller, for the same reason—being $\chi^{(3)}$ multiplied by the factor $\gamma_{\mathbf{k}}^2$—is the four-magnon contribution coming from $\Pi^{(8)}$, $\Pi^{(9)}$, and $\Pi^{(10)}$.

In conclusion, summing all the second-order diagrams contributing to $\Pi^{(i)}$, $i=1-10$, the main result is that, for $\tilde{\omega}>2$, the scattering intensity given by the two-magnon correlation function G_{Λ_0} is very small and can be even negative, due to the self-energy diagrams, as can be seen from Figs. 7 (dashed lines).

A first correction to this result comes from adding ladder interactions to the main two Raman magnons in these second-order diagrams. As an example, let us consider again the self-energy diagram $\mathcal{E}_1$ contributing to $\Pi^{(3)}$. In the energy region $\tilde{\omega}>2$, this diagram represents the process in which two off-shell magnons are created by light and one of them decays into three magnons giving rise to a state of four on-shell magnons. As we saw in Sec. III A 1, the two main magnons, α and β, are created close together in real space and undergo to repeated scattering. Therefore, also in this case, instead of the single diagram $\mathcal{E}_1$, we should sum an infinite number of

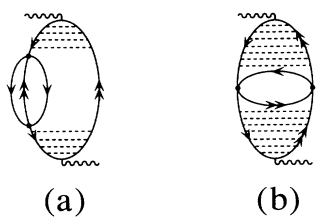

FIG. 8. The two main Raman magnons interact repeatedly via ladders before the off-shell decay occurs. The ladder interaction is simply a positive factor smaller than 1 for $\tilde{\omega}>2$; but it takes into account the Van Hove singularity for $\tilde{\omega}<2$. (a) Self-energy diagram. (b) Vertex insertion diagram.

terms, as shown in Fig. 8. A similar procedure should be carried out for the vertex corrections (e.g., diagram $\mathcal{E}_5$) as well. The calculation of this sum can be carried out using the same techniques of Sec. III A 2. If we make the approximation $1/\varepsilon_{\mathbf{k}}^{m}\approx 1$, then the calculation is quite simple and the result amounts to multiplying the bare Green's function of the two main magnons, $1/(\tilde{\omega}-2\varepsilon_{\mathbf{k}}+i\eta)$, by the RPA denominator

$$\frac{1}{\{1+[1/zS\alpha(S)]I^{(0)}(\omega)\}} = \frac{1}{\left\{1+[1/zS\alpha(S)]\sum_{\mathbf{k}} f_{\mathbf{k}}^{2}[1/(\omega-2\varepsilon_{\mathbf{k}}+i\eta)]\right\}}, \tag{3.34}$$

which, for $\tilde{\omega}>2$, is just a real positive function of $\tilde{\omega}$ smaller than 1. Therefore, the total intensity coming from the second-order diagrams contributing to $\Pi^{(3)}$ is reduced by the interaction of the two main magnons as shown in Figs. 7 (the solid curves are for $S=\frac{1}{2}$ and the dotted curves for $S=1$). In particular, the negative intensity peak has been reduced by more than 50% for $S=\frac{1}{2}$.

We now turn to the discussion of the line shape in the energy region $0<\tilde{\omega}<2$. It is rather important to see how the two-magnon SW line shape derived in Sec. III A 2 is modified by the second-order diagrams when the imaginary part of these is taken at the level of the two-magnon states (namely, the two *main magnons* in the diagram are the ones *on shell).* We will see that, in fact, all of these diagrams hardly change the previous line shape at all, leaving, in particular, the narrow two-magnon peak almost unmodified. As far as the self-energy diagrams contributing to $\Pi^{(3)}$ are concerned, we will take them into account by dressing the bare magnon/propagators, as discussed at the beginning of this section. In order to do this, we need to compute numerically both the real and the imaginary part of $\Sigma_{\alpha\alpha}^{(2)}(\mathbf{k},\omega)$ and subsequently the "dressed" noninteracting bubble diagram contributing to $\Pi^{(3)}$ (see Fig. 9)

$$b_{dr}(\mathbf{k},\omega)=i\int\frac{d\omega'}{2\pi}\frac{1}{\omega+\omega'-\varepsilon_{\mathbf{k}}-\Sigma_{\alpha\alpha}^{(2)}(\mathbf{k},\omega+\omega')} \times\frac{-1}{\omega'+\varepsilon_{\mathbf{k}}+\Sigma_{\beta\beta}^{(2)}(\mathbf{k},\omega')} . \tag{3.35}$$

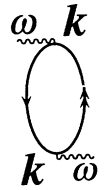

FIG. 9. Dressed noninteracting bubble diagram contributing to $\Pi^{(3)}$: the magnon propagators have been dressed by the second-order self-energy.

We need to compute $b_{dr}(\mathbf{k},\omega)$ again as a function of $\mathbf{k}$ and ω. This calculation is numerically rather subtle because $\mathrm{Im}\Sigma_{\alpha\alpha}^{(2)}(\mathbf{k},\omega)$ changes sign and can be both positive and negative.

The "dressed" functions $L_{dr}^{(m)}(\omega)$ are given by

$$L_{dr}^{(m)}(\omega)=\frac{1}{\Omega_{\max}}\frac{1}{N}\sum_{\mathbf{k}}\frac{f_{\mathbf{k}}^{2}}{\varepsilon_{\mathbf{k}}^{m}}b_{dr}(\mathbf{k},\omega) . \tag{3.36}$$

Once $L_{dr}^{(0)}(\omega)$, $L_{dr}^{(1)}(\omega)$, $L_{dr}^{(2)}(\omega)$ are calculated, we can use Eq. (3.22) to compute the two-interacting-magnon Green's function, which now contains possible *off-shell* decay terms. The result of this calculation for $S=\frac{1}{2}$ is shown in Fig. 10, where, by comparison, we have superimposed the two-magnon SW line shape previously obtained from the same Eq. (3.22) but without adding the second-order self-energy to the magnon propagators [see Fig. 6(a)]. The wigglings and secondary peaks in this picture are due to finite-lattice effects [the bubble $b_{dr}(\mathbf{k},\omega)$, as a function of $\mathbf{k}$, has been calculated for a lattice of 20×20 points]. We see that, apart from these finite-lattice effects, the two curves are very close for $\tilde{\omega}<2$. In particular, the position of the two-magnon peak turns out to be unchanged because, as we have said above, the correction to the magnon dispersion due to the second-order self-energy is very small (see Appendix D). We known that, in the previously derived two-magnon SW line shape for $S=\frac{1}{2}$, the peak position happened to be close to the experimental value, if we used a reasonable value for the exchange constant ($J\approx 1000\ \mathrm{cm}^{-1}$). Therefore, this correct feature is preserved in this modified calculation. Notice, in contrast, that an analogous calculation performed using the HP vertices would shift considerably the peak position towards lower frequencies, since, as we have mentioned above, the HP second-order self-energy near the zone boundary decreases the spin-wave dispersion by an amount almost equal to the first-order (Oguchi) correction.[30] For $\tilde{\omega}>2$ we have checked that the line shape of Fig. 10 almost coincides with the line

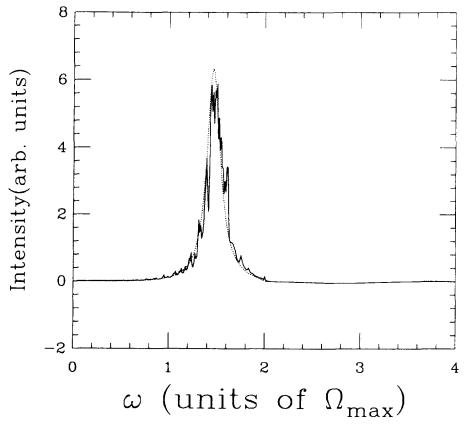

FIG. 10. Line shape of the two-magnon SW Raman scattering for $S=\frac{1}{2}$ obtained when the one-magnon Green's functions have been dressed by second-order self-energy insertions so that off-shell decay into three-magnon states is possible. As a comparison we have superimposed Fig. 6(a) (dotted line here).

shape of Fig. 7(a), solid line, obtained by summing the two self-energy insertion diagrams (diagrams $\mathcal{E}_1$ and $\mathcal{E}_2$ of Appendix E). As anticipated, this proves that, indeed, these two diagrams are the leading order correction in a $1/S$ expansion due to the second-order self-energy. This gives us some confidence that the single second-order diagrams (diagrams $\mathcal{E}_5$–$\mathcal{E}_8$) also would represent the leading-order correction of the modified theory obtained when $\mathcal{V}^{\alpha\beta}$ is corrected by second-order vertex interactions. Therefore, we can simply study the contribution of these diagrams for $\tilde{\omega}<2$, after we have added ladder interactions to the initial (final) main magnons. An example is given in Fig. 8(b). It turns out that the effect of these diagrams for $\tilde{\omega}<2$ is completely negligible, since their intensity is 2 orders of magnitude smaller than the two-magnon SW peak intensity of Fig. 6.

Finally, a similar analysis of all the other correlation functions $\Pi^{(i)}$, $i=1,2,4,\ldots,10$ does not reveal any surprises: their contribution for $\tilde{\omega}<2$ can be completely neglected as well. Therefore, the conclusion is that the second-order self-energy and vertex corrections do not modify substantially the line shape obtained in Sec. III A 2 for $\tilde{\omega}<2$ and give quite a small contribution for $\tilde{\omega}>2$. In particular, the off-shell decay completely fails to broaden the two-magnon peak. Finally, the negative intensity problem will be fixed when we add the other terms—that we are going to study now—that contribute to the total Raman-scattering *spin* correlation function.

B. Direct four-magnon production

We now turn to the computation of $G_{\Lambda_1}(\omega)$ which describes the direct creation, by the Raman Hamiltonian, of four magnons and their possible scattering. Processes involving the direct production of four magnons should be the most likely to provide the high-energy tail far beyond the two-magnon cutoff observed in the experiment. Of course, there is little hope of performing a fully interacting Green's-function calculation of four-magnon processes. In fact, we will be forced to compute just the lowest-order approximation of $G_{\Lambda_1}(\omega)$, namely, the noninteracting case. We want to compute

$$G^{(0)}_{\Lambda_1}(t_1-t_2)=-i\langle 0|\mathcal{T}\Lambda_1(t_1)\Lambda_1(t_2)|0\rangle\ , \tag{3.37}$$

where $|0\rangle$ is the LSW ground state and the time dependence of Λ_1 is given by the unperturbed LSW Hamiltonian, H_0 [see Eq. (2.29)]. Since $G_{\Lambda_1}(\omega)$ has been normal ordered with respect to the magnon operators α and β, it is easy to see that

$$G^{(0)}_{\Lambda_1}(t_1-t_2)=G^{(0)}_{4m(+)}(t_1-t_2)+G^{(0)}_{4m(-)}(t_1-t_2)\ , \tag{3.38}$$

where

$$G_{4m(+)}(t_1-t_2)=-i(B/2)^2\left[\frac{z}{4N}\right]^2 g(\mathbf{E}_{\rm inc},\mathbf{E}_{\rm sc})$$
$$\times\sum_{\substack{1234\\1'2'3'4'}}\delta_G(1+2-3-4)\delta_{G'}(1'+2'-3'-4')\tilde{V}^{(8)}_{(1234)}\tilde{V}^{(7)}_{(1'2'3'4')}$$
$$\times\langle 0|\mathcal{T}\beta_1(t_1)\beta_2(t_1)\alpha_3(t_1)\alpha_4(t_1)\alpha^\dagger_{1'}(t_2)\alpha^\dagger_{2'}(t_2)\beta^\dagger_{3'}(t_2)\beta^\dagger_{4'}(t_2)|0\rangle\ , \tag{3.39}$$

$$G^{(0)}_{4m(-)}(t_1-t_2)=G^{(0)}_{4m(+)}(t_2-t_1)\ . \tag{3.40}$$

$G^{(+)}_{4m(+)}$ and $G^{(0)}_{4m(-)}$ represent the creation of four on-shell, noninteracting, magnons by the scattering operator, as shown by the diagram in Fig. 11. Remembering that, in this case,

$$\alpha^\dagger_{\mathbf{k}}(t)=e^{i\Omega_k t}\alpha^\dagger_{\mathbf{k}}\ ,\quad \beta^\dagger_{\mathbf{k}}(t)=e^{i\Omega_k t}\beta^\dagger_{\mathbf{k}}\ ,$$

the Fourier transform of $G^{(0)}_{4m(+)}(t_1-t_2)$ is easily computed

$$G^{(0)}_{4m(+)}(\omega)=N(B/2)^2 g(\mathbf{E}_{\rm inc},\mathbf{E}_{\rm sc})(z/4)^2\left[\frac{1}{\Omega_{\max}}\right]\frac{4}{N^3}\sum_{1234}\delta_G(1+2-3-4)\tilde{V}^{(7)}_{(1234)}\tilde{V}^{(8)}_{(3412)}\left[\frac{1}{\tilde{\omega}-\varepsilon_1-\varepsilon_2-\varepsilon_3-\varepsilon_4+i\eta}\right]\ . \tag{3.41}$$

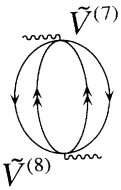

FIG. 11. Raman-scattering contribution due to four on-shell noninteracting magnons created directly by the quartic term of the Raman operator.

In deriving Eq. (3.41), we will have used the symmetry properties of $\tilde{V}^{(7)}$ and $\tilde{V}^{(8)}$ under the interchange of momentum variables (see Appendix B), so that the four possible Wick's pairings give just a factor of 4. Notice that $G^{(0)}_{4m(+)}(\omega)$ is of $O(S^0)$, that is the same order of the indirect four-magnon production studied in the previous section. Since the dominant two-magnon contribution is of $O(S^2)$, this means that the *relative intensity* of the four-magnon contribution to the two magnon is roughly four times bigger for the $S=\frac{1}{2}$ case then the $S=1$ case.

We have numerically computed the imaginary part of $G^{(0)}_{4m(+)}(\omega)$ which gives the contribution of the direct four-magnon production to the Raman spectrum. The result is shown in Fig. 12(b), while in Fig. 12(a) we show the four-magnon density of states obtained from

$$\rho_{4m}(\tilde{\omega})=\frac{1}{N^3}\sum_{1234}\delta_G(1+2-3-4)\delta(\tilde{\omega}-\varepsilon_1-\varepsilon_2-\varepsilon_3-\varepsilon_4)\ . \tag{3.42}$$

In contrast with the joint density of states of two magnon, $\rho_{4m}(\tilde{\omega})$ does not have any Van Hove singularity because of the large phase space available, even though the curve has a peak near $\tilde{\omega}=4$ which is the maximum energy that a four-noninteracting-magnon state can have. The total area has been normalized to one.

The line shape of the direct four-magnon intensity [Fig. 12(b)] resembles a little the density of states, even though its intensity and total area is a small fraction of one. We would like to emphasize that the direct four-magnon intensity is essentially positive in the whole frequency range, despite the fact that its matrix element does not occur in a positive definite combination due to the non-Hermiticity of the Raman Hamiltonian Λ. This is an example of the fact that the non-Hermiticity of the DM formalism is quite harmless for on-shell processes like the creation of four on-shell, noninteracting magnons. For $S=\frac{1}{2}$, the four-magnon peak has an intensity about 200 times smaller than the two-magnon peak and its integrated area is about 1.9% of the two-magnon area. If we plot the sum of the two contributions, the four-magnon contribution is so tiny that it does not seem to modify the two-magnon line shape at all. However, its peak occurs at such high frequencies (approximately at $\tilde{\omega}=3$) that the second cumulant is increased almost by a factor of 2. The ratio of the first two cumulants is changed from 0.107 to 0.194. For $S=1$, the four-magnon intensity seems to be completely negligible; but again the ratio between the first two cumulants increases from 0.099 to 0.12 in striking, though probably accidental, agreement with the results obtained by Singh in his series-expansion calculation.[14] Of course, we must sum all the four-magnon contributions before we can say anything definite about the moments of the line shape.

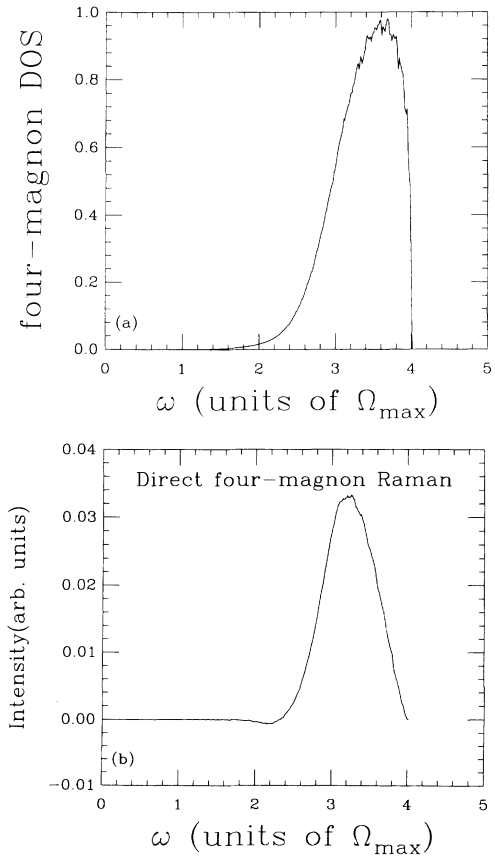

FIG. 12. (a) Four-magnon density of states from Eq. (3.42). (b) Raman intensity from direct four-magnon production. The four magnons are on-shell and not interacting.

Finally, we would like to conclude this section saying a few words about how magnon interaction can possibly modify the direct four-magnon intensity, obtained in the noninteracting case. From simple phase-space considerations, we should expect magnon interactions among the four magnons to cause a less drastic change in the line shape than in the two-magnon case. Nevertheless, since the interaction is attractive—at least the part coming from the Ising part—it is conceivable that magnon interaction will move the four-magnon peak towards lower frequencies: indeed, it costs less energy to flip four spins adjacent on the same plaquette or row than to flip four spins laying on sites that are not nearest neighbors. The interaction could, in fact, give rise to a four-magnon bound state, in which case it is not impossible that the scattering intensity could increase in correspondence of the energy of this collective excitation. We discuss this problem in more detail in Sec. III D.

C. Interference

The last boson correlation function that we need to study is $G_{\Lambda_{10}}(t_1-t_2)$, which represents the interference between the two-magnon and the four-magnon processes. The computation of $G_{\Lambda_{10}}$ is not much simpler than that of G_{Λ_1} and therefore we are forced, once again, to look at the lowest-order terms in perturbation theory. One can immediately see that, in the unperturbed case, $G^{(0)}_{\Lambda_{10}}$ vanishes identically. Once again this comes about because Λ_1 and Λ_0 have been normal ordered and $T=0$. The first nonvanishing contribution is obtained at first order in perturbation theory, where $G_{\Lambda_{10}}$ is given by

$$G^{(1)}_{\Lambda_{10}}(t_1-t_2)=-i(-i/\hbar)\int_{-\infty}^{+\infty}dt'\langle 0|\mathcal{T}\Lambda_1(t_1)\Lambda_0(t_2)V_{\rm DM}(t')|0\rangle\ . \tag{3.43}$$

In order to evaluate Eq. (3.43), the best way to proceed is to realize that, in this case, the topological structure of the possible diagrams is quite simple. Indeed, there is just one basic diagram, which is shown in Fig. 13(a). All

the different contributions are obtained by assigning arrows to the lines of this diagram in all the possible ways. Each diagram will always involve two quartic vertices: $\tilde{V}^{(i)}$, coming from Λ_1 and $V^{(j)}$, coming from $V_{\rm DM}$. Furthermore, as we explain in greater detail in Appendix D, since we are at zero temperature, we must remember that two lines of the same species cannot run between two vertices in opposite directions, otherwise the diagram vanishes. Using these rules, one can see that Eq. (3.43) gives only 12 different contributions. Both their diagrammatic and analytical expressions are given in Appendix F. Summing all of them up we obtain

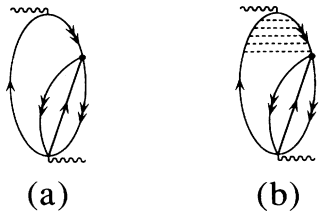

FIG. 13. (a) Typical first-order interference diagram; (b) ladder interaction has been added at level of the two-magnon state.

$$G^{(1)}_{\Lambda_{10}}(\omega)+G^{(1)}_{\Lambda_{01}}(\omega)=G^{(1)}_{\Lambda_{10}}(\omega)+G^{(1)}_{\Lambda_{10}}(-\omega)$$
$$=8N(B/2)^2 g(\mathbf{E}_{\rm inc},\mathbf{E}_{\rm sc})\left[\frac{z}{4}\right]^1\frac{1}{\Omega_{\max}}[\mathcal{I}_1(\tilde{\omega})+\mathcal{I}_2(\tilde{\omega})+\mathcal{I}_3(\tilde{\omega})+\mathcal{I}_1(-\tilde{\omega})+\mathcal{I}_2(-\tilde{\omega})+\mathcal{I}_3(-\tilde{\omega})]\,, \quad (3.44)$$

where

$$\mathcal{I}_1(\tilde{\omega})=\frac{1}{N^3}\sum_{(1234)}\delta_G(1+2-3-4)\tilde{V}^{(7)}_{(4321)}\left[V^{(2)}_{(1234)}\frac{\tilde{\gamma}_1}{\varepsilon_1}\frac{1}{\tilde{\omega}-2\varepsilon_1+i\eta}+V^{(5)}_{(1234)}\frac{\tilde{\gamma}_4}{\varepsilon_4}\frac{1}{\tilde{\omega}-2\varepsilon_4+i\eta}\right]$$
$$\times\frac{1}{\tilde{\omega}-\varepsilon_1-\varepsilon_2-\varepsilon_3-\varepsilon_4+i\eta}\,, \quad (3.45)$$

$$\mathcal{I}_2(\tilde{\omega})=\frac{1}{N^3}\sum_{(1234)}\delta_G(1+2-3-4)2\tilde{V}^{(7)}_{(1234)}V^{(8)}_{(3412)}\left[\frac{\gamma_1\tilde{\gamma}_1}{\varepsilon_1}+\frac{\gamma_3\tilde{\gamma}_3}{\varepsilon_3}\right]\frac{1}{\varepsilon_1+\varepsilon_2+\varepsilon_3+\varepsilon_4}\frac{1}{\tilde{\omega}-\varepsilon_1-\varepsilon_2-\varepsilon_3-\varepsilon_4}\,, \quad (3.46)$$

$$\mathcal{I}_3(\tilde{\omega})=-\frac{1}{N^3}\sum_{(1234)}\delta_G(1+2-3-4)V^{(7)}_{(4321)}\left[\tilde{V}^{(2)}_{(1234)}\frac{\tilde{\gamma}_1}{\varepsilon_1}\frac{1}{\tilde{\omega}-2\varepsilon_1+i\eta}+\tilde{V}^{(5)}_{(1234)}\frac{\tilde{\gamma}_4}{\varepsilon_4}\frac{1}{\tilde{\omega}-2\varepsilon_4+i\eta}\right]$$
$$\times\frac{1}{\varepsilon_1+\varepsilon_2+\varepsilon_3+\varepsilon_4}\,. \quad (3.47)$$

Notice that these interference diagrams, which are the leading, nonvanishing contribution to the interference Green's function, are of $O(S^0)$, just like the direct four-magnon term studied in Sec. III B and the indirect four-magnon terms considered in Sec. III A. Therefore, we conclude that all the first, nonvanishing contributions to the Raman scattering, involving four magnons, are of $O(S^0)$.

All the first-order interference diagrams have as main ingredients two vertex functions $\tilde{V}(i)V(j)$ and two energy denominators. $\mathcal{I}_1(\tilde{\omega})$ is the sum of diagrams $\mathcal{F}_1$, $\mathcal{F}_3$, $\mathcal{F}_5$, and $\mathcal{F}_7$, which are characterized by the product of the two energy denominators

$$\frac{1}{\tilde{\omega}-2\varepsilon_1+i\eta}\frac{1}{\tilde{\omega}-\varepsilon_1-\varepsilon_2-\varepsilon_3-\varepsilon_4+i\eta}\,, \quad (3.48)$$

and are the most intuitive to interpret: they describe an off-shell decay of one of the two-main magnons, created originally by light, into three magnons, generating a four-on-shell-magnon final state; or, the inverse process, in which three off-shell magnons—out of four created by light—converge into one, on-shell magnon, generating a two-magnon final state. $\mathcal{I}_2(\tilde{\omega})$ is the sum of diagrams $\mathcal{F}_2$, $\mathcal{F}_4$, $\mathcal{F}_6$, and $\mathcal{F}_8$ which contain

$$\frac{1}{\varepsilon_1+\varepsilon_2+\varepsilon_3+\varepsilon_4}\frac{1}{\tilde{\omega}-\varepsilon_1-\varepsilon_2-\varepsilon_3-\varepsilon_4+i\eta}\,, \quad (3.49)$$

and, finally, $\mathcal{I}_3(\tilde{\omega})$ is the sum of diagrams $\mathcal{F}_9$, $\mathcal{F}_{10}$, $\mathcal{F}_{11}$, and $\mathcal{F}_{12}$, with the energy denominators

$$\frac{1}{\varepsilon_1+\varepsilon_2+\varepsilon_3+\varepsilon_4}\frac{1}{\tilde{\omega}-2\varepsilon_1} \quad (3.50)$$

These diagrams are of a more difficult interpretation. The denominator $1/(\varepsilon_1+\varepsilon_2+\varepsilon_3+\varepsilon_4)$ comes about because of vacuum fluctuations, due to the quartic term of the exchange Hamiltonian, which creates four particles even before the light comes in. The other energy denominator can be either $1/(\tilde{\omega}-\varepsilon_1-\varepsilon_2-\varepsilon_3-\varepsilon_4+i\eta)$ or $1/(\tilde{\omega}-2\varepsilon_1+i\eta)$, depending on the way the different operators, coming from Λ_0, Λ_1, and $V_{\rm DM}$, respectively, occur in the time ordering. Notice that $\mathcal{I}_3(\tilde{\omega})$ will con-

tribute only in the $0<\tilde{\omega}<2$ region.

In order to cure the Van Hove singularity occurring when a two-magnon state, characterized by $1/(\tilde{\omega}-2\varepsilon_1+i\eta)$, is present, we need to sum again an infinite number of terms with ladder interactions, as we did previously (see Sec. III A 3). A typical interference diagram, with ladder interactions at the level of the two-magnon state, is shown in Fig. 13(b). We know already that the result of summing this series gives approximately a RPA denominator modifying the bare two-magnon Green's function $1/(\tilde{\omega}-2\varepsilon_1+i\eta)$, as shown in Eq. (3.34). For $\tilde{\omega}>2$, this RPA denominator is simply a real positive number greater than one, which decreases the scattering intensity; while for $0<\tilde{\omega}<2$, its effect is more complicated because it is a complex number, the real part of which changes sign.

The results are shown in Fig. 14. Notice that $\mathcal{I}_2(\tilde{\omega})$ is much smaller than $\mathcal{I}_1(\tilde{\omega})$ because it contains the factor $\gamma_{\mathbf{k}}$ which vanishes when $\mathbf{k}$ is close to the boundary of the HAFM Brillouin zone. Again, the total interference intensity [Fig. 14(d)] is partially negative. Notice that the intensity coming from "interference" terms can be negative even when the theory is an ordinary, good Hermitian theory, as far as the *total* intensity from all the terms comes out to be positive. Finally, as anticipated, the ladder interactions reduce the intensity when $\tilde{\omega}>2$ and eliminate the singularity at $\tilde{\omega}=2$.

D. Total Raman scattering

In this section we will discuss the total Raman-scattering line shape resulting from the two-magnon and four-magnon scattering. We shall first consider separately the total intensity coming from four-magnon production.

1. Total four-magnon intensity

In Fig. 15 we show the scattering intensity coming from the sum of all the *four-magnon* contributions which have been discussed in Sec. III A 3, III B, and III C. The solid curve is for the $S=\frac{1}{2}$ case, the dotted curve for the $S=1$ case, and the dashed curve for the $S=\infty$ case. For the indirect four-magnon production we have just considered all of the second-order diagrams contributing to $\Pi^{(i)}$, $i=1,\ldots,10$ (see Appendix E) attaching to them ladder interactions between the two main magnons (see Fig. 8). The same ladder interactions have been attached

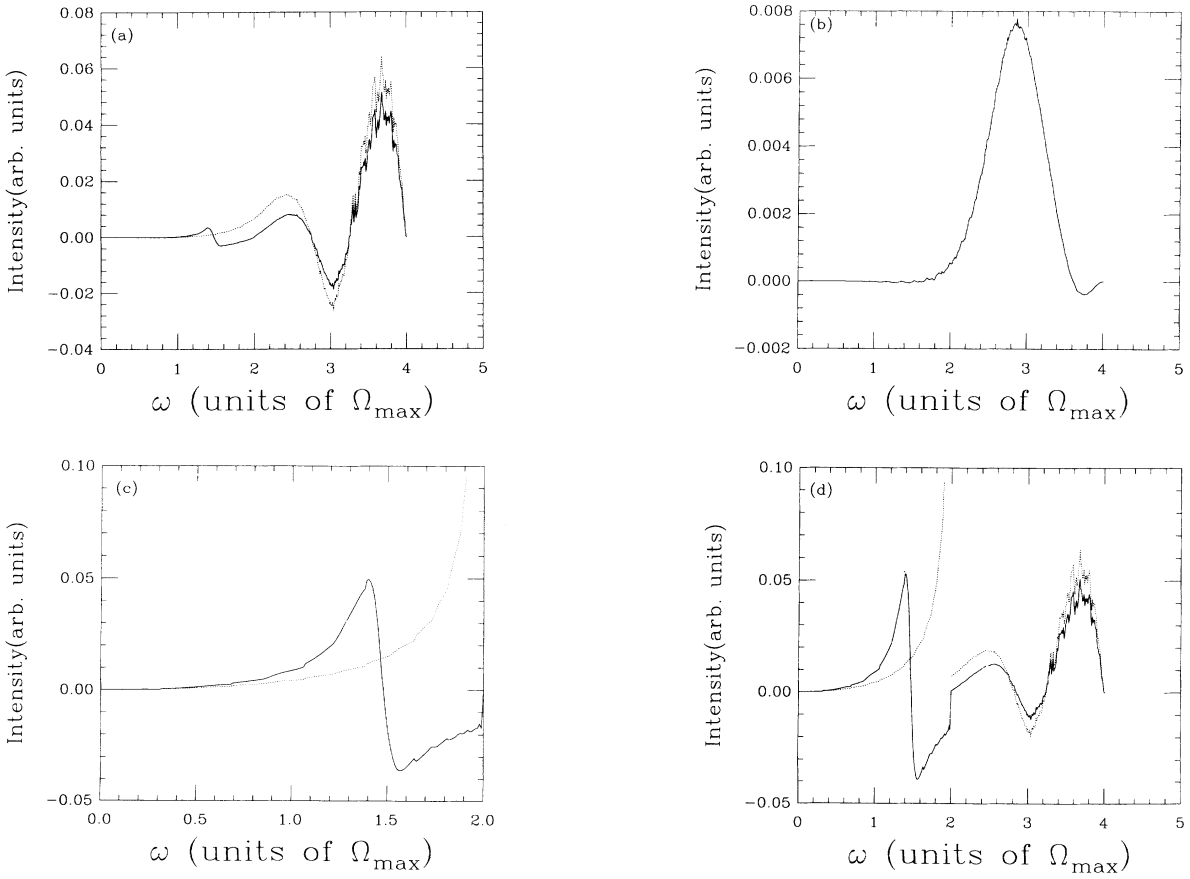

FIG. 14. Scattering intensity from interference diagrams. Dotted lines: without ladder; solid lines: with ladders (for $S=\frac{1}{2}$). (a) $\mathcal{I}_1(\tilde{\omega})$, (b) $\mathcal{I}_2(\tilde{\omega})$, (c) $\mathcal{I}_3(\tilde{\omega})$, (d) total sum. Notice that $\mathcal{I}_1(\tilde{\omega})$ has more noise—due to numerical effects—than the other six-dimensional integrals calculated in this paper.

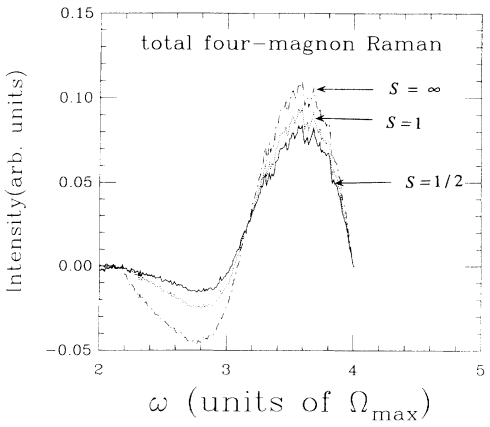

FIG. 15. Total four-magnon scattering intensity. The solid line is the $S=\frac{1}{2}$ case, the dotted line is $S=1$, the dashed line represents the $S=\infty$ case which is equivalent to the noninteracting case.

at the level of the two-magnon states in the interference diagrams [see Fig. 13(b)]. The sum of all the diagrams *without* ladders represents the leading four-magnon contribution in a $1/S$ expansion. As we saw in the previous sections, this contribution is of $O(1/S^0)$ [if we disregard the trivial energy scale $\Omega_{\max}=JzS\alpha(S)$, which appears as an overall factor in front of all the different terms of the Raman correlation function]. We also saw that the sum of the ladders gives essentially the RPA denominator shown in Eq. (3.34), which depends on S and it is responsible for the slight difference of the spectrum for different values of the spin. For the case $S=\infty$, this denominator is equal to one and therefore this case is equivalent to the noninteracting (no ladders) case. All the Van Hove singularities in the energy region $\tilde{\omega}<2$ are cured by summing the ladders. The four-magnon contribution in the energy region $\tilde{\omega}<2$ is irrelevant: it will be completely washed out by the overwhelming two-magnon contribution (cf. Fig. 6) which is positive and 2 orders of magnitude greater than the four-magnon part. The important region is for $\tilde{\omega}>2$, where the four-magnon contribution shown in Fig. 15 is the dominant part. There we can see that, apart from the small negative dip that extends from $\tilde{\omega}=2$ to $\tilde{\omega}=3$, the total four-magnon contribution is positive and has a rather well-defined peak at $\tilde{\omega}\approx 3.6$. Notice that the four-magnon density of states [see Fig. 12(a)] has a peak at $\tilde{\omega}=3.5$. The small negative dip is still something to worry about. It is more pronounced for bigger values of the spin, even though it is also true that the whole four-magnon contribution becomes less and less important with the increase of the spin and it is infinitesimally small for $S=\infty$ with respect to the two-magnon intensity which is proportional to S^2. We do not know if this residual negative intensity is the result of some numerical inaccuracies in our multidimensional integrals, in a region where a very large number of terms with different sign occur, or it is something more fundamental, connected with the non-Hermitian nature of the DM formalism.

2. *Total two-magnon–four-magnon SW Raman scattering: spin $S=\frac{1}{2}$*

In Fig. 16 we show the total Raman intensity coming from two-magnon and four-magnon scattering for the $S=\frac{1}{2}$ case. As anticipated, we see that the four-magnon contribution hardly modifies the two-magnon SW line shape: it yields simply a small bump, at quite large frequencies, of very small intensity. The numbers a_{2m} and a_{4m} represent, respectively, the integrated intensities of the two-magnon part and the four-magnon part. The four-magnon area is approximately 2.9% of the two-magnon area. The dotted line in the picture represents a δ function whose strength is equal to a_{4m} and whose position is chosen so that the sum of the δ function plus the two-magnon contribution yields the correct first moment of the solid curve. The two-magnon and four-magnon peaks, in units of J, are situated at

$$\omega_2\simeq 3.38$$

and

$$\omega_4\simeq 8.66 .$$

It is useful to compare these results with what one would expect to find from the following qualitative arguments. If the ground state were a classical Néel state, the energy cost to flip a pair of nearest-neighbor spins would be $3J_{\text{eff}}$ (six bonds are broken), whereas the energy cost would be $4J_{\text{eff}}$ if the flipped spins were not nearest neighbors (eight bonds are broken). Therefore, one would expect the Raman line shape to have a peak around $3J_{\text{eff}}$ that is, in proximity to the energy of a "bound pair." If we use the Oguchi correction and take $J_{\text{eff}}\approx 1.16J$, for $S=\frac{1}{2}$, this result is consistent with the position of our two-magnon peak. On the other hand, if we flip four spins, the energy

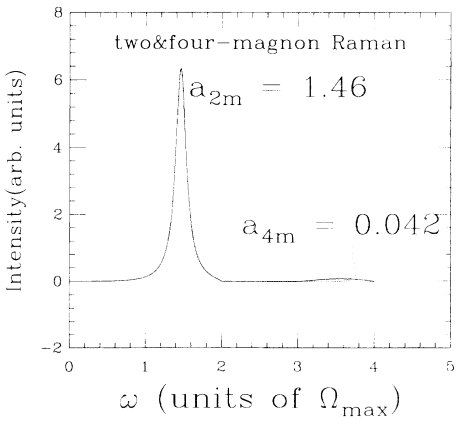

FIG. 16. Line shape of the total two-magnon–four-magnon SW Raman scattering for $S=\frac{1}{2}$. The numbers a_{2m} and a_{4m} represent, respectively, the integrated intensities of the two-magnon part and the four-magnon part. The dotted line in the picture represents a δ function (smeared out by an arbitrary width) whose strength is equal to a_{4m} and whose position is chosen so that the sum of the δ plus the two-magnon contribution yields the correct first moment of the solid curve.

cost will be $4J_{\text{eff}}$ if the four spins are around a plaquette, $5J_{\text{eff}}$ if they are neighbors in a row, $6J_{\text{eff}}$ if they are two separated bound pairs, and finally $8J_{\text{eff}}$ if all four spins are not nearest neighbors of each other. Therefore, in the Raman spectrum we would expect to find a four-magnon peak, coming from a four-magnon bound state, around $5J_{\text{eff}}$, with nonzero intensity between $4J_{\text{eff}}$ and $6J_{\text{eff}}$. A naive argument also allows one to give a rough estimate of the ratio of the intensities of the four-magnon and two-magnon contribution. Since we are interested essentially in nearest-neighbor spin flips, this ratio is related to the probability of having a pair of nearby spin flips in the ground state. The Raman operator flips a pair of neighboring spins, and if there happen to be no other nearby spins flipped in the ground state, then this will likely produce a two-magnon excited state. If, however, the quantum fluctuation occurs on a pair immediately neighboring the pair flipped by the Raman operator, this presumably has a significant amplitude to be a four-magnon excited state. In lowest-order perturbation theory about the Néel state, the probability of a given bond being flipped is $(\frac{1}{6})^2$. Since the bond flipped by the Raman operator has four neighbors, we may roughly estimate the rate of four-magnon to two-magnon production to be $4\times(\frac{1}{6})^2=\frac{1}{9}$. Therefore, the four-magnon intensity should be about 10% of the two-magnon intensity, more than three times larger than what we obtain in our spin-wave calculation.

At this point it is also useful to consider the results obtained from finite-size calculations. For 4×4 lattices, several authors[9–12] have found that the dominant two-magnon peak is located at $2.976J$, whereas there are basically two four-magnon peaks: one very small at $4.47J$ and a bigger one $5.48J$. The total four-magnon intensity is somewhat more than 10% of the two-magnon intensity. Calculations performed on larger lattices (18 sites and 20 sites) (Refs. 12 and 13) show that the structure seen on 4×4 clusters persists: no new peaks appear, while the old ones shift slightly to higher frequencies (see, however, Ref. 31). These results roughly agree with the qualitative arguments presented above, in contrast with what we obtain for the position and relative intensity of the four-magnon peak, which are respectively $7.5J_{\text{eff}}$ and 2.9%. The disagreement in the peak position can easily be explained if we remember that, in all our calculations, we have considered the four magnons as noninteracting (the only condition that they satisfy is that the total momentum is zero). Therefore, it is not surprising that the four-magnon peak is dominated by phase-space effects and hence occurs close to $4\Omega_{\max}$, where the density of states has a maximum [cf. Fig. 12(a)]. As we saw for the two-magnon scattering, adding repeated ladder interactions to these four magnons will very likely give rise to a four-magnon bound state with an energy approximately equal to $5J_{\text{eff}}$. This, in turn, will shift the four-magnon peak in the Raman spectrum towards lower frequencies. Unfortunately, it is very hard to study four-magnon bound states and we have not tried to do that. This prevents us from making a precise estimate of where the four-magnon peak will be located and especially of how the relative four-magnon intensity will be modified by the interaction. It is not impossible that the four-magnon interaction will increase the intensity to 10%, as estimated above, but we cannot prove this statement. Even if this does occur, however, qualitative disagreement will remain between the theoretical line shape—characterized by two well-separated narrow peaks—and the broad asymmetric experimental line shape.

We now turn to the discussion of the first three frequency moments and cumulants of the total Raman line shape. In Table I we show the first three cumulants [see Eqs. (3.31) and (3.32) for the definition] for several cases. In the first column we have the cumulants relative to the two-magnon SW line shape shown in Fig. 6(a). The second column contains the cumulants obtained from the total two-magnon–four-magnon SW line shape that we have first described (see Fig. 16). The third column contains the series-expansion results.[7] The fourth column contains the cumulants obtained from exact diagonalization of small clusters[9–12] and, finally, the last column represents the experimental values of the cumulants obtained from Raman experiments on La_2CuO_4.[4,7,5] If we compare the first two columns, we see that the four-magnon contribution modifies slightly the first cumulant, the value of which gets closer to the series-expansion result. On the other hand, the second and third cumulants are changed quite a lot by the four-magnon scattering. In particular, the second cumulant is enhanced by a factor of 2 with respect to the two-magnon result, and the parameter-free ratio M_2/M_1 changes from 0.11 to 0.26, which is even bigger than the series-expansion result. The third cumulant, which in our two-magnon SW calculation is negative,[28] becomes positive when we add the four-magnon contribution and the ratio M_3/M_1 is two times bigger than the series-expansion result, while it compares a little better with the finite-size diagonalization result. The fact that the value of M_3/M_1 that we get is considerably bigger than the series-expansion result is again an indication that the four-magnon peak of our theory is situated at too large frequencies, as a result of having completely neglected the interactions among the four magnons. We can also estimate how the four-magnon intensity should change, if the interaction lowered the four-magnon peak down to $5J_{\text{eff}}$, in order for our first two cumulants to remain close to the series-expansion values. Suppose that the four-magnon peak is now at $5J_{\text{eff}}\approx5.8J$. Let us accordingly fix its intensity so that the first cumulant is equal to the Singh *et al.* result $3.58J$ (which is only slightly larger than our value, $3.50J$). One easily finds that the four-magnon intensity should be about a factor of 3.4 larger than our spin-wave result, that is, roughly 10% of the two-magnon intensity. Using these values for the intensity and peak position of the four-magnon part, we can now evaluate the second and third cumulants (we represent the four-magnon intensity as a function). We find that $M_2=0.78J$, $M_3=0.95$, $M2/M1=0.22$, $M_3/M1=0.26$, in very good agreement with the series-expansion results. Therefore, if magnon interaction shifts the four-magnon peak down to $5J_{\text{eff}}$ and, at the same time, increases its intensity by a factor of 3.4, the agreement with the series-expansion re-

sults is excellent and the whole picture is consistent.

In conclusion, the four-magnon contribution, calculated within DM spin-wave theory, does not seem to modify substantially the two-magnon line shape. Therefore, the resulting two-magnon–four-magnon SW line shape (cf. Fig. 16) is still in rather poor agreement with the line shape obtained from the experiments on La_2CuO_4.[7] On the other hand, the four-magnon contribution does modify appreciably the first three frequency moments of the line shape, yielding values for the first three cumulants and their ratios that are in better agreement with the series expansion results than the simple two-magnon SW line shape. The discrepancies that still remain between our results and the results obtained from series expansion and exact diagonalization (particularly evident for the position of the four-magnon peak and the value of the third cumulant), should probably be fixed by developing a more sophisticated analysis of the four-magnon scattering, namely, by adding interaction to the four-magnon states. Even in this case, however, we believe that the theoretical spectrum will consist of two well-separated two-magnon and four-magnon peaks—the former much larger than the latter—still not resembling the broad and long-tailed line shape seen in the experiments.

3. *Total two-magnon–four-magnon Raman scattering: spin $S=1$*

Finally, we want to consider briefly the total Raman scattering from two magnons and four magnons for the case $S=1$. The relative intensity of the four-magnon part with respect to the two-magnon part is approximately 0.87, smaller, as expected, than for the $S=\frac{1}{2}$ case, and apparently completely negligible. More interesting is the study of the frequency moments and cumulants of the curve, given in Table II. We can see that the four-magnon contribution causes a very small increase in the first cumulant but has a less negligible effect on the second and the third one. In particular, the ratio M_2/M_1 is enhanced by 50% with respect to the two-magnon result, whereas, in the series-expansion calculation,[14] the same ratio is increased only by 30%. This rather large discrepancy between the series-expansion result and ours is, however, not as bad as it might appear: the uncertainties in M_2/M_1 are large in this case because the width of the curve is extremely narrow[14] compared to the $S=\frac{1}{2}$ case. Also, in this case adding interactions to the four-magnon states will push down the four-magnon peak, making our result in better agreement with the series-expansion calculation. In any case, again the four-magnon contribution changes the ratio M_2/M_1 in the right direction, but in a less pronounced way than for $S=\frac{1}{2}$.

IV. CONCLUSIONS

In this paper we have studied the line shape of the Raman scattering in the two-dimensional quantum HAFM at zero temperature, within the framework of spin-wave theory based on the Dyson-Maleev formalism. Besides the well-known two-magnon scattering, we have carried out a systematic evaluation of all the leading-order four-magnon contributions. We found that the spectral density is essentially positive, despite the fact that the Dyson-Maleev Hamiltonian is non-Hermitian. The four-magnon intensity is much smaller than the dominant two-magnon scattering so that the two-magnon line shape is apparently not appreciably modified by the four-magnon contribution. As a result, the overall line shape that we obtain for $S=\frac{1}{2}$, when we include the four-magnon contribution, is still in rather poor agreement with the experimental line shape obtained in Raman-scattering experiments on the undoped phase of La_2CuO_4. On the other hand, the first three frequency cumulants of the line shape are conspicuously modified by the four-magnon scattering, particularly for the $S=\frac{1}{2}$ case. For $S=\frac{1}{2}$ the values that we get for the first two cumulants and their ratios are in fairly good agreement with the results obtained from series-expansion calculations by Singh *et al.*, which are believed to be very accurate and are also considered to be in very good agreement with the experimental values.[7] However, the value of the third cumulant (which is an extremely sensitive function of the skewness of the line shape) is much larger than that obtained by Singh *et al.*, signaling that our four-magnon peak is located at too high frequencies. As we discussed above, this could, in principle, be taken care of by developing a fully interacting picture for the four-magnon scattering. In any case, our calculation shows that a systematic inclusion of the four-magnon contribution gives better results for the first three cumulants than the two-magnon scattering alone. The comparison with the $S=1$ case also gives a consistent picture.

If we accept that the two-magnon–four-magnon Raman line shape presented here (possibly improved by adding interactions to the four-magnon states), correctly reproduces the values of the first three cumulants obtained by series-expansion calculations, there remains to be explained why for $S=\frac{1}{2}$ this line shape looks so different from the experimental line shape. Of course, it is possible that the agreement with the series-expansion results, which is not perfect, is only a coincidence and our spin-wave calculation is not, in fact, adequate to treat the $S=\frac{1}{2}$ case. In that case a more suitable approach might give a rather different line shape, in better agreement with the experiment. However, it is known that the spin-wave expansion at $T=0$ is an useful asymptotic expansion in calculating many properties[32,33] of the $S=\frac{1}{2}$ HAFM, which agrees very well with more recent, sophisticated numerical techniques. An example of this agreement has been provided here by the calculation of the second-order correction of the renormalization factor of the spin-wave velocity, Z_c. The $1/S^2$ correction is less than 2% and increases Z_c up to 1.177 for $S=\frac{1}{2}$, in excellent agreement with the value 1.18 ± 0.02 derived by series expansion.[24] Therefore, we think that a complete failure of this perturbation expansion for this particular problem of the Raman scattering is not likely. Another possibility is that the claimed agreement of the series-expansion calculations with the experiments is, in fact, a coincidence. In that case we might think that the *model*

within which the Raman scattering in La_2CuO_4 has been studied, namely, an $S=\frac{1}{2}$ HAFM for the unperturbed system plus a photon–spin-pair coupling for the scattering operator, is not correct. Recently a cyclic four-spin Hamiltonian, rather than an $S=\frac{1}{2}$ HAFM, has been proposed[34] as a more suitable model for the undoped phase La_2CuO_4. This Hamiltonian is derived from a multiband Hubbard-type model for cuprates. Some preliminary calculations of the Raman scattering carried out by exact numerical methods on small clusters[35,36] shown that the Raman line shape is strongly influenced by the four-spin interaction. Notice that in these calculations the Raman interaction employed is still the Fleury-Elliott-Parkinson Hamiltonian used in this paper. The results obtained on a 4×4 lattice show some more structure for $\omega>4J$ than the previous analogous calculations[9–11] carried out for the Heisenberg model. Further investigation in this direction is certainly very desirable. However, since the $S=\frac{1}{2}$ HAFM has been so successful in explaining[37] many other properties of La_2CuO_4, mainly at long wavelengths, the problem for the Raman scattering could simply lie in the scattering operator describing the effective coupling between light and spin system. A recent study[38] of Raman scattering in Mott-Hubbard systems has indeed provided a more general effective spin Hamiltonian for the scattering operator, involving different Raman modes. For the B_{1g} symmetry, besides a leading-order term proportional to the Fleury-Elliott-Parkinson Hamiltonian used in this paper, there is also another spin-pair term involving third-nearest-neighbor interactions. This term could become very important in the resonance regime.[39] A study of this term contributing to the B_{1g} mode, together with an analysis of other Raman-active modes observed also in experiments on La_2CuO_4,[5] will be the topic of a forthcoming publication.

ACKNOWLEDGMENTS

This work was supported by NSF-DMR-9113911 and a grant of computer time from the National Center for Supercomputer Applications. The authors thank A. H. MacDonald and S. Chakravarty for several useful conversations and suggestions and Mats Wallin for his valuable help in the numerical calculation of the spin-wave renormalization factor.

APPENDIX A: THE DYSON-MALEEV REPRESENTATION

The representations used in Eqs. (2.2) and (2.3) are obtained by using, respectively, (1) direct Dyson-Maleev representation on the "rotated" sublattice A, and (2) conjugate Dyson-Maleev representation on sublattice B. The direct DM representation reads

$$S^z=-S+a^\dagger a\ , \tag{A1a}$$

$$S^+=(2S)^{1/2}a^\dagger\ , \tag{A1b}$$

$$S^-=(2S)^{1/2}\left[1-\frac{a^\dagger a}{2S}\right]a\ . \tag{A1c}$$

The conjugate DM representation reads

$$S^z=-S+a^\dagger a\ , \tag{A2a}$$

$$S^+=(2S)^{1/2}a^\dagger\left[1-\frac{a^\dagger a}{2S}\right]\ , \tag{A2b}$$

$$S^-=(2S)^{1/2}a\ . \tag{A2c}$$

It is easy to check that both these representations are indeed good representations of the spin-SU(2) algebra, namely, the operators defined in Eqs. (A1) and (A2) satisfy the spin commutation relations

$$[S^+,S^z]=S^+\ ,\quad [S^-,S^z]=-S^-\ ,\quad [S^+,S^-]=2S^z\ , \tag{A3a}$$

$$\mathbf{S}\cdot\mathbf{S}=S^zS^z+\tfrac{1}{2}(S^+S^-+S^-S^+)=S(S+1)\ . \tag{A3b}$$

These representations are not Hermitian in the sense that S^+ is not the Hermitian conjugate of S^-:

$$(S^+)^\dagger\neq S^-\ . \tag{A4}$$

As a result, operators which are Hermitian in the spin variables may not be so in the boson variables.

A "rotated" lattice is the system that we get when we perform the following operations:

$$\begin{aligned} &S^z\rightarrow -S^z\ ,\\ &S^+\rightarrow S^-\ ,\\ &S^-\rightarrow S^+\ . \end{aligned} \tag{A5}$$

One can immediately see that the "rotation" preserves the commutation relations, Eq. (A3). This transformation is convenient when we have a two-sublattice antiferromagnet, where, as a first approximation, namely, in the classical limit, $S\rightarrow\infty$, the ground state is the Néel state: $+S$ on the A sublattice, $-S$ on the B sublattice. By rotating the A sublattice, the ground state, in the large-S limit, looks ferromagnetic; as a result, when we bosonize the spins, the ground state of the system (again, in the large-S limit) is the vacuum state for both the a and b operators. Notice that, of course, the antiferromagnetic Heisenberg Hamiltonian given in Eq. (2.1) does not become *completely* ferromagnetic under this transformation. Indeed, we get

$$H^{\rm rot}=-J\sum_{\langle ij\rangle}S_i^zS_j^z+\frac{J}{2}\sum_{\langle ij\rangle}(S_i^+S_i^-+S_i^-S_j^-)\ , \tag{A6}$$

that is, only the Ising part (S^z component) is equal to the ferromagnetic case.

APPENDIX B: THE DYSON-MALEEV VERTICES

1. Hamiltonian

The quartic part of the Heisenberg Hamiltonian in terms of the boson operators is [cf. Eq. (2.7)]

$$V'_{\rm DM}=-J\sum_{\langle ij\rangle}(a_i^\dagger a_i b_j^\dagger b_j+\tfrac{1}{2}a_i^\dagger a_i a_i b_j+\tfrac{1}{2}a_i^\dagger b_j^\dagger b_j^\dagger b_j)\ . \quad \text{(B1)}$$

Let us introduce the Fourier transforms of a's and b's in a careful way. Let us assume that all the four wave vectors, $\mathbf{k}_1$, $\mathbf{k}_2$, $\mathbf{k}_3$, $\mathbf{k}_4$, lie within the HAFM Brillouin zone. Let us take the origin—in real space—to be on the A sublattice. Then $\mathbf{r}_i$ is a vector of the A sublattice but any vector $\mathbf{r}_j$ of the B sublattice must be written in the form $\mathbf{r}_j=\mathbf{r}_i+\delta$. We obtain

$$V'_{\rm DM}=-\frac{Jz}{4N}\sum_{(1234)}\delta_{\rm G}(1+2-3-4)(\gamma_{2-4}a_1^\dagger a_3 b_4^\dagger b_2+\gamma_{1-4}a_2^\dagger a_3 b_4^\dagger b_1+\gamma_{2-3}a_1^\dagger a_4 b_3^\dagger b_2+\gamma_{1-3}a_2^\dagger a_4 b_3^\dagger b_1$$
$$+\gamma_2 a_1^\dagger a_3 a_4 b_2+\gamma_1 a_2^\dagger a_3 a_4 b_1+\gamma_{2-3-4}a_1^\dagger b_3^\dagger b_4^\dagger b_2+\gamma_{1-3-4}a_2^\dagger b_3^\dagger b_4^\dagger b_1)\ , \quad \text{(B2)}$$

where we have used

$$\sum_{\mathbf{r}_i}e^{-i(\mathbf{k}_1+\mathbf{k}_2-\mathbf{k}_3-\mathbf{k}_4)\cdot\mathbf{r}_i}=N\delta_{\rm G}(1+2-3-4)\ , \quad \text{(B3)}$$

and $\mathbf{G}$ is a reciprocal-lattice vector. Equation (B3) expresses momentum conservation to within a reciprocal-lattice vector. It must be interpreted in the following way:

$$\delta_{\rm G}(1+2-3-4)\rightarrow\mathbf{k}_4=\mathbf{k}_1+\mathbf{k}_2-\mathbf{k}_3+\mathbf{G}\ , \quad \text{(B4)}$$

namely, $\mathbf{k}_1$, $\mathbf{k}_2$, $\mathbf{k}_3$ vary freely inside the HAFM Brillouin zone and $\mathbf{G}$ is the only reciprocal-lattice vector which "umklapp" the sum $(\mathbf{k}_1+\mathbf{k}_2-\mathbf{k}_3)$ back to the HAFM Brillouin zone and it is equal to zero whenever $(\mathbf{k}_1+\mathbf{k}_2-\mathbf{k}_3)$ is already inside it. We choose to write $V'_{\rm DM}$ in the particularly symmetric form[22] given in Eq. (B2) because, as was shown by Kopietz,[23] this exposes some underlying symmetries of the vertices and allows one to handle more effectively the infrared divergences that occur in them.[22,23] When we write a's and b's in terms of α's and β's, we obtain Eq. (2.24) for the normal-ordered part of $V'_{\rm DM}$ and the nine vertex functions are given by

$$V^{(1)}_{(1234)}=-\mathcal{U}_{1234}\{x_1[x_4(x_3\gamma_{1-3-4}-\gamma_{1-4})-(x_3\gamma_{1-3}-\gamma_1)]+x_2[x_4(x_3\gamma_{2-3-4}-\gamma_{2-4})-(x_3\gamma_{2-3}-\gamma_2)]\}\ , \quad \text{(B5)}$$

$$V^{(2)}_{(1234)}=-2\mathcal{U}_{1234}\{x_1x_2[x_4(\gamma_{1-4}-x_3\gamma_{1-3-4})-(\gamma_1-x_3\gamma_{1-3})]+[x_4(\gamma_{2-4}-x_3\gamma_{2-3-4})-(\gamma_2-x_3\gamma_{2-3})]\}\ , \quad \text{(B6)}$$

$$V^{(3)}_{(1234)}=-2\mathcal{U}_{1234}\{x_1[(\gamma_{1-3}-x_3\gamma_1)-x_4(\gamma_{1-3-4}-x_3\gamma_{1-4})]+x_2[(\gamma_{2-3}-x_3\gamma_2)-x_4(\gamma_{2-3-4}-x_3\gamma_{2-4})]\}\ , \quad \text{(B7)}$$

$$V^{(4)}_{(1234)}=-4\mathcal{U}_{1234}\{x_1x_2[(x_3\gamma_{1-3-4}-\gamma_{1-4})-x_4(x_3\gamma_{1-3}-\gamma_1)]+[(x_3\gamma_{2-3-4}-\gamma_{2-4})-x_4(x_3\gamma_{2-3}-\gamma_2)]\}\ , \quad \text{(B8)}$$

$$V^{(5)}_{(1234)}=-2\mathcal{U}_{1234}\{x_2[x_4(x_3\gamma_{1-3}-\gamma_1)-(x_3\gamma_{1-3-4}-\gamma_{1-4})]+x_1[x_4(x_3\gamma_{2-3}-\gamma_2)-(x_3\gamma_{2-3-4}-\gamma_{2-4})]\}\ , \quad \text{(B9)}$$

$$V^{(6)}_{(1234)}=-2\mathcal{U}_{1234}\{x_1x_2[(x_3\gamma_{2-4}-\gamma_{2-3-4})-x_4(x_3\gamma_2-\gamma_{2-3})]+[(x_2\gamma_{1-4}-\gamma_{1-3-4})-x_4(x_3\gamma_1-\gamma_{1-3})]\}\ , \quad \text{(B10)}$$

$$V^{(7)}_{(1234)}=-\mathcal{U}_{1234}\{x_1[(\gamma_{1-3-4}-x_3\gamma_{1-4})-x_4(\gamma_{1-3}-x_3\gamma_1)]+x_2[(\gamma_{2-3-4}-x_3\gamma_{2-4})-x_4(\gamma_{2-3}-x_3\gamma_2)]\}\ , \quad \text{(B11)}$$

$$V^{(8)}_{(1234)}=-\mathcal{U}_{1234}\{x_2[x_4(x_3\gamma_{1-3-4}-\gamma_{1-4})-(x_3\gamma_{1-3}-\gamma_1)]+x_1[x_4(x_3\gamma_{2-3-4}-\gamma_{2-4})-(x_3\gamma_{2-3}-\gamma_2)]\}\ , \quad \text{(B12)}$$

$$V^{(9)}_{(1234)}=-\mathcal{U}_{1234}\{x_2[(\gamma_{1-3-4}-x_3\gamma_{1-4})-x_4(\gamma_{1-3}-x_3\gamma_1)]+x_1[(\gamma_{2-3-4}-x_3\gamma_{2-4})-x_4(\gamma_{2-3}-x_3\gamma_2)]\}\ , \quad \text{(B13)}$$

where $\mathcal{U}_{1234}=u_1u_2u_3u_4$.

The diagrammatic representation of the nine vertices is shown in Fig. 17. Since $V^{(4)}$ is the relevant vertex in the two-interacting-magnon Raman scattering, at the lowest order, where the vertex function satisfies a "ladder" Bethe-Salpeter equation [cf. Eq. (3.21)], we have preferred to represent $V^{(4)}$ with the ladder diagram shown in the picture.

The vertex functions have the following symmetry properties under the interchange of the momentum labels:

$$V^{(1)}_{(1234)}=V^{(1)}_{(2134)}=V^{(1)}_{(1243)}\ , \quad \text{(B14a)}$$

$$V^{(2)}_{(1234)}=V^{(2)}_{(1243)}\ , \quad \text{(B14b)}$$

$$V^{(3)}_{(1234)}=V^{(3)}_{(2134)}\ , \quad \text{(B14c)}$$

$$V^{(5)}_{(1234)}=V^{(5)}_{(2134)}\ , \quad \text{(B14d)}$$

$$V^{(6)}_{(1234)}=V^{(6)}_{(1243)}\ , \quad \text{(B14e)}$$

$$V^{(7)}_{(1234)}=V^{(7)}_{(2134)}=V^{(7)}_{(1243)}\ , \quad \text{(B14f)}$$

$$V^{(8)}_{(1234)}=V^{(8)}_{(2134)}=V^{(8)}_{(1243)}\ , \quad \text{(B14g)}$$

$$V^{(9)}_{(1234)}=V^{(9)}_{(2134)}=V^{(9)}_{(1243)}\ . \quad \text{(B14h)}$$

The four momenta labeling the vertex functions $V^{(i)}_{(1234)}$ are not independent because the vertices are always meant to be multiplied by $\delta_{\rm G}(1+2-3-4)$. When $\mathbf{G}=\mathbf{0}$, and therefore $\mathbf{k}_1+\mathbf{k}_2=\mathbf{k}_3+\mathbf{k}_4$, it is easy to see that the following equalities hold:

$$V^{(1)}_{(1234)}=V^{(9)}_{(1234)}\ , \quad \text{(B15a)}$$

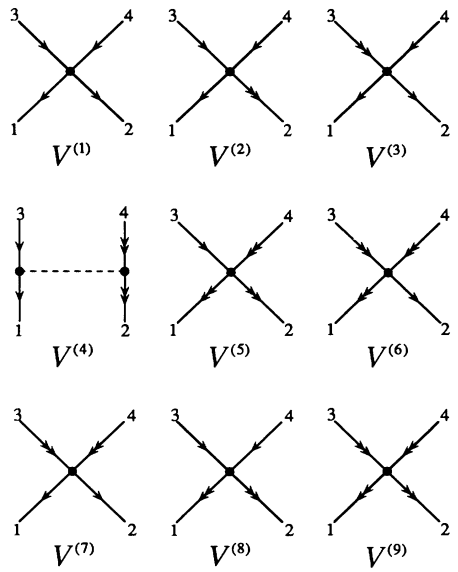

FIG. 17. Feynman diagrams for the nine quartics vertices of the Hamiltonian.

$$V^{(2)}_{(1234)} = V^{(6)}_{(1234)} , \tag{B15b}$$

$$V^{(3)}_{(1234)} = V^{(5)}_{(1234)} , \tag{B15c}$$

$$V^{(7)}_{(1234)} = V^{(8)}_{(1234)} , \tag{B15d}$$

$$V^{(4)}_{(1234)} = V^{(4)}_{(2143)} . \tag{B15e}$$

2. *Raman-scattering operator*

The quartic part of the Raman operator given in Eq. (2.65) can easily be written in the following form:

$$\Lambda'_1 = -\frac{B}{2}\mathcal{P}(\mathbf{E}_{\rm inc},\mathbf{E}_{\rm sc}) \times \sum_{i,\delta}(\pm)[a_i^\dagger a_i b_{i+\delta}^\dagger b_{i+\delta} + \tfrac{1}{2}(a_i^\dagger a_i a_i b_{i+\delta} + a_i^\dagger b_{i+\delta}^\dagger b_{i+\delta} b_{i+\delta})] , \tag{B16}$$

where $(\pm)$ means that vertical bonds must be summed with the *plus* sign whereas horizontal bonds have a *minus* sign in front [cf. Eq. (2.54)]. Notice that this $(\pm)$ is the only important difference with respect to $V'_{\rm DM}$. Proceeding exactly in the same way as we did for $V'_{\rm DM}$, we arrive at Eq. (2.63), where the vertex functions $\tilde{V}^{(1)}_{1234}$, $\tilde{V}^{(2)}_{1234}$, etc., are obtained, respectively, from V_{1234}, $V^{(2)}_{1234}$, etc., simply by replacing, in Eqs. (B5) and (B13), $\gamma_{\mathbf{k}}$ by $\tilde{\gamma}_{\mathbf{k}}$. For instance,

$$\tilde{V}^{(1)}_{(1234)} = -\mathcal{U}_{1234}\{x_1[x_4(x_3\tilde{\gamma}_{1-3-4}-\tilde{\gamma}_{1-4}) - (x_3\tilde{\gamma}_{1-3}-\tilde{\gamma}_1)] + x_2[x_4(x_3\tilde{\gamma}_{2-3-4}-\tilde{\gamma}_{2-4}) - (x_3\tilde{\gamma}_{2-3}-\tilde{\gamma}_2)]\} . \tag{B17}$$

In Fig. 18 we show the Feynman diagrams representing these nine vertices. The symmetry properties given in Eqs. (B14) and (B15) hold for the $\tilde{V}^{(i)}_{(1234)}$'s as well.

Let us consider now the problem of the infrared divergences in $V^{(i)}_{1234}$, $\tilde{V}^{(i)}_{1234}$, $i=1,\ldots,9$. For small values of $k=|\mathbf{k}|$, we have

$$x_{\mathbf{k}} = 1-\frac{k}{\sqrt{2}}+\frac{k^2}{4}+O(k^3) , \tag{B18}$$

$$\gamma_{\mathbf{k}} = 1-\frac{k^2}{4}+O(k^4) , \tag{B19}$$

$$u_{\mathbf{k}} = \left[\frac{\sqrt{2}}{2}\right]^{1/2}\frac{1}{\sqrt{k}}+O(\sqrt{k}) , \tag{B20}$$

$$\tilde{\gamma}_{\mathbf{k}} = \tfrac{1}{4}(k_y^2-k_x^2)+O(k_y^2-k_x^2) . \tag{B21}$$

Therefore, the singular behavior of the DM vertices $V^{(i)}_{1234}$ and $\tilde{V}^{(i)}_{1234}$ is entirely contained in the front factor $\mathcal{U}_{1234}=u_1u_2u_3u_4$: whenever anyone of the four momenta goes to zero, the vertex function has a square-root singularity. Notice, however, that when $\mathbf{k}_3$ or $\mathbf{k}_4$ goes to zero, the arguments of the two square brackets precisely vanish and one can check that the vertex functions are finite in this case. Hence, products of *two* vertices of the form $V^{(i)}_{1234}V^{(j)}_{3412}$, $\tilde{V}^{(i)}_{1234}\tilde{V}^{(j)}_{3412}$, and $V^{(i)}_{1234}\tilde{V}^{(j)}_{3412}$ are finite whenever *any* of the four momenta approaches zero. It turns out that, in all the leading-order four-magnon processes that we study in this paper [which are of $O(1/S^0)$], the product of two vertices—either both from the Hamiltonian, or both from the Raman operator, or one from each—appears in the above combinations; as a result, the matrix elements remain finite even when any of the four momenta vanishes: all the unphysical singularities exactly cancel. This nice characteristic of the DM formalism justifies the use of perturbation theory and it is not shared by the Holstein-Primakoff formalism, where the cancellation of the singularities of the *quartic* terms does not occur.

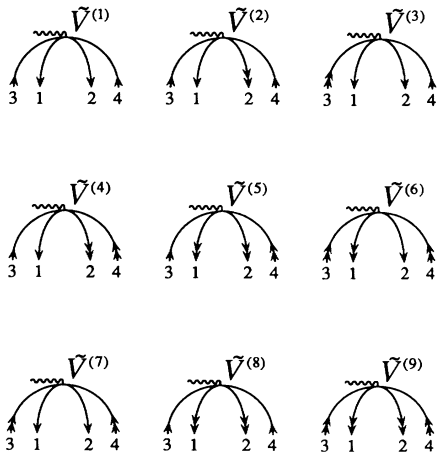

FIG. 18. Feynman diagrams for the nine quartic vertices of the Raman-scattering operator.

APPENDIX C: SOLUTION OF THE LADDER BETHE-SALPETER EQUATION

In the appendix we derive Eq. (3.22) starting from Eqs. (3.20) and (3.21). We will need the following two relations:

$$\sum_{\mathbf{k}} \tilde{\gamma}_{\mathbf{k}} \gamma_{\mathbf{k}} g_{\mathbf{k}} = 0 \ , \tag{C1}$$

$$\sum_{\mathbf{k}} \tilde{\gamma}_{\mathbf{k}} \gamma_{\mathbf{k}-\mathbf{k}_1} g_{\mathbf{k}} = \tilde{\gamma}_{\mathbf{k}_1} \sum_{\mathbf{k}} \tilde{\gamma}_{\mathbf{k}}^2 g_{\mathbf{k}} \ , \tag{C2}$$

or, in terms of $f_{\mathbf{k}} = 2\tilde{\gamma}_{\mathbf{k}}$

$$\sum_{\mathbf{k}} f_{\mathbf{k}} \gamma_{\mathbf{k}} g_{\mathbf{k}} = 0 \ , \tag{C3}$$

$$z \sum_{\mathbf{k}} f_{\mathbf{k}} \gamma_{\mathbf{k}-\mathbf{k}_1} g_{\mathbf{k}} = f_{\mathbf{k}_1} \sum_{\mathbf{k}} f_{\mathbf{k}}^2 g_{\mathbf{k}} \ . \tag{C4}$$

Here $g_{\mathbf{k}}$ is a generic function having the symmetry of the square lattice. We will also need the explicit expression of $V^{(4)}_{\mathbf{k}\mathbf{k}_1\mathbf{k}_1\mathbf{k}}$, which can be rewritten in the form

$$\tfrac{1}{4} V^{(4)}_{\mathbf{k}\mathbf{k}_1\mathbf{k}_1\mathbf{k}} = \left[\frac{1}{2} \gamma_{\mathbf{k}-\mathbf{k}_1} \left(\frac{1}{\varepsilon_{\mathbf{k}}} \frac{1}{\varepsilon_{\mathbf{k}_1}} + 1 \right) - \frac{1}{2} \gamma_{\mathbf{k}} \gamma_{\mathbf{k}_1} \frac{1}{\varepsilon_{\mathbf{k}}} \frac{1}{\varepsilon_{\mathbf{k}_1}} \right] . \tag{C5}$$

Let us rewrite here the two basic equations

$$G^{+}_{\Lambda_0}(\omega) = C \frac{i}{N} \int \frac{d\omega'}{2\pi} \sum_{\mathbf{k}} \frac{f_{\mathbf{k}}}{\varepsilon_{\mathbf{k}}} G^{(0)}_{\alpha\alpha}(\mathbf{k}, \omega+\omega') \times G^{(0)}_{\beta\beta}(\mathbf{k}, \omega') \Gamma_{\mathbf{k}}(\omega, \omega') \ , \tag{C6}$$

$$\Gamma_{\mathbf{k}}(\omega, \omega') = \frac{f_{\mathbf{k}}}{\varepsilon_{\mathbf{k}}} + \frac{Jz}{N} \left[\frac{-i}{\hbar} \right] \times \sum_{\mathbf{k}_1} \int \frac{d\omega_1}{2\pi} \frac{1}{4} V^{(4)}_{\mathbf{k}\mathbf{k}_1\mathbf{k}_1\mathbf{k}} \times G^{(0)}_{\alpha\alpha}(\mathbf{k}_1, \omega+\omega_1) \times G^{(0)}_{\beta\beta}(\mathbf{k}, \omega_1) \Gamma_{\mathbf{k}_1}(\omega, \omega_1) \ , \tag{C7}$$

where $C = N(B/2)^2 g(\mathbf{E}_{\text{inc}}, \mathbf{E}_{\text{sc}}) z [S\alpha(S)]^2$. First, let us substitute Eq. (C7) into Eq. (C6). We obtain

$$G^{+}_{\Lambda_0}(\omega) = C L^{(2)}(\omega) = \mathcal{A}_1(\omega) \ , \tag{C8}$$

where $L^{(2)}(\omega)$ is given in Eq. (3.15) and $\mathcal{A}_1(\omega)$ is defined by

$$\mathcal{A}_1(\omega) = C \frac{i}{N} \sum_{k} \int \frac{d\omega'}{2\pi} \frac{f_{\mathbf{k}}}{\varepsilon_{\mathbf{k}}} G^{(0)}_{\alpha\alpha}(\mathbf{k}, \omega+\omega') G^{(0)}_{\beta\beta}(\mathbf{k}, \omega') \times \frac{Jz}{N} \left[\frac{-i}{\hbar} \right] \sum_{\mathbf{k}_1} \int \frac{d\omega_1}{2\pi} \frac{1}{4} V^{(4)}_{\mathbf{k}\mathbf{k}_1\mathbf{k}_1\mathbf{k}} G^{(0)}_{\alpha\alpha}(\mathbf{k}_1, \omega+\omega_1) G^{(0)}_{\beta\beta}(\mathbf{k}_1, \omega_1) \Gamma_{\mathbf{k}_1}(\omega, \omega_1) \ . \tag{C9}$$

In order to compute $\mathcal{A}_1(\omega)$, we use the explicit expression of $V^{(4)}_{\mathbf{k}\mathbf{k}_1\mathbf{k}_1\mathbf{k}}$ and first we carry out $\sum_k$ using Eqs. (C3) and (C4). We obtain

$$\mathcal{A}_1(\omega) = C \frac{i}{N} \frac{Jz}{N} \left[\frac{-i}{\hbar} \right] \sum_{\mathbf{k}_1} \int \frac{d\omega_1}{2\pi} \frac{f_{\mathbf{k}_1}}{2z} G^{(0)}_{\alpha\alpha}(\mathbf{k}_1, \omega+\omega_1) G^{(0)}_{\beta\beta}(\mathbf{k}_1, \omega_1) \Gamma_{\mathbf{k}_1}(\omega, \omega_1) \times \sum_{\mathbf{k}} \int \frac{d\omega'}{2\pi} \frac{f_{\mathbf{k}}^2}{\varepsilon_{\mathbf{k}}} \left(\frac{1}{\varepsilon_{\mathbf{k}}} \frac{1}{\varepsilon_{\mathbf{k}_1}} + 1 \right) G^{(0)}_{\alpha\alpha}(\mathbf{k}, \omega+\omega') G^{(0)}_{\beta\beta}(\mathbf{k}, \omega') \tag{C10}$$

$$= \left[\frac{-J}{\hbar} \right] G^{+}_{\Lambda_0}(\omega) \tfrac{1}{2} L^{(2)}(\omega) + \mathcal{A}_2(\omega) \ , \tag{C11}$$

where

$$\mathcal{A}_2(\omega) = \tfrac{1}{2} L^{(1)}(\omega) \left[C \left[\frac{-i}{\hbar} \right] \frac{J}{N} \sum_{\mathbf{k}_1} f_{\mathbf{k}_1} \int \frac{d\omega_1}{2\pi} G^{(0)}_{\alpha\alpha}(\mathbf{k}_1, \omega+\omega_1) G^{(0)}_{\beta\beta}(\mathbf{k}_1, \omega_1) \Gamma_{\mathbf{k}_1}(\omega, \omega_1) \right] . \tag{C12}$$

Now, again, we put Eq. (C7) into Eq. (C12), we use Eqs. (C3) and (C4) to disentangle the two sums and we replace the obtained expression for $\mathcal{A}_2$ into Eq. (C11) with the result

$$\mathcal{A}_1(\omega)=\frac{1}{2}\left[\frac{-J}{\hbar}\right]L^{(2)}(\omega)G^{+}_{\Lambda_0}(\omega)+\tfrac{1}{2}C\left[\frac{-J}{\hbar}\right]L^{(1)}(\omega)L^{(1)}(\omega)$$
$$+L^{(1)}(\omega)\tfrac{1}{2}C\left[\frac{-i}{\hbar}\right]\frac{J}{N}\left[\frac{Jz}{N}\left[\frac{-i}{\hbar}\right]\right]$$
$$\times\sum_{\mathbf{k}_2}\int\frac{d\omega_2}{2\pi}\tfrac{1}{2}f_{\mathbf{k}_2}G^{(0)}_{\alpha\alpha}(\mathbf{k}_2,\omega+\omega_2)G^{(0)}_{\beta\beta}(\mathbf{k}_2,\omega_2)\Gamma_{\mathbf{k}_2}(\omega,\omega_2)$$
$$\times\sum_{\mathbf{k}_1}\int\frac{d\omega_1}{2\pi}f^2_{\mathbf{k}_1}\left[\frac{1}{\varepsilon_{\mathbf{k}}}\frac{1}{\varepsilon_{\mathbf{k}_1}}+1\right]G^{(0)}_{\alpha\alpha}(\mathbf{k}_1,\omega+\omega_1)G^{(0)}_{\beta\beta}(\mathbf{k}_1,\omega_1) \tag{C13}$$

$$=\frac{1}{2}\left[\frac{-J}{\hbar}\right]L^{(2)}(\omega)G^{+}_{\Lambda_0}(\omega)+\tfrac{1}{2}C\left[\frac{-J}{\hbar}\right]L^{(1)}(\omega)L^{(1)}(\omega)$$
$$+\frac{1}{4}\left[\frac{J}{\hbar}\right]^2L^{(1)}(\omega)L^{(1)}(\omega)G^{+}_{\Lambda_0}(\omega)+\frac{1}{2}\left[\frac{-J}{\hbar}\right]L^{(0)}(\omega)\mathcal{A}_2(\omega)\ . \tag{C14}$$

Finally, we replace $\mathcal{A}_1(\omega)$ by Eq. (C8) and $\mathcal{A}_2(\omega)$ by Eq. (C11) and we obtain

$$G^{+}_{\Lambda_0}(\omega)-CL^{(2)}(\omega)=-\frac{1}{2}\frac{J}{\hbar}L^{(2)}(\omega)G^{+}_{\Lambda_0}(\omega)-\tfrac{1}{2}C\frac{J}{\hbar}L^{(1)}(\omega)L^{(1)}(\omega)+\frac{1}{4}\left[\frac{J}{\hbar}\right]^2L^{(1)}(\omega)L^{(1)}G^{+}_{\Lambda_0}(\omega)$$
$$-\frac{1}{2}\frac{J}{\hbar}L^{(0)}(\omega)\left[G^{+}_{\Lambda_0}(\omega)-CL^{(2)}(\omega)+\frac{1}{2}\frac{J}{\hbar}L^{(2)}(\omega)G^{+}_{\Lambda_0}(\omega)\right]\ . \tag{C15}$$

At this point we can easily solve for $G^{+}_{\Lambda_0}(\omega)$ and we obtain Eq. (3.22).

Note that, from Eqs. (C3) and (C4), together with the expression of the $V^{(4)}_{\mathbf{k}\mathbf{k}_1\mathbf{k}_1\mathbf{k}}$ given by Eq. (C5), one can see that the only effective part of the vertex function $V^{(4)}_{\mathbf{k}\mathbf{k}_1\mathbf{k}_1\mathbf{k}}$ is the one coming from the Ising term of the Hamiltonian, S^zS^z. The part coming from S^+S^-, which is non-Hermitian in the DM formalism, *does not contribute* in this calculation. Furthermore, exactly for this reason, we would get the same result using the corresponding vertex function $V^{(4)}_{\mathbf{k}\mathbf{k}_1\mathbf{k}_1\mathbf{k}}$ obtained in the Holstein-Primakoff formalism when $\sqrt{1-a^\dagger a/2S}$ is expanded to first order.

APPENDIX D: MAGNON SELF-ENERGY AT $T=0$

In this appendix we study the irreducible self-energy $\Sigma_{\alpha\alpha}(\mathbf{k},\omega)$ relative to the α-magnon propagator up to second order in perturbation theory, namely, at $O(1/S)$ level. The self-energy of the β magnon can then be obtained from the relation $\Sigma_{\beta\beta}(\mathbf{k},\omega)=\Sigma_{\alpha\alpha}(\mathbf{k},-\omega)$. The computation of $\Sigma_{\alpha\alpha}(\mathbf{k},\omega)$ will allow us to determine a correction to the magnon dispersion given in Eq. (2.30) to $O(1/S)$. Indeed the renormalized excitation energy, $\omega_{\mathbf{k}}$, for an α spin wave with wave vector $\mathbf{k}$ is given by the real part of the pole of the propagator $G_{\alpha\alpha}(\mathbf{k},\omega)$, that is, by the real part of the solution of the equation, for fixed $\mathbf{k}$,

$$\omega-\Omega_{\mathbf{k}}-\Sigma_{\alpha\alpha}(\mathbf{k},\omega)=0\ , \tag{D1}$$

where $\Omega_{\mathbf{k}}$ is the linear-spin-wave dispersion renormalized by Oguchi corrections, given in Eq. (2.30),

$$\Omega_{\mathbf{k}}=\Omega_{\max}\varepsilon_{\mathbf{k}}=\frac{Jz}{\hbar}\left[S+\frac{r}{2}S^0\right]\varepsilon_{\mathbf{k}}\ . \tag{D2}$$

Since the perturbation scheme that we use in this paper is based on the assumption that self-energy corrections are small compared with $\Omega_{\mathbf{k}}$, we expect that the solution of Eq. (D1) is given approximately by[40]

$$\omega_{\mathbf{k}}\simeq\Omega_{\mathbf{k}}+\mathrm{Re}\Sigma_{\alpha\alpha}(\mathbf{k},\Omega_{\mathbf{k}})\ . \tag{D3}$$

We will refer to $\Sigma_{\alpha\alpha}(\mathbf{k},\omega_{\mathbf{k}})\simeq\Sigma_{\alpha\alpha}(\mathbf{k},\Omega_k)$ as the *on-shell* self-energy and to $\Sigma_{\alpha\alpha}(\mathbf{k},\omega)$ as the *off-shell* self-energy, when $\omega\neq\omega_{\mathbf{k}}$.

The magnon damping is defined by

$$\hbar\Gamma(\mathbf{k},\omega)=-\mathrm{Im}\Sigma_{\alpha\alpha}(\mathbf{k},\omega)\ , \tag{D4}$$

and again we shall refer to $\Gamma(\mathbf{k},\omega_{\mathbf{k}})$ as the on-shell damping and to $\Gamma(\mathbf{k},\omega)$—when $\omega\neq\omega_{\mathbf{k}}$—as the off-shell damping, respectively.

The rotational invariance of the Hamiltonian in spin space guarantees that the elementary excitations of the system are gapless, namely,

$$\lim_{\mathbf{k}\to0}\omega_{\mathbf{k}}=0\ . \tag{D5}$$

Since $\Omega_{\mathbf{k}}=O(k)$ for small $\mathbf{k}$, this implies that

$$\lim_{\mathbf{k}\to0}\Sigma_{\alpha\alpha}(\mathbf{k},\omega=0)=0\ . \tag{D6}$$

More generally we have

$$\lim_{\mathbf{k}\to0}\Sigma_{\mu\nu}(\mathbf{k},\omega=0)=0\ . \tag{D7}$$

We shall prove that this condition is satisfied order by order in perturbation theory.

We now proceed to study $\Sigma_{\alpha\alpha}(\mathbf{k},\omega)$ at first and second order. Some simple rules, valid for Feynman diagrams of bosons systems at $T=0$, turn out to be very useful in deciding which are the nonvanishing terms that will contribute. We are studying a boson theory at $T=0$, where the unperturbed ground state is the boson vacuum. Therefore, the bare propagator $G^{(0)}_{\alpha\alpha}(\mathbf{k};t-t') = -i\langle 0|\mathcal{T}\alpha_{\mathbf{k}}(t)\alpha^{\dagger}_{\mathbf{k}}(t')|0\rangle$ vanishes if $t'<t$. Thus, $G^{(0)}_{\alpha\alpha}$ only propagates forward in time: in contrast to the degenerate Fermi system case, there is no hole propagation. In fact, since the β propagator has been defined according to Eq. (2.34), it follows that $G^{(0)}_{\beta\beta}$ vanishes if $t'>t$. Formally this resembles more a "hole" propagation. In this case no "particle" propagation ($t'<t$) is possible. We can think of the α magnon as a "particle" and the β magnon as a "hole." This has two consequences. First, there cannot be any contraction within any of the vertices $V^{(i)}$ since the vertices have already been normal ordered and the contraction

$$\langle 0|\mathcal{T}\alpha^{\dagger}_{\mathbf{k}}(t)\alpha_{\mathbf{k}}(t)|0\rangle \equiv \langle 0|\mathcal{T}\alpha^{\dagger}_{\mathbf{k}}(t^{+})\alpha_{\mathbf{k}}(t)|0\rangle = 0 \ . \tag{D8}$$

Thus, a Feynman diagram vanishes if there is a particle (hole) line $G^{(0)}_{\alpha\alpha}$ ($G^{(0)}_{\beta\beta}$) that closes on itself. Secondly, we know that a Feynman diagram is integrated over all internal variables, which means that all possible time orderings are included. No diagram can contribute unless there is some time ordering in which all the particle lines $G^{(0)}_{\alpha\alpha}$ run forward in time and the hole lines $G^{(0)}_{\beta\beta}$ run backwards. As a result, diagrams, at any order in perturbation theory, in which two particle (hole) lines have their ends joined by the *same two interactions* and run in *opposite* directions, are identically zero. These two restrictions eliminate all the self-energy diagrams, of any order in perturbation theory, as long as we restrict ourselves to the $V^{(1)}$, $V^{(4)}$, $V^{(9)}$, that is, vertices which conserve the particle number separately for the α and β magnons: indeed, these vertices commute with $N_{\alpha}=\sum_{\mathbf{k}}\alpha^{\dagger}_{\mathbf{k}}\alpha_{\mathbf{k}}$ and $N_{\beta}=\sum_{\mathbf{k}}\beta^{\dagger}_{\mathbf{k}}\beta_{\mathbf{k}}$ and therefore the diagrams that they generate always contain two particles (holes) running in opposite directions and joining the same two vertices.

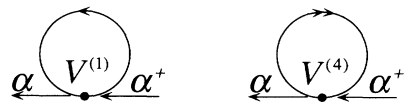

FIG. 19. First-order self-energy diagrams for α magnon.

By using these rules it is easy to see that all the first-order self-energy diagrams, shown in Fig. 19, vanish at $T=0$. Therefore, Eq. (D1) does not give any correction to the spin-wave dispersion at first order. This, however, was to be expected because a correction of $O(S^0)$ to the LSW dispersion has already been taken into account by the Oguchi correction, which comes about exactly from the normal ordering of the quartic interactions.

A nonzero self-energy is obtained at second order. Second-order self-energy diagrams are shown in Fig. 20. The diagrams shown in Fig. 20(a) vanish because of the rules that we have just discussed. In Fig. 20(b) we show all the nonzero second-order diagrams. The second-order self-energy is given by

$$\Sigma^{(2)}_{\alpha\alpha}(\mathbf{k},\omega) = \Omega_{\max}\frac{1}{[4S\alpha(S)]^2}\frac{1}{N^2} \times \sum_{(234)}\delta_{\mathbf{G}}(\mathbf{k}+2-3-4)\left[2V^{(2)}_{(\mathbf{k}234)}V^{(3)}_{(432\mathbf{k})}\frac{1}{\tilde{\omega}-\varepsilon_2-\varepsilon_3-\varepsilon_4+i\eta} - 8V^{(7)}_{(\mathbf{k}234)}V^{(8)}_{(432\mathbf{k})}\frac{1}{\tilde{\omega}+\varepsilon_2+\varepsilon_3+\varepsilon_4-i\eta}\right] . \tag{D9}$$

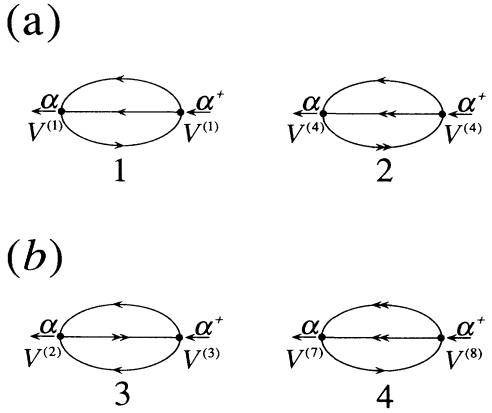

FIG. 20. Second-order self-energy diagrams for α magnon. (a) Diagrams 1 and 2 vanish at $T=0$; (b) diagrams 3 and 4 are the only nonzero contributions.

In deriving Eq. (D9) we have used the symmetry properties of the vertex functions under the interchange of momentum labels [cf. Eqs. (B14) and (B15)].

As we can see from the diagrams, these self-energy insertions correspond to "three-one" (confluence-splitting) mechanisms, in which, for example, a particle of momentum $\mathbf{k}$ and energy ω decays into three particles, conserving momentum, and energy. From Eq. (D9) we can also see that the imaginary part of the on-shell self-energy is rigorously zero because the two conditions $\delta(\mathbf{k}+2-3-4)$ and $\delta(\varepsilon_{\mathbf{k}}-\varepsilon_2-\varepsilon_3-\varepsilon_4)$ cannot be satisfied simultaneously. This is due to fact that the dispersion $\varepsilon_{\mathbf{k}}$ is a convex function of $\mathbf{k}$ for all $\mathbf{k}$, and therefore a spontaneous decay of one on-shell magnon into n on-shell magnons, in which energy and momentum are simultaneously conserved, is not possible (cf. Appendix E of Ref. 22). Hence, the on-shell magnon damping calculated up to second order in perturbation theory at $T=0$ is zero for

any $\mathbf{k}$. In fact, it follows easily that

$$\Gamma^{(2)}(\mathbf{k},\omega)=0 \quad \text{for } |\omega|\leq\Omega_{\mathbf{k}} . \tag{D10}$$

We expect this result—based on the negative curvature of the magnon dispersion—to hold at any order in perturbation theory, since we shall soon see that $\mathrm{Re}\|\underline{\Sigma}(\mathbf{k},\omega)\|/\Omega_{\mathbf{k}}\ll 1$, so that the renormalized magnon energy will be also a convex function of $\mathbf{k}$.

Recently the Dyson-Maleev formalism has been used to calculate the magnon damping in the two-dimensional HAFM at asymptotically low temperatures, both at long wavelengths[29] and at short wavelengths.[23] In all cases it was shown that the damping for all momenta is much smaller than the frequency of excitations, so that even in two dimensions, magnons are very well-defined quasiparticles, provided that $k\xi\gg 1$, where ξ is the correlation length, which is of order of $\exp(\mathrm{const}/T)$. The vanishing of the on-shell damping at $T=0$ is quite independent of the value of the spin S and the wave vector $\mathbf{k}$. However, it has been derived within the context of spin-wave theory which is generally believed to be valid for large S. Therefore, one could wonder if these arguments still hold for small S. For long wavelengths this picture is certainly still valid if the ground state is *ordered* because, following Dyson,[20] kinematic restrictions due to the finite value of S are not important in this case. This follows also from the renormalization-group analysis of Chakravarty, Halperin, and Nelson,[37] which shows that, at $T=0$, if the ground state is ordered, the long-wavelength limit of a small-S is equivalent to the large-S limit. Of course, the problem is that, for the Raman scattering, we are particularly interested in the case of $S=\frac{1}{2}$ and short wavelengths. One can image that, in this case, some other formalism that takes into account the real quantum nature of the spins better that spin-wave theory might yield a class of elementary excitations essentially different from spin waves.[9] In this paper, however, we shall remain in the framework of spin-wave theory, with the hope that, even in this extreme situation of small S and short wavelengths, its results are still valid, provided that we use the correct quantum-fluctuation-renormalized values for the magnon dispersion and spin stiffness constant.

We now turn to the study of the second-order self-energy in greater detail. First, we want to show that the gaplessness of the spin-wave modes is preserved by the second-order self-energy correction. We are interested in $\Sigma^{(2)}_{\alpha\alpha}(\mathbf{k},\omega=0)$ for $\mathbf{k}\approx 0$. We shall need the following limiting expressions:[23]

$$x_{\mathbf{k}}=1-\frac{k}{\sqrt{2}}+\frac{k^2}{4}+O(k^3) , \tag{D11}$$

$$\gamma_{\mathbf{k}}=1-\frac{k^2}{4}+O(k^4) , \tag{D12}$$

$$u^2_{\mathbf{k}}=\frac{\sqrt{2}}{2}\frac{1}{k}+O(k^0) , \tag{D13}$$

$$\gamma_{\mathbf{q}-\mathbf{k}}=\gamma_{\mathbf{q}}+\tfrac{1}{2}\mathbf{V}_{\mathbf{q}}\cdot\mathbf{k}-\tfrac{1}{4}\mathbf{k}\mathcal{M}_{\mathbf{q}}\mathbf{k}+O(k^3) , \tag{D14}$$

where the vector $\mathbf{V}_{\mathbf{q}}$ and the matrix $\mathcal{M}_{\mathbf{q}}$ are defined by

$$\mathbf{V}^{\mu}_{\mathbf{q}}\equiv -2\partial^{\mu}\gamma_{\mathbf{q}}=\sin q^{\mu} , \tag{D15}$$

$$\mathcal{M}^{\mu\nu}_{\mathbf{q}}\equiv -2\partial^{\mu}\partial^{\nu}\gamma_{\mathbf{q}}=\delta^{\mu\nu}\cos q^{\mu} . \tag{D16}$$

Using these equations, we now expand the two matrix elements in Eq. (D9) around $\mathbf{k}=0$. Let us consider, for instance, $V^{(2)}_{(\mathbf{k}234)}V^{(3)}_{(432\mathbf{k})}$,

$$\begin{aligned}2V^{(2)}_{(\mathbf{k}234)}V^{(3)}_{(432\mathbf{k})}=4(u_{\mathbf{k}}u_2u_3u_4)^2\{&x_{\mathbf{k}}x_2[x_4(\gamma_{\mathbf{k}-4}-x_3\gamma_{\mathbf{k}-3-4})-(\gamma_{\mathbf{k}}-x_3\gamma_{\mathbf{k}-3})]\\&+[x_4(\gamma_{2-4}-x_2\gamma_{2-3-4})-(\gamma_2-x_3\gamma_{2-3})]\}\\\times\{&x_4[(\gamma_{4-2}-x_2\gamma_4)-x_{\mathbf{k}}(\gamma_{4-2-\mathbf{k}}-x_2\gamma_{4-\mathbf{k}})]+x_3[(\gamma_{3-2}-x_2\gamma_3)-x_{\mathbf{k}}(\gamma_{3-2-\mathbf{k}}-x_2\gamma_{3-k})]\} .\end{aligned} \tag{D17}$$

The prefactor contains $u^2_{\mathbf{k}}$ which diverges like $1/k$. However, the argument of the second curly bracket vanishes at $\mathbf{k}=0$. Expanding we get

$$\begin{aligned}2V^{(2)}_{(\mathbf{k}234)}V^{(3)}_{(432\mathbf{k})}=8(u_2u_3u_4)^2\left[\frac{\sqrt{2}/2}{k}+O(1)\right]&\{x_2[x_4(\gamma_4-x_3\gamma_{3+4})-(1-x_3\gamma_3)]\\&+[x_4(\gamma_{2-4}-x_2\gamma_{2-3-4})-(\gamma_2-x_3\gamma_{2-3})]+f(\mathbf{k})\}\\\times\Bigg[&\left[\frac{k}{\sqrt{2}}-\frac{k^2}{4}\right][x_4(\gamma_{4-2}-x_2\gamma_4)+x_3(\gamma_{3-2}-x_2\gamma_3)]\\&-\frac{1}{2}\left[1-\frac{\sqrt{2}k}{2}+\frac{k^2}{4}\right][x_4(\mathbf{V}_{4-2}-x_2\mathbf{V}_4)+x_3(\mathbf{V}_{3-2}-x_2\mathbf{V}_3)]\cdot\mathbf{k}\\&+\mathbf{k}[x_4(\mathcal{M}_{4-2}-x_2\mathcal{M}_4)+x_3(\mathcal{M}_{3-2}-x_2\mathcal{M}_3)]\mathbf{k}+O(k^4)\Bigg] ,\end{aligned} \tag{D18}$$

where $f(\mathbf{k})$ is a function than vanishes linearly with $\mathbf{k}$. Similarly for the other matrix element we obtain

$$8V^{(8)}_{(\mathbf{k}234)}V^{(7)}_{(432\mathbf{k})}=8(u_2u_3u_4)^2\left[\frac{\sqrt{2}/2}{k}+O(1)\right]\{x_2[x_4(\gamma_4-x_3\gamma_{3+4})-(1-x_3\gamma_3)]$$
$$+[x_4(\gamma_{2-4}-x_2\gamma_{2-3-4})-(\gamma_2-x_3\gamma_{2-3})]+g(\mathbf{k})\}$$
$$\times\left[-\left[\frac{k}{\sqrt{2}}-\frac{k^2}{4}\right][x_4(\gamma_{4-2}-x_2\gamma_4)+x_3(\gamma_{3-2}-x_2\gamma_3)]\right.$$
$$-\frac{1}{2}[x_4(\mathbf{V}_{4-2}-x_2\mathbf{V}_4)+x_3(\mathbf{V}_{3-2}-x_2\mathbf{V}_3)]\cdot\mathbf{k}$$
$$\left.+\mathbf{k}[x_4(\mathcal{M}_{4-2}-x_2\mathcal{M}_4)+x_3(\mathcal{M}_{3-2}-x_2\mathcal{M}_3)]\mathbf{k}+O(k^4)\right], \tag{D19}$$

where, again, $g(\mathbf{k})$ is a function that vanishes linearly with $\mathbf{k}$.

Summing up the two terms we get

$$2V^{(2)}_{(\mathbf{k}234)}V^{(3)}_{(432\mathbf{k})}+8V^{(8)}_{(\mathbf{k}234)}V^{(7)}_{(432\mathbf{k})}=-4\sqrt{2}(u_2u_3u_4)^2\{x_2[x_4(\gamma_4-x_3\gamma_{3+4})-(1-x_3\gamma_3)]$$
$$+[x_4(\gamma_{2-4}-x_2\gamma_{2-3-4})-(\gamma_2-x_3\gamma_{2-3})]\}$$
$$\times\{x_4(\mathbf{V}_{4-2}-x_2\mathbf{V}_4)+x_3(\mathbf{V}_{3-2}-x_2\mathbf{V}_3)\}\cdot\hat{\mathbf{k}}+O(k)\,. \tag{D20}$$

The term proportional to the unit vector $\hat{\mathbf{k}}$ vanishes when we sum the matrix elements over $\mathbf{k}_2$, $\mathbf{k}_3$, $\mathbf{k}_4$ in Eq. (D9) because the self-energy has the point-group symmetry of the square lattice [cf. Eq. (2.47)]. Therefore, the conclusion is that the on-shell self-energy $\Sigma^{(2)}_{\alpha\alpha}(\mathbf{k},\omega=0)$ vanishes *linearly* when $\mathbf{k}\to 0$. For small k we can therefore write

$$\Sigma^{(2)}_{\alpha\alpha}(\mathbf{k},\Omega_{\mathbf{k}})=\Omega_{\max}\frac{\delta}{[2S\alpha(S)]^2}\frac{\sqrt{2}}{2}ak+O(k^2)\,, \tag{D21}$$

where, as we shall see, δ is a small *positive* constant.

We have computed numerically, for several values of $\mathbf{k}$ inside the HAFM Brillouin zone, $\Gamma^{(2)}_{\alpha\alpha}(\mathbf{k},\omega)$ as a function of ω. From this, using the Kronig-Kramers relation, we have evaluated the real part of $\Sigma^{(2)}_{\alpha\alpha}(\mathbf{k},\omega)$, as a function of ω. This allowed us to estimate the magnon dispersion corrected by the second-order self-energy, namely, at $O(1/S)$.

In Figs. 21 we show the second-order self-energy—real and imaginary parts—for a $\mathbf{k}$ vector close to the center of the HAFM Brillouin zone [Fig. 21(a)] and a $\mathbf{k}$ vector on the Brillouin-zone boundary [Fig. 21(b)]. [The solid line is $\Gamma^{(2)}_{\alpha\alpha}(\mathbf{k},\omega)$, the dotted line is $\mathrm{Re}\Sigma^{(2)}_{\alpha\alpha}(\mathbf{k},\omega)$.] $\Gamma^{(2)}_{\alpha\alpha}(\mathbf{k},\omega)$ as a function of $\tilde{\omega}=\omega/\Omega_{\max}$, for fixed $\mathbf{k}$, is zero for $|\tilde{\omega}|\le\varepsilon_{\mathbf{k}}$, as expected. For $|\tilde{\omega}|>\varepsilon_{\mathbf{k}}$, $\Gamma^{(2)}_{\alpha\alpha}(\mathbf{k},\omega)$ starts out very soft but positive, so that the condition

$$-\mathrm{Im}\left[\frac{1}{\omega-\Omega_{\mathbf{k}}-\Sigma^{(2)}_{\alpha\alpha}(\mathbf{k},\omega)}\right]\ge 0 \tag{D22}$$

is satisfied for $\tilde{\omega}\approx\varepsilon_k$, namely, around the on-shell position. Quite soon, however, for $\tilde{\omega}>\varepsilon_{\mathbf{k}}$, $\Gamma^{(2)}_{\alpha\alpha}(\mathbf{k},\omega)$ changes sign becoming negative and it keeps decreasing until it reaches a minimum around $\tilde{\omega}=2$. Then it starts to increase again, it changes sign and, after reaching a maximum around $\tilde{\omega}=2.6$–2.8, it drops suddenly to zero at

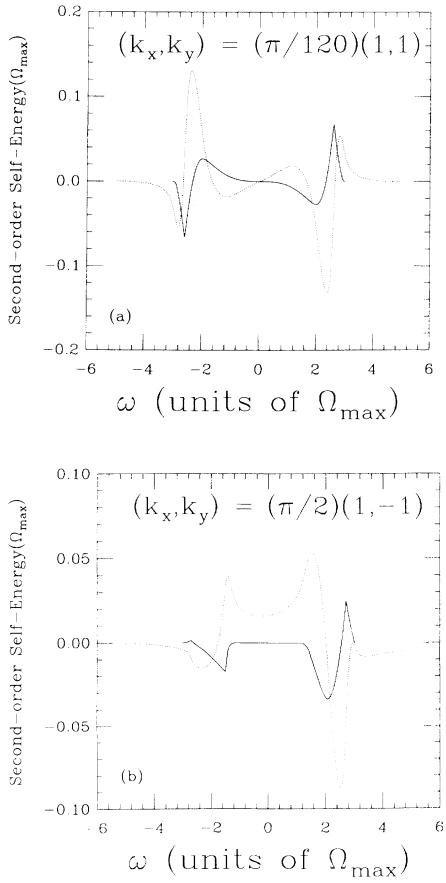

FIG. 21. Second-order self-energy for $S=\frac{1}{2}$ as a function of $\tilde{\omega}$ for two different values of $\mathbf{k}$. The solid curve is $-(1/\pi)\mathrm{Im}\Sigma^{(2)}$. The dotted curve is $\mathrm{Re}\Sigma^{(2)}$. (a) $\mathbf{k}=(\pi/120)(1,1)$ (it is close to the zone center); (b) $\mathbf{k}=(\pi/2)(1,-1)$ (it is on the zone boundary).

$\tilde{\omega}=3$. Notice that for $\mathbf{k}$ close to the zone center, the self-energy is almost, but not perfectly, antisymmetric with respect to the y axis; whereas for $\mathbf{k}$ on the zone boundary, the behavior of the self-energy for negative $\tilde{\omega}$ is similar to the behavior for positive $\tilde{\omega}$. From Figs. 21 we see that, away from the mass shell, the self-energy is not so small; nevertheless, the condition $|\Sigma^{(2)}_{\alpha\alpha}(\mathbf{k},\omega)|/\varepsilon_{\mathbf{k}} \ll 1$ is certainly satisfied for $\tilde{\omega}\approx\varepsilon_{\mathbf{k}}$. The fact that the imaginary part of the self-energy—and therefore the magnon spectral density—can be negative is due to the non-Hermiticity of the boson Hamiltonian. Of course, we expect other more physically relevant quantities, e.g., the spin spectral density, namely, the imaginary part of the spin-spin correlation function, to be positive definite, when all the different contributions are properly summed.

From the real part of $\Sigma^{(2)}_{\alpha\alpha}(\mathbf{k},\omega)$ we have computed, through Eq. (D3), the correction to the magnon dispersion at $O(1/S)$ level. We find that the correction is small and positive—i.e., the magnon dispersion becomes slightly stiffer. In Fig. 22 we show the result for

$$R_{\mathbf{k}}=[2S\alpha(S)]^2\frac{\Sigma^{(2)}_{\alpha\alpha}(\mathbf{k},\Omega_{\mathbf{k}})}{\Omega_{\mathbf{k}}} \tag{D23}$$

as a function of $\mathbf{k}$ inside the antiferromagnetic Brillouin zone. $R_{\mathbf{k}}$ is about 0.021 for $\mathbf{k}$ close to the zone center where it develops a very soft minimum. This is in agreement with Eq. (D21) with $\delta\approx 0.021$. $R_{\mathbf{k}}$ has a maximum on the zone boundary at $\mathbf{k}=(\pm\pi/2,\pm\pi/2)$, where its value is ≈ 0.039 but then it drops again to 0.021 for $\mathbf{k}=(\pm\pi/2,0)$ and $\mathbf{k}=(0,\pm\pi/2)$. The value of δ allows us to estimate the value of the renormalization constant of the spin-wave velocity at $O(1/S^2)$ level.

The spin-wave velocity c is defined as the coefficient such that

$$\omega_{\mathbf{k}}\approx ck \tag{D24}$$

as $k\rightarrow 0$.

Linear-spin-wave theory gives

$$\omega_{\mathbf{k}}=\frac{JzS}{\hbar}\varepsilon_{\mathbf{k}}\approx\frac{\sqrt{2}}{2}\frac{JazS}{\hbar}k\ , \tag{D25}$$

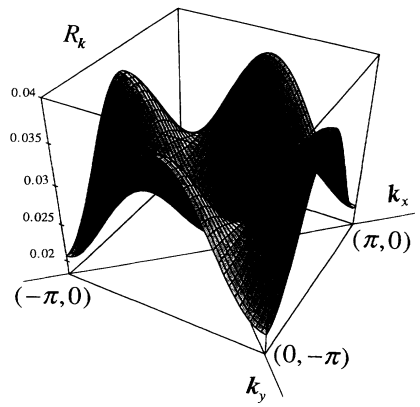

FIG. 22. Normalized self-energy $R_{\mathbf{k}}$, defined in Eq. (D23), as a function of the wave vector inside the HAFM Brillouin zone.

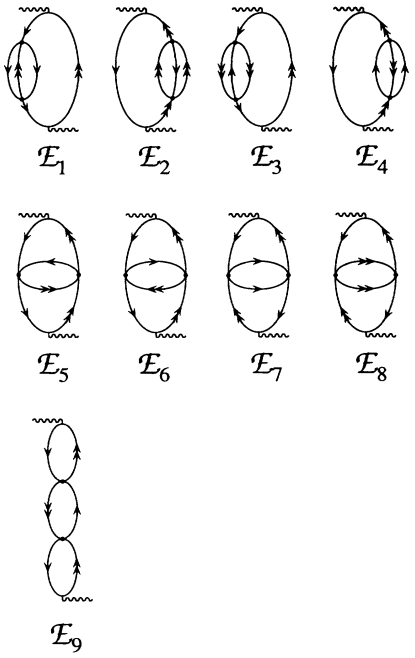

FIG. 23. Second-order diagrams contributing to $\Pi^{(3)}$.

so that

$$c_{\mathrm{LSW}}=\frac{\sqrt{8}JaS}{\hbar}\ . \tag{D26}$$

If we add the Oguchi correction

$$\omega_{\mathbf{k}}=\Omega_{\mathbf{k}}=\frac{JzS\alpha(S)}{\hbar}\varepsilon_{\mathbf{k}}\approx\frac{\sqrt{2}}{2}\frac{JazS\alpha(S)}{\hbar}k \tag{D27}$$

and

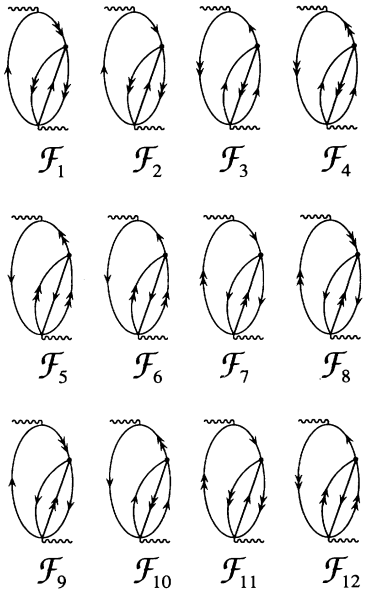

FIG. 24. First-order (the lowest nonvanishing) interference diagrams.

$$c_{\mathrm{Og}}=\frac{\sqrt{2}}{2}\frac{JazS\alpha(S)}{\hbar}=Z_{\mathrm{Og}}c_{\mathrm{LSW}}\ , \tag{D28}$$

with

$$Z_{\mathrm{Og}}=\alpha(S)=1+\frac{0.158}{2S}\ . \tag{D29}$$

If we consider the correction coming from the second-order self-energy, we have

$$\omega_{\mathbf{k}}=\Omega_{\mathbf{k}}+\Sigma^{(2)}_{\alpha\alpha}(\mathbf{k},\Omega_{\mathbf{k}})\approx\Omega_{\max}\frac{\sqrt{2}}{2}\left[1+\frac{\delta}{[2S\alpha(S)]^2}\right]ak\ . \tag{D30}$$

The spin-wave velocity is

$$c=\Omega_{\max}a\frac{\sqrt{2}}{2}\left[1+\frac{\delta}{[2S\alpha(S)]^2}\right]=Z_c c_{\mathrm{LSW}}\ , \tag{D31}$$

with

$$Z_c=\left[1+\frac{\delta}{[2S\alpha(S)]^2}\right]\alpha(S)\ . \tag{D32}$$

For $S=\frac{1}{2}$ we get $Z_c\approx 1.177$, which is very close to the series-expansion result,[24] $Z_c=1.18\pm0.02$. Notice that, near the zone center, the numerical evaluation of the function $R_{\mathbf{k}}$ is quite tricky because, for $\mathbf{k}\approx\mathbf{0}$, the self-energy is given by the difference between almost equal terms, whose magnitude diverges as $\mathbf{k}\to\mathbf{0}$. A careful numerical analysis of this problem, showing how the value of δ has actually been achieved, has been given elsewhere.[33]

APPENDIX E: SECOND-ORDER DIAGRAMS FOR $\Pi^{(3)}_{\mathbf{kk}'}(\omega)$

In this appendix we write down the analytical expressions of all the second-order diagrams that contribute to $\Pi^{(3)}_{\mathbf{kk}'}(\omega)$. The diagrams are shown in Fig. 23. (Notice that the ladder diagrams studied explicitly in Sec. III A 2 are not included here.) As discussed in Sec. III A 3, these diagrams are the most important contributions—in fact, the only relevant ones—to the *indirect* four-magnon production. Similar expressions have been computed for the other nine correlation functions $\Pi^{(3)}_{\mathbf{kk}'}(\omega)$, $i=1,2,4,\ldots,10$, but they are not reported here:

$$\mathcal{E}_1=2C\delta_{\mathbf{kk}'}\left[\frac{1}{\tilde{\omega}-2\varepsilon_{\mathbf{k}}+i\eta}\right]^2\sum_{(234)}\left[\delta_{\mathrm{G}}(\mathbf{k}+2-3-4)V^{(2)}_{(\mathbf{k}234)}V^{(3)}_{(432\mathbf{k})}\frac{1}{\tilde{\omega}-\varepsilon_{\mathbf{k}}-\varepsilon_2-\varepsilon_3-\varepsilon_4+i\eta}\right]\ , \tag{E1}$$

$$\mathcal{E}_2=\mathcal{E}_1\ , \tag{E2}$$

$$\mathcal{E}_3=-8C\delta_{\mathbf{kk}'}\left[\frac{1}{\tilde{\omega}-2\varepsilon_{\mathbf{k}}+i\eta}\right]^2\sum_{(234)}\left[\delta_{\mathrm{G}}(\mathbf{k}+2-3-4)V^{(7)}_{(342\mathbf{k})}V^{(8)}_{(2\mathbf{k}34)}\frac{\tilde{\omega}-\varepsilon_{\mathbf{k}}+\varepsilon_2+\varepsilon_3+\varepsilon_4}{(\varepsilon_{\mathbf{k}}+\varepsilon_2+\varepsilon_3+\varepsilon_4)^2}\right]\ , \tag{E3}$$

$$\mathcal{E}_4=\mathcal{E}_3\ , \tag{E4}$$

$$\mathcal{E}_5=4C\sum_{(1234)}\left[\delta_{\mathrm{G}}(1+2-3-4)\delta_{\mathbf{k}1}\delta_{\mathbf{k}'3}V^{(2)}_{(1234)}V^{(6)}_{(3412)}\frac{1}{\tilde{\omega}-2\varepsilon_1+i\eta}\frac{1}{\tilde{\omega}-2\varepsilon_3+i\eta}\frac{1}{\tilde{\omega}-\varepsilon_1-\varepsilon_2-\varepsilon_3-\varepsilon_4+i\eta}\right]\ , \tag{E5}$$

$$\mathcal{E}_6=4C\sum_{(1234)}\left[\delta_{\mathrm{G}}(1+2-3-4)\delta_{\mathbf{k}1}\delta_{\mathbf{k}'3}V^{(3)}_{(1243)}V^{(5)}_{(4321)}\frac{1}{\tilde{\omega}-2\varepsilon_1+i\eta}\frac{1}{\tilde{\omega}-2\varepsilon_3+i\eta}\frac{1}{\tilde{\omega}-\varepsilon_1-\varepsilon_2-\varepsilon_3-\varepsilon_4+i\eta}\right]\ , \tag{E6}$$

$$\mathcal{E}_7=4C\sum_{(1234)}\left[\delta_{\mathrm{G}}(1+2-3-4)\delta_{\mathbf{k}1}\delta_{\mathbf{k}'2}V^{(2)}_{(1243)}V^{(3)}_{(4312)}\frac{1}{\tilde{\omega}-2\varepsilon_1+i\eta}\frac{1}{\tilde{\omega}-2\varepsilon_2+i\eta}\frac{1}{\tilde{\omega}-\varepsilon_1-\varepsilon_2-\varepsilon_3-\varepsilon_4+i\eta}\right]\ , \tag{E7}$$

$$\mathcal{E}_8=\mathcal{E}_7\ , \tag{E8}$$

$$\mathcal{E}_9=-16C\sum_{1}\left[V^{(7)}_{(1\mathbf{k}\mathbf{k}1)}V^{(8)}_{(1\mathbf{k}'\mathbf{k}'1)}\frac{1}{\tilde{\omega}-2\varepsilon_{\mathbf{k}}+i\eta}\frac{1}{\tilde{\omega}-2\varepsilon_{\mathbf{k}'}+i\eta}\frac{1}{\tilde{\omega}+2\varepsilon_1-i\eta}\right]\ , \tag{E9}$$

where $C=(1/\Omega_{\max})[1/S\alpha(S)]^2(1/4N)^2$. In deriving Eqs. (E2) and (E8), we have used the following symmetry property of the DM vertices:

$$\delta_{\mathrm{G}}(\mathbf{k}+2-3-4)V^{(2)}_{(\mathbf{k}234)}V^{(3)}_{(432\mathbf{k})}=\delta_{\mathrm{G}}(\mathbf{k}+2-3-4)V^{(6)}_{(\mathbf{k}234)}V^{(5)}_{(432\mathbf{k})}\ . \tag{E10}$$

APPENDIX F: INTERFERENCE DIAGRAMS

In this appendix we consider all of the interference diagrams contributing to $G_{\Lambda_{10}}$ at the lowest order in V_{DM}. These diagrams are shown in Fig. 24. Here are their analytical expressions:

$$\mathcal{I}_1=4K\sum_{(1234)}\left[\delta_G\frac{\tilde{\gamma}_4}{\varepsilon_4}\tilde{V}^{(7)}_{(4321)}V^{(5)}_{(1234)}\frac{1}{\tilde{\omega}+2\varepsilon_4-i\eta}\frac{1}{\tilde{\omega}+\varepsilon_1+\varepsilon_2+\varepsilon_3+\varepsilon_4-i\eta}\right], \tag{F1}$$

$$\mathcal{I}_2=-8K\sum_{(1234)}\left[\delta_G\frac{\gamma_1\tilde{\gamma}_1}{\varepsilon_1}\tilde{V}^{(7)}_{(1234)}V^{(8)}_{(3412)}\frac{1}{\varepsilon_1+\varepsilon_2+\varepsilon_3+\varepsilon_4}\frac{1}{\tilde{\omega}+\varepsilon_1+\varepsilon_2+\varepsilon_3+\varepsilon_4-i\eta}\right], \tag{F2}$$

$$\mathcal{I}_3=4K\sum_{(1234)}\left[\delta_G\frac{\tilde{\gamma}_1}{\varepsilon_1}\tilde{V}^{(7)}_{(4321)}V^{(2)}_{(1234)}\frac{1}{\tilde{\omega}+2\varepsilon_1-i\eta}\frac{1}{\tilde{\omega}+\varepsilon_1+\varepsilon_2+\varepsilon_3+\varepsilon_4-i\eta}\right], \tag{F3}$$

$$\mathcal{I}_4=-8K\sum_{(1234)}\left[\delta_G\frac{\gamma_3\tilde{\gamma}_3}{\varepsilon_3}\tilde{V}^{(7)}_{(1234)}V^{(8)}_{(3412)}\frac{1}{\varepsilon_1+\varepsilon_2+\varepsilon_3+\varepsilon_4}\frac{1}{\tilde{\omega}+\varepsilon_1+\varepsilon_2+\varepsilon_3+\varepsilon_4-i\eta}\right], \tag{F4}$$

$$\mathcal{I}_5=4K\sum_{(1234)}\left[\delta_G\frac{\tilde{\gamma}_1}{\varepsilon_1}\tilde{V}^{(8)}_{(4321)}V^{(6)}_{(1234)}\frac{1}{\tilde{\omega}-2\varepsilon_1+i\eta}\frac{1}{\tilde{\omega}-\varepsilon_1-\varepsilon_2-\varepsilon_3-\varepsilon_4+i\eta}\right], \tag{F5}$$

$$\mathcal{I}_6=8K\sum_{(1234)}\left[\delta_G\frac{\gamma_3\tilde{\gamma}_3}{\varepsilon_3}\tilde{V}^{(8)}_{(1234)}V^{(7)}_{(3412)}\frac{1}{\varepsilon_1+\varepsilon_2+\varepsilon_3+\varepsilon_4}\frac{1}{\tilde{\omega}-\varepsilon_1-\varepsilon_2-\varepsilon_3-\varepsilon_4+i\eta}\right], \tag{F6}$$

$$\mathcal{I}_7=4K\sum_{(1234)}\left[\delta_G\frac{\tilde{\gamma}_4}{\varepsilon_4}\tilde{V}^{(8)}_{(4321)}V^{(3)}_{(1234)}\frac{1}{\tilde{\omega}-2\varepsilon_4+i\eta}\frac{1}{\tilde{\omega}-\varepsilon_1-\varepsilon_2-\varepsilon_3-\varepsilon_4+i\eta}\right], \tag{F7}$$

$$\mathcal{I}_8=8K\sum_{(1234)}\left[\delta_G\frac{\gamma_1\tilde{\gamma}_1}{\varepsilon_1}\tilde{V}^{(8)}_{(1234)}V^{(7)}_{(3412)}\frac{1}{\varepsilon_1+\varepsilon_2+\varepsilon_3+\varepsilon_4}\frac{1}{\tilde{\omega}-\varepsilon_1-\varepsilon_2-\varepsilon_3-\varepsilon_4+i\eta}\right] \tag{F8}$$

$$\mathcal{I}_9=4K\sum_{(1234)}\left[\delta_G\frac{\tilde{\gamma}_1}{\varepsilon_1}\tilde{V}^{(2)}_{(1234)}V^{(7)}_{(3412)}\frac{1}{\tilde{\omega}+2\varepsilon_1-i\eta}\frac{1}{\varepsilon_1+\varepsilon_2+\varepsilon_3+\varepsilon_4}\right], \tag{F9}$$

$$\mathcal{I}_{10}=-4K\sum_{(1234)}\left[\delta_G\frac{\tilde{\gamma}_4}{\varepsilon_4}\tilde{V}^{(3)}_{(1234)}V^{(8)}_{(3412)}\frac{1}{\tilde{\omega}-2\varepsilon_4+i\eta}\frac{1}{\varepsilon_1+\varepsilon_2+\varepsilon_3+\varepsilon_4}\right], \tag{F10}$$

$$\mathcal{I}_{11}=-4K\sum_{(1234)}\left[\delta_G\frac{\tilde{\gamma}_1}{\varepsilon_1}\tilde{V}^{(6)}_{(1234)}V^{(8)}_{(3412)}\frac{1}{\tilde{\omega}-2\varepsilon_1+i\eta}\frac{1}{\varepsilon_1+\varepsilon_2+\varepsilon_3+\varepsilon_4}\right], \tag{F11}$$

$$\mathcal{I}_{12}=4K\sum_{(1234)}\left[\delta_G\frac{\tilde{\gamma}_4}{\varepsilon_4}\tilde{V}^{(5)}_{(1234)}V^{(7)}_{(3412)}\frac{1}{\tilde{\omega}+2\varepsilon_4+i\eta}\frac{1}{\varepsilon_1+\varepsilon_2+\varepsilon_3+\varepsilon_4}\right], \tag{F12}$$

where $K=(B/2)^2g(\mathbf{E}_{\rm inc},\mathbf{E}_{\rm sc})(z/4)^2(1/\Omega_{\max})/N^2$ and δ_G stands for $\delta_G(1+2-3-4)$. The sum of $\mathcal{I}_i$, $i=1,\ldots,12$ gives $G_{\Lambda_{10}}$ at first order. Now let us consider the sum $G^{(1)}_{\Lambda_{10}}+G^{(1)}_{\Lambda_{01}}$. We obtain

$$\begin{aligned}
G^{(1)}_{\Lambda_{10}}(\omega)+G^{(1)}_{\Lambda_{01}}(\omega)&=G^{(1)}_{\Lambda_{10}}(\omega)+G^{(1)}_{\Lambda_{10}}(-\omega)\\
&=4K\sum_{(1234)}\delta_G\left\{\left[(\tilde{V}^{(7)}_{(4321)}V^{(2)}_{(1234)}+\tilde{V}^{(8)}_{(4321)}V^{(6)}_{(1234)})\frac{\tilde{\gamma}_1}{\varepsilon_1}\frac{1}{\tilde{\omega}-2\varepsilon_1+i\eta}\right.\right.\\
&\quad+(\tilde{V}^{(7)}_{(4321)}V^{(5)}_{(1234)}+\tilde{V}^{(8)}_{(4321)}V^{(3)}_{(1234)})\frac{\tilde{\gamma}_4}{\varepsilon_4}\frac{1}{\tilde{\omega}-2\varepsilon_4+i\eta}\\
&\quad+2(\tilde{V}^{(8)}_{(1234)}V^{(7)}_{(3412)}+\tilde{V}^{(7)}_{(1234)}V^{(8)}_{(3412)})\left(\frac{\gamma_1\tilde{\gamma}_1}{\varepsilon_1}+\frac{\gamma_3\tilde{\gamma}_3}{\varepsilon_3}\right)\\
&\quad\left.\times\frac{1}{\varepsilon_1+\varepsilon_2+\varepsilon_3+\varepsilon_4}\right]\frac{1}{\tilde{\omega}-\varepsilon_1-\varepsilon_2-\varepsilon_3-\varepsilon_4+i\eta}\\
&\quad+\left[-(\tilde{V}^{(2)}_{(1234)}V^{(7)}_{(4321)}+\tilde{V}^{(6)}_{(1234)}V^{(8)}_{(4321)})\frac{\tilde{\gamma}_1}{\varepsilon_1}\frac{1}{\tilde{\omega}-2\varepsilon_1+i\eta}\right.\\
&\quad\left.+(\tilde{V}^{(3)}_{(1234)}V^{(8)}_{(4321)}+\tilde{V}^{(5)}_{(1234)}V^{(7)}_{(4321)})\frac{\tilde{\gamma}_4}{\varepsilon_4}\frac{1}{\tilde{\omega}-2\varepsilon_4+i\eta}\right]\\
&\quad\left.\times\frac{1}{\varepsilon_1+\varepsilon_2+\varepsilon_3+\varepsilon_4}+(\tilde{\omega}\to-\tilde{\omega})\right\}.
\end{aligned} \tag{F13}$$

Finally, using the following identities in Eq. (F13):

$$\delta_G \tilde{V}^{(7)}_{(4321)} V^{(2)}_{(1234)} = \delta_G \tilde{V}^{(8)}_{(4321)} V^{(6)}_{(1234)} , \tag{F14a}$$

$$\delta_G \tilde{V}^{(7)}_{(4321)} V^{(5)}_{(1234)} = \delta_G \tilde{V}^{(8)}_{(4321)} V^{(3)}_{(1234)} , \tag{F14b}$$

$$\delta_G \tilde{V}^{(8)}_{(1234)} V^{(7)}_{(3412)} = \delta_G \tilde{V}^{(7)}_{(1234)} V^{(8)}_{(3412)} , \tag{F14c}$$

$$\delta_G \tilde{V}^{(2)}_{(1234)} V^{(7)}_{(4321)} = \delta_G \tilde{V}^{(6)}_{(1234)} V^{(8)}_{(4321)} , \tag{F14d}$$

$$\delta_G \tilde{V}^{(3)}_{(1234)} V^{(8)}_{(4321)} = \delta_G \tilde{V}^{(5)}_{(1234)} V^{(7)}_{(4321)} , \tag{F14e}$$

we immediately obtain Eq. (3.44) of Sec. III C.

[1]P. A. Fleury and R. Loudon, Phys. Rev. **166**, 514 (1968).

[2]J. B. Parkinson, J. Phys. C **2**, 2012 (1969).

[3]P. A. Fleury and H. J. Guggenheim, Phys. Rev. Lett. **24**, 1346 (1970).

[4]K. B. Lyons, P. A. Fleury, J. P. Remeika, A. S. Cooper, and T. J. Negran, Phys. Rev. B **37**, 2353 (1988).

[5]K. B. Lyons, P. E. Sulewski, P. A. Fleury, H. L. Carter, A. S. Cooper, G. P. Espinosa, and Z. Fisk, Phys. Rev. B **39**, 9693 (1989). For more recent results, see P. E. Sulewski *et al.*, *ibid.* **41**, 225 (1990).

[6]S. Sugai, S. Shamoto, and M. Sato, Phys. Rev. B **38**, 6436 (1988).

[7]R. R. P. Singh, P. A. Fleury, K. B. Lyons, and P. E. Sulewski, Phys. Rev. Lett. **62**, 2736 (1989).

[8]S. M. Girvin (unpublished).

[9]S. Chakravarty, in *High Temperature Superconductivity, Proceedings of the Los Alamos Symposium 1989, Los Alamos, New Mexico,* edited by K. S. Bedell, D. Coffey, D. E. Meltzer, D. Pines, and J. R. Schrieffer (Addison-Wesley, Reading, MA, 1990).

[10]E. Gagliano and S. Bacci, Phys. Rev. B **42**, 8772 (1990).

[11]Elbio Dagotto and Didier Poilblanc, Phys. Rev. B **42**, 7940 (1990).

[12]S. Bacci, E. Gagliano, and F. Nori, in *Strongly Correlated Electron Systems II,* edited by G. Baskaran, A. E. Ruckenstein, E. Tosatti, and Yu Lu (World Scientific, Singapore, 1991); S. Bacci, and E. Gagliano, Phys. Rev. B **43**, 6224 (1991).

[13]See the discussion by E. B. Stechel, in *High Temperature Superconductivity* (Ref. 9), p. 191.

[14]R. R. P. Singh, Phys. Rev. B **41**, 4873 (1990).

[15]Theodore C. Hsu, Phys. Rev. B **41**, 11 379 (1990).

[16]Y. R. Wang, Phys. Rev. B **43**, 3786 (1991).

[17]Y. R. Wang, Phys. Rev. B **43**, 13 774 (1991).

[18]I. Affleck and J. B. Marston, Phys. Rev. B **37**, 3664 (1988).

[19]K. B. Lyons and P. A. Fleury, J. Appl. Phys. **64**, 6075 (1988); W. H. Weber and G. W. Ford, Phys. Rev. B **40**, 6890 (1989).

[20]F. J. Dyson, Phys. Rev. **102**, 1217 (1956); **102**, 1230 (1956).

[21]S. V. Maleev, Zh. Eksp. Theor. Fiz. **30**, 1010 (1957) [Sov. Phys. JETP **64**, 654 (1958)].

[22]A. B. Harris, D. Kumar, B. I. Halperin, and P. C. Hohenberg, Phys. Rev. B **3**, 961 (1971).

[23]P. Kopietz, Phys. Rev. B **41**, 9228 (1990).

[24]R. R. P. Singh, Phys. Rev. B **39**, 9760 (1989); R. R. P. Singh and D. A. Huse, *ibid.* **40**, 7247 (1989).

[25]T. Oguchi, Phys. Rev. **117**, 117 (1960).

[26]R. J. Elliott and M. F. Thorpe, J. Phys. C **2**, 1630 (1969).

[27]R. W. Davis, S. R. Chinn, and H. J. Zeiger, Phys. Rev. B **4**, 992 (1971).

[28]From Parkinson's theory the values of the cumulants for $S=\frac{1}{2}$ are $M_1/J=2.78$, $M_2/J=0.297$, $M_3/J=0.155$, $M_2/M_1=0.107$, $M_3/M_1=0.056$. Notice that in this case the third cumulant is *positive* for $S=\frac{1}{2}$, while it is negative for any other spin; see also R. R. P. Singh, Phys. Rev. B **41**, 4873 (1990).

[29]Stéphane Tyč and B. I. Halperin, Phys. Rev. B **42**, 2096 (1990).

[30]Jun-ichi Igarashi and Akihiro Watabe, Phys. Rev. B **43**, 13 456 (1991).

[31]E. Stechel (private communication) reports unpublished results on 18- and 20-site clusters in which the peaks split and shift around significantly in position and amplitude, indicating that, even for these larger lattices, finite-size effects are quite significant and depend on the choice of the boundary conditions. These results are in disagreement with the results published so far for the 20 sites (see Ref. 12). However, Stechel's results indicate for both the 18- and 20-site clusters a total weight in the high-energy satellite of about 5%, which is intermediate between our spin-wave estimate of 2.9% and the naive spin-flip estimate of 10%.

[32]Guillermo E. Castilla and S. Chakravarty, Phys. Rev. B **43**, 13 687 (1991).

[33]C. M. Canali, S. M. Girvin, and M. Wallin, Phys. Rev. B (to be published).

[34]S. Sugai *et al.*, Phys. Rev. B **42**, 1045 (1990).

[35]Y. Kuramoto (unpublished).

[36]M. Roger and J. M. Delrieu, Phys. Rev. B **39**, 2299 (1989).

[37]S. Chakravarty, B. I. Halperin, and D. R. Nelson, Phys. Rev. B **39**, 7443 (1988).

[38]B. Sriram Shastry and Boris I. Shraiman, Phys. Rev. Lett. **65**, 1068 (1990).

[39]In Ref. 38 the effective spin scattering Hamiltonian is obtained perturbatively as an expansion in $t/(U-\omega_i)$, where t and U are the parameters of the original one-band Hubbard model, and ω_i is the initial energy of the photon field, which couples to the charge degrees of freedom. In the resonant regime $\omega_i \sim U$, the "higher-order" terms are no longer small compared with the "zeroth"-order term given by the Elliott-Fleury-Loudon Hamiltonian.

[40]Notice that the approximation made in Eq. (D3) is consistent with the approximation that we have made to derive Eq. (2.48) and therefore Eq. (D1). As we said in Sec. II B, these equations are correct to leading order in $\|\underline{\Sigma}(\mathbf{k},\omega)\|/\Omega_{\mathbf{k}}$. The justification of this approximation will come *a posteriori* by proving in this appendix that indeed $\Sigma_{\gamma\delta}(\mathbf{k},\omega)$ is small compared to the unpertubed energy $\Omega_{\mathbf{k}}$.

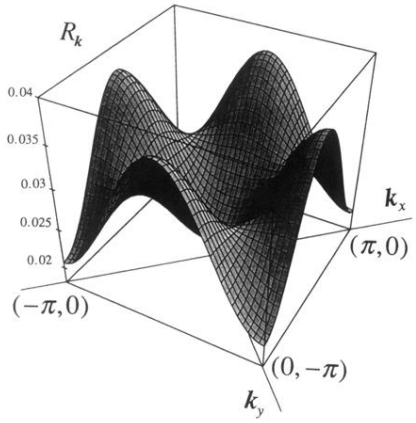

FIG. 22. Normalized self-energy $R_{\mathbf{k}}$, defined in Eq. (D23), as a function of the wave vector inside the HAFM Brillouin zone.